國 立 交 通 大 學

電子物理研究所

碩士論文

鍺基紅外光偵測器應用於光連接系統之設計與建模

Design and modeling of Germanium based Photodetectors for on-chip optical interconnects

指導教授：趙天生 博士

研 究 生：吳立盈

中華民國 一百零一 年 九 月

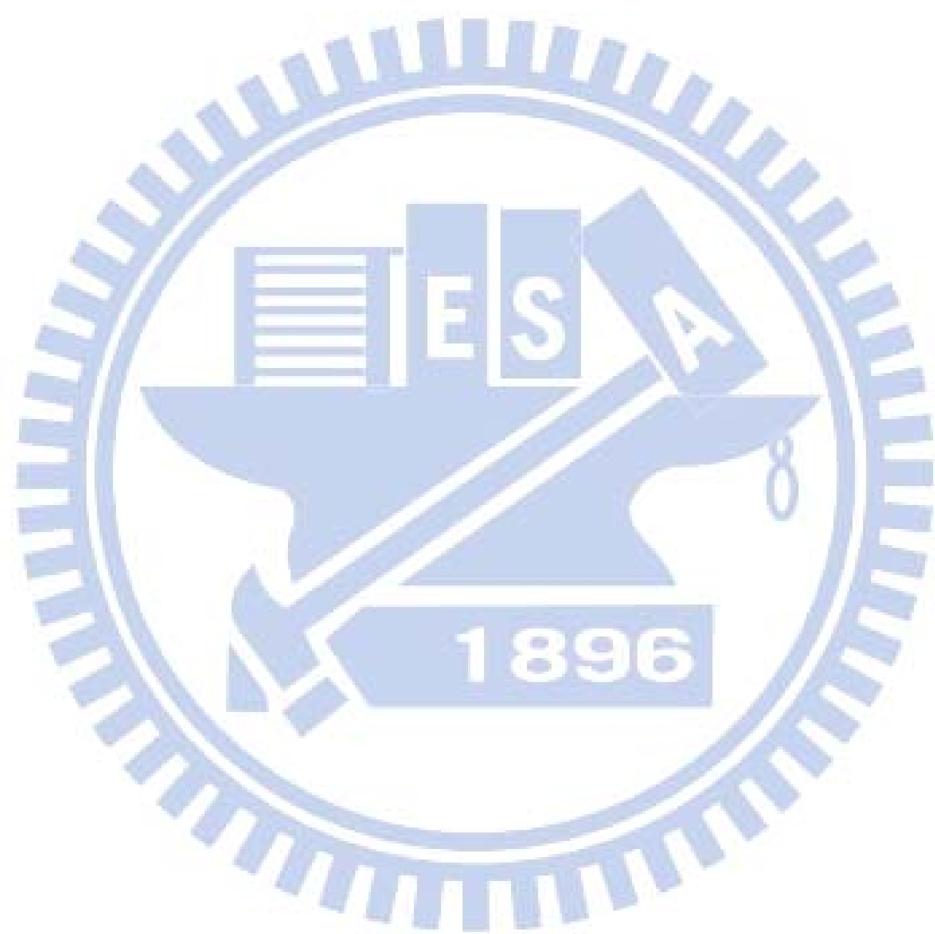

鍺基紅外光偵測器應用於光連接系統之

設計與建模

Design and modeling of Germanium based Photodetectors for on-chip optical interconnects

指導教授 ：趙天生 博士　　**Advisor : Dr. Tien-Sheng Chao**

研究生：吳立盈　　**Student : Li-Ying Wu**

國立交通大學

電子物理所碩士班

碩士論文

Institute of Electrophysics

National Chiao Tung University

A Thesis Submitted to Department of Electronphysics College of Science National Chiao Tung University in Partial Fulfillment of the Requirements for the Degree of Master of Science in Electrophysics.

September 2012,

Hsinchu, Taiwan, Republic of China.

中華民國 一百零一 年 九 月

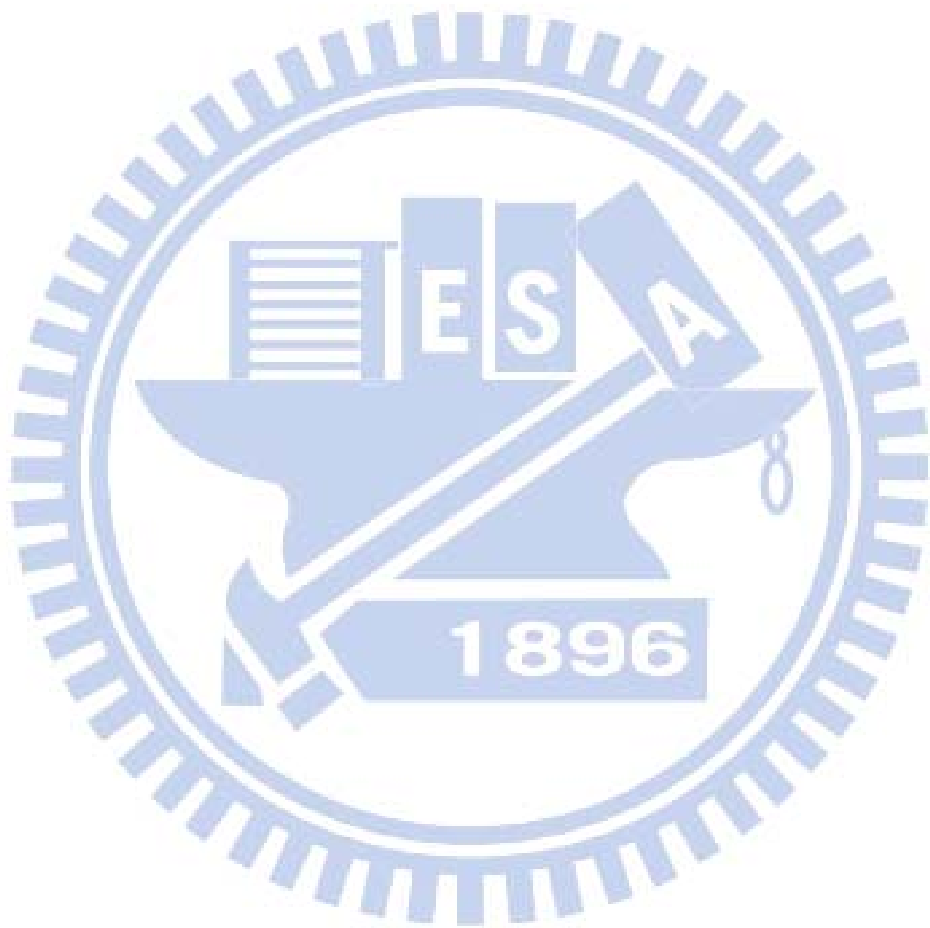
E S A
1896

Abstract

As one of the crucial components in optical interconnect system, germanium photodiodes (GePD) are promising due to its corresponding bandgap (0.66 eV) to absorb infra-red light and the compatibility to silicon-based photonics and electronics. However, many researchers have shown that the key issue of GePD is high dark current, and efforts were done to suppress the dark current and to increase gain-bandwidth product by improving GePD efficiency and speed. This thesis aims to systematically find the photo-electrical behavior based on the simplest P-i-N germanium photodiodes. To investigate the main physical mechanism behind the dark current of germanium photodiode, analysis of temperature dependence ofexperimentally measured dark current is performed. After that, several guidelines toward the GePD structure are provided in this thesis with the aid of TCAD simulation, which can be a useful reference when fabricating high-efficiency and low-power consumption germanium photodetector with lateral P-i-N structure.

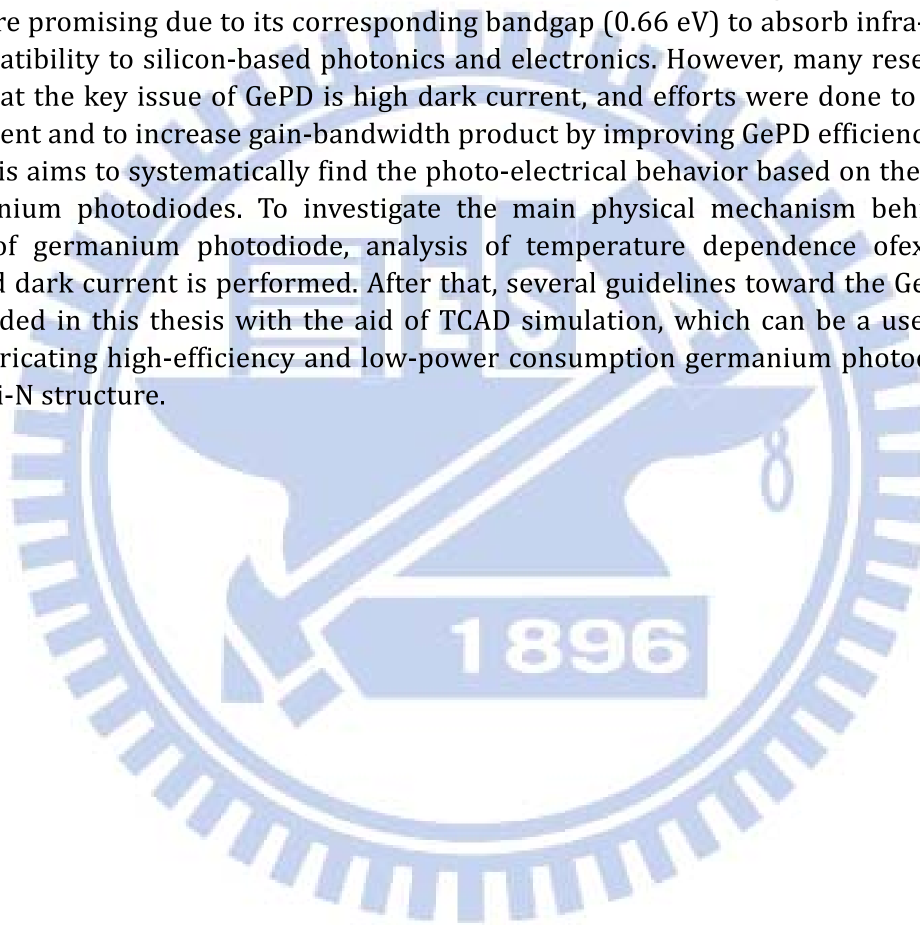

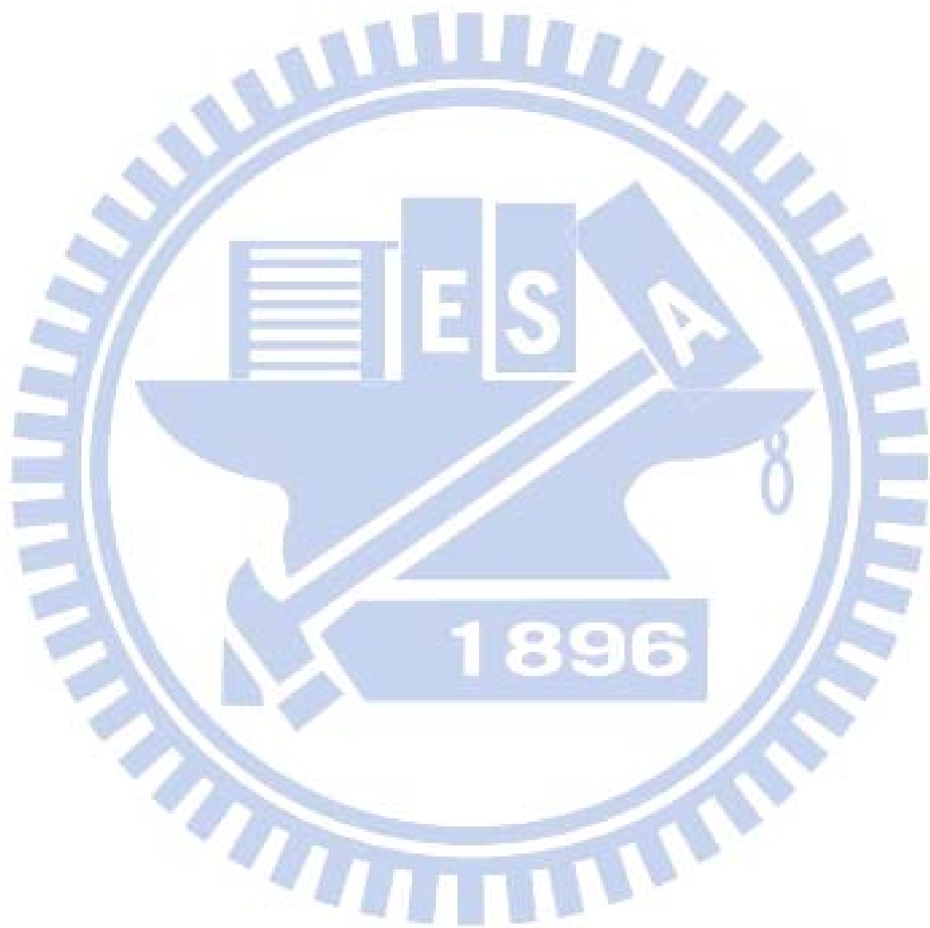
E
S
A
1896

摘要

在取代積體電路銅導線的光連接傳輸系統中，紅外光偵測器是光學訊號接收端的重要元件，其中，鍺的能隙(0.66 eV) 使得鍺基元件能夠有效吸收紅外光訊號，鍺基紅外光偵測器近年來成為許多研究的題目。文獻指出，鍺基紅外光偵測器的主要缺點是暗電流過高，造成訊號干擾以及額外功率消耗。本篇論文以水平 P-i-N 結構的鍺基紅外光偵測器為研究對象，首先透過變溫量測與分析，得知在室溫以及小偏壓操作下，暗電流來自於 Shockley-Read-Hall 載子產生過程 (SRH generation)。接著利用 TCAD 模擬軟體，取用上述 SRH 模型，模擬不同幾何參數對於偵測器之暗電流、光電流以及傳輸速度的影響，探討各參數的權衡與最佳化，為未來提供製造低雜訊、高效率以及高頻寬的鍺基紅外光偵測器的方針。

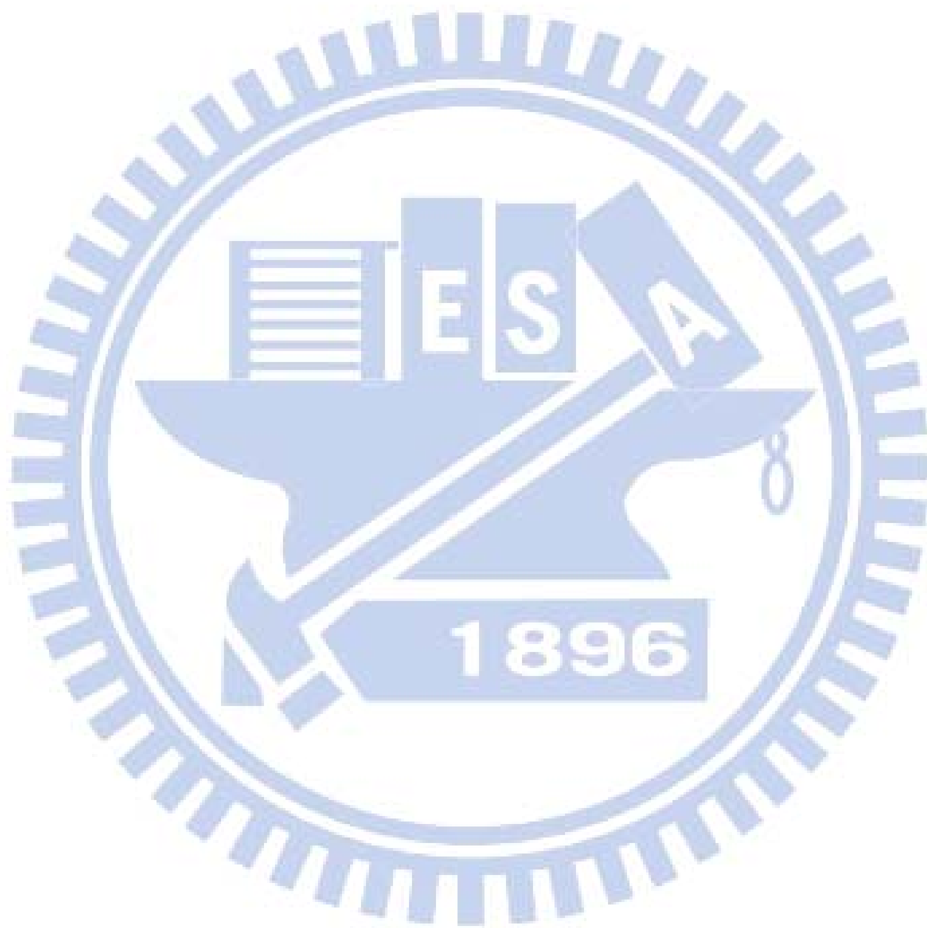

Foreword

I'd like to acknowledge the contribution of two persons to this thesis. One is Prof. Marc Heyns, the thesis supervisor, whose advisement enables this thesis more physically logical. One is Dr. Geert Hellings, my daily supervisor; I deeply appreciate him for his generous teaching, continued guidance, and endless patience.

I am also grateful to members in KULeuven University and National Chiao-Tung University who are in charge of the dual-degree Master program, which provided me such a wonderful opportunity to study here. For the two-year research days in Taiwan, I'd like to acknowledge Prof. Tien-Sheng Chao, who is not only an encouraging teacher but also a supporting mentor. In the free and respectful research environment he provides, I am lucky to meet all the members in the Advanced Semiconductor Device Fabrication and Measurement Lab, and the times we spent together studying and doing experiments in the clean room are definitely memorable.

Finally a big thank you goes to my dear family, wherever in Taiwan or Belgium, I never stop feeling their immediate love and support.

Li-Ying Wu

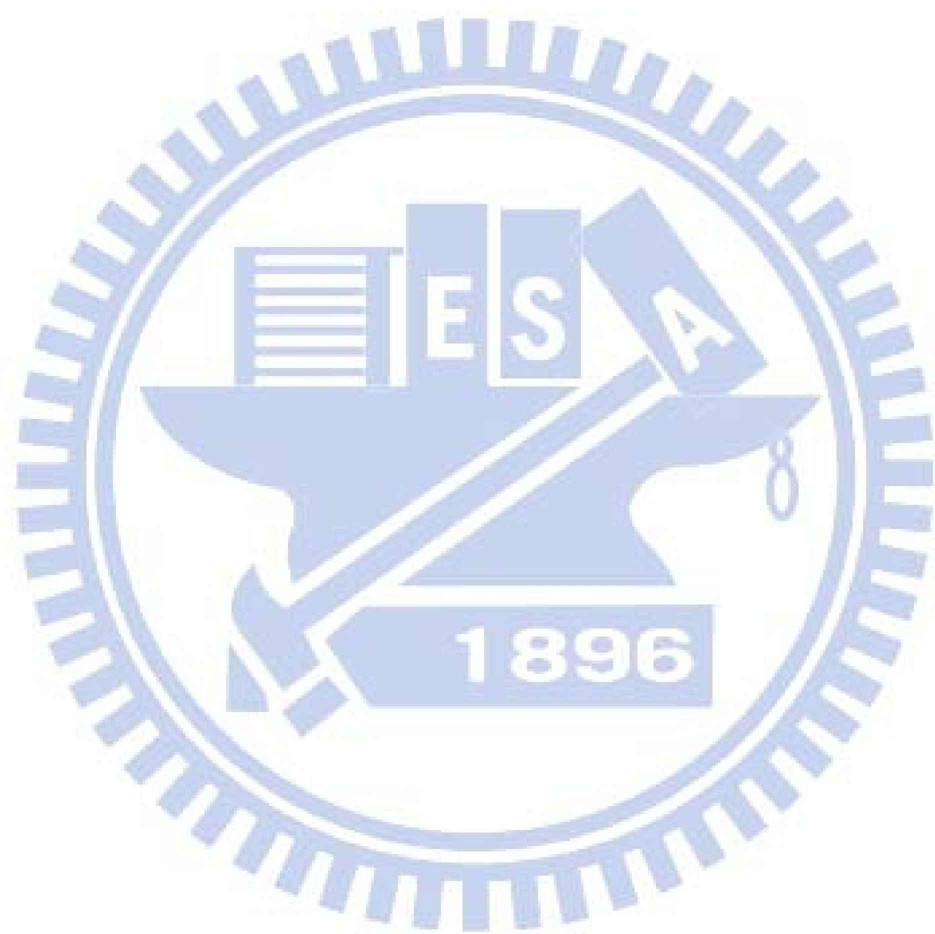
E
S
A
1896

Table of Contents

Abstract v

摘要 vii

Foreword ix

Table of Contents xi

List of figures and tables xiii

List of figures xiii

List of Tables xv

Chapter 1 Introduction 1

1.1 Optical Interconnect: A System Overview 1

1.1.1 History 1

1.1.2 Photodiodes in optical interconnect system 2

1.2 Working principle of P-i-NGePD 3

Chapter 2 Experimental Investigation of Dark Current in Germanium photodiodes 5

2.1 Dark Current Mechanisms in Ge Photodiode 5

2.1.1 Diffusion Currents 5

2.1.2 SRH current 7

2.1.3 Tunneling and Impact Ionization 9

2.2 Measurements of Germanium photodiodes 10

2.2.1 Structure of GePD 10

2.2.2 Temperature dependence measurement 11

2.3 Temperature Dependence of dark current 13

2.4 Conclusion 19

Chapter 3 Dark Current in Germanium photodiodes: TCAD simulation 21

3.1 TCAD Models 21

3.1.1Default Models in TCAD (including Diffusion) 21

3.1.2 SRH: The Shockley-Read-Hall Model 21

3.2 Base structure formed in TCAD 22

3.3TCAD Optimization of Dark Current 26
3.3.1 Alterations in thickness 26
3.3.2 Alterations in width 29
3.3.3 Alterations in implant energy 32
3.4 Conclusion 33
Chapter 4 Quantum Efficiency Optimization 35
4.1 Optical Generation and definition of Quantum Efficiency 35
4.1.1 Optical Generation Method 35
4.1.2 Definition of Quantum Efficiency (QE) 37
4.2 QE in respect of Structural parameters 38
4.2.1 QE dependence on thickness and width of GePD 38
4.2.2 QE dependence on doping separation 40
4.3 QE improvement by Junction engineering 42
4.4 Conclusion 44
Chapter 5 Transient Response Optimization 45
5.1 The Role of Transient Response 45
5.2Speed in respect of structural parameters 47
5.3 Length effect 50
5.3.1 Capacitance in length direction 50
5.3.2 Absorption in length direction 51
5.4 Frequency response 53
5.4.1 Bit stream input 53
5.4.2 Eye diagram 53
5.5 Conclusion 55
Chapter 6 Conclusion 57
Appendices 61
Appendix A: Command codes in TCAD simulator 63
Sprocess 63
Sdevice for IV 67
Sdevice for C-V 70
Sdevice for transient 72
Bibliography 75

List of figures and tables

List of figures

Fig. 1-1 System overview of optical interconnection[4]. 2

Fig. 1-2Illustration and band diagram of a lateral PiN GePD in reverse bias. 3

Fig. 2-1 Energy band diagram of p-n junction in reverse bias. 6

Fig. 2-2 Shockley-Read-Hall generation process[9]. 7

Fig. 2-3 Band diagram and tunneling process of heavily doped diodes[9][15]. 9

Fig. 2-4 Structure of germanium photodiode. 10

Fig. 2-5 Large distribution of dark current vs. Length of GePD. 12

Fig. 2-6 Temperature dependence of I-V characteristics (with parasitic leakage) 12

Fig. 2-7 Temperature dependence of I-V characteristics. 13

Fig. 2-8 Activation energy versus reverse bias from experimental data. 14

Fig. 2-9 Reverse Currents (A/μm) versus 1000/T(K^{-1}). 16

Fig. 2-10 Total reverse current subtracted by diffusion current. 17

Fig. 2-11 Variation of recombination lifetime versus effective dopant concentration[18]. 18

Fig. 3-1 Simulated structure of germanium photodiode in TCAD, showing dopant profiles, meshing. 22

Fig. 3-2 Simulated structure with exponential (top) and constant (bottom) defect distribution profile. 23

Fig. 3-3 Dark current experiment data and results of Exponential defect profile (Top) simulation and constant defect profile (bottom) simulation. 24

Fig. 3-4 Defect determined forward swing behavior indicated accuracy of the defect density level acquired from simulation of dark current. 25

Fig. 3-5 Simulated dark current as a function of Total Ge thickness. 27

Fig. 3-6 Trap number comparison between constant and exponential defects........ 28

Fig. 3-7 Effects of the width of germanium on dark current........ 29

Fig. 3-8Dark current of different diodes versus doping separation ratio........ 30

Fig. 3-9 Electric field distribution in diodes with different doping separation........ 31

Fig. 3-10 Dark current versus implant energy ratio........ 32

Fig. 3-11 Electric field distribution of diodes with different junction depth 32

Fig. 4-1 The 2Dsingle-modeinfrared light intensity distribution inside a 2D Germanium structure of 2-μm-wide and 0.2-μm-thick. 35

Fig. 4-2 Two-dim Gaussian optical signal in the TCAD simulator........ 36

Fig. 4-3 Light distribution in photodiodes with different width and thickness. 38

Fig. 4-4 Effects of Ge thickness and width on QE. 39

Fig. 4-5 QE dependence on doping separation. 41

Fig. 4-6Dark current and QE as a function of implant energy. 42

Fig. 4-7 Deep junctions and shallow junctions. 43

Fig. 4-8 Effects of deep-and-shallow junctions on dark current and QE........ 43

Fig. 4-9 The optimum structure for low dark current and high QE. 44

Fig. 5-1 Illustration of rise time definition........ 45

Fig. 5-2 Effective circuit of a PIN photodiode[20][21]........ 46

Fig. 5-3 C-V characteristics of simulated photodiode with various structures. 48

Fig. 5-4 Speed of GePD is inversely proportional to wGe........ 48

Fig. 5-5.Speed evaluation of GePDs with different Wi and wGe. 49

Fig. 5-6Parasitic Capacitance C_{PD}obtained with length of GePD........ 50

Fig. 5-7 Optical absorption coefficient of Si, Ge, and SiGe alloys[22]. 51

Fig. 5-8 Absorption ratio versus length of germanium photodiode. 52

Fig. 5-9 The bit stream input contains combinations three bits........ 53

Fig. 5-10 Eye diagram of the GePD with speed 30GHz. 54

List of Tables

Table 2-1 Structural parameters of GePD. 11

Table 6-1 Several Guidelines for designing GePD. 59

Table 6-2 GePD equivalent circuit [19] [20]and acquired value of components. 60

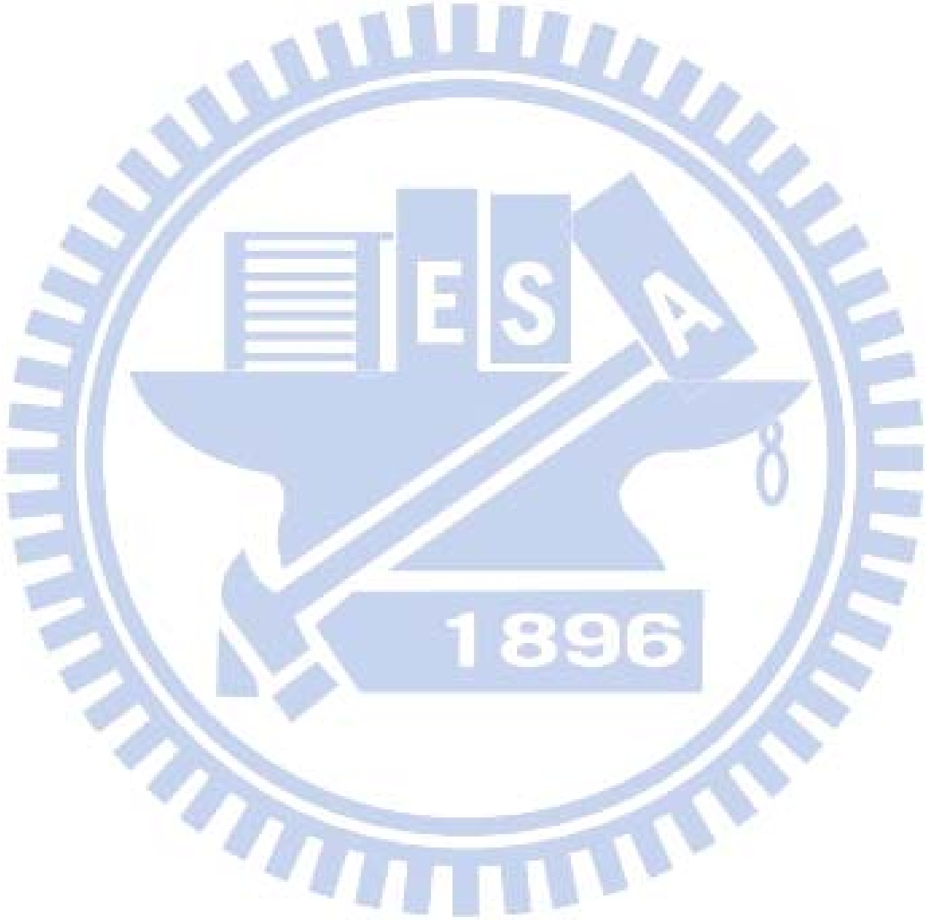

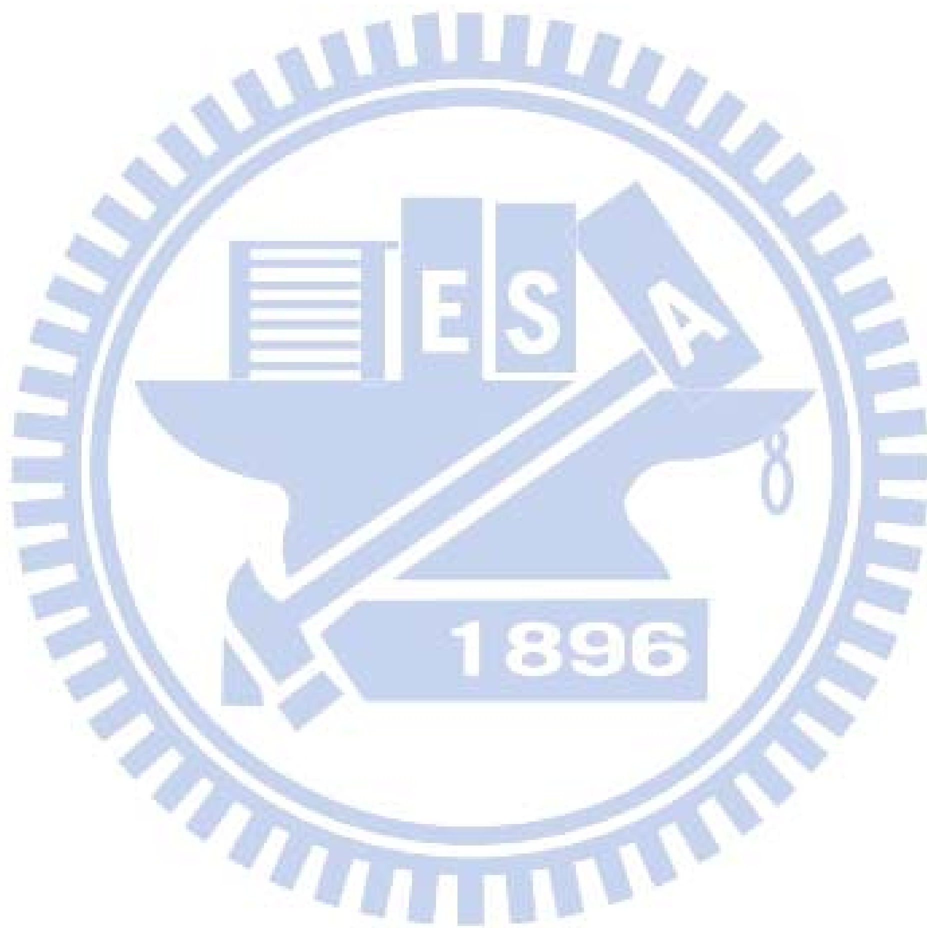

Chapter 1 Introduction

The objective of this thesis is to find an optimum structure of the germanium photodiode inside the optical interconnect system. To start, a system overview of optical interconnect is introduced, and the working principal of a photodiode is given.

1.1 Optical Interconnect: A System Overview

1.1.1 History

Information processing relies on linear and non-linear devices and circuits for logic and storage functions, and also requires interconnections to carry the signal from one place to another. As the counting reduction in feature sizes on electronic chips leads to a larger numbers of faster devices at lower cost per device, the scaling of electrical interconnections doesn't keep up with the growth of electrical devices. The traffic in long-distance is limited by various problems of electrical wiring, for example, high resistance and high parasitic capacitance of long wires. This degrades the speed improvement via devices researches, and global interconnects will become very difficult if people keep using conventional method[1].

The research for optical interconnects starting as early as semiconductor diode laser had been invented, and the first idea that optical interconnects can be utilized in very-large scale-integration (VLSI) was proposed and analyzed by Goodman, *et al.* in 1984. Same year, the quantum confined Stark effect was discovered in III-V semiconductor quantum wells, which enables efficient high-speed optical modulators. Integrated waveguide versions of such modulators are extensively today for high-performance applications[2].

The advantages of using optical interconnects makes development attractive, such as less distance dependency on performance, ability to have 2-D interconnects rather than connect from edge, and feasibility of wavelength division multiplexed interconnects without using any electrical multiplexing circuitry. More details were enumerated in literatures[1][3].

1.1.2 Photodiodes in optical interconnect system

Optical interconnects require the integration of various technologies. Fig. 1-1 shows the overview of a simple set of photonic transceiver and receiver [4], where electrical-optical signal transition happens. Left-hand side of Fig. 1-1 is a silicon modulator consists of optical ring resonators. The modulator takes electrical signals and monochromic laser lights as inputs and generates optical signals of infrared frequency as optical data, which then passages through a silicon waveguide routed on the chip and arrives at the destination chip. At right-hand side, a germanium photodetector is there to capture transmitted optical data, and then transfer optical signals into pulses of electrical currents.

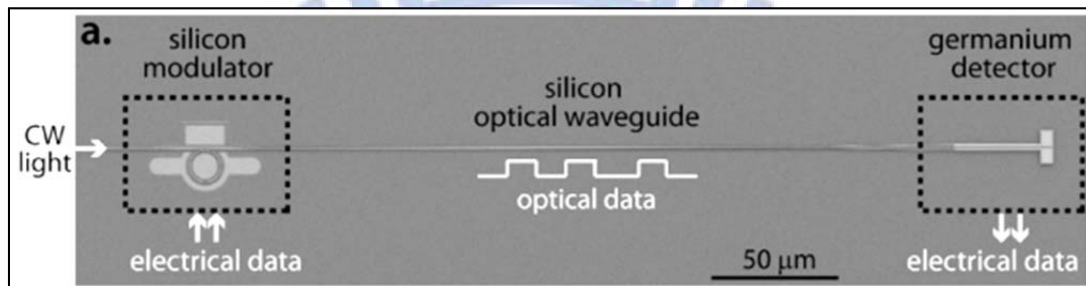

Fig. 1-1 System overview of optical interconnection[4].

As one of the crucial components in optical interconnect system, germanium photodetectors, or Germanium photodiodes (GePDs), have been broadly investigated due to its corresponding bandgap to absorb infrared light at 1.55-μm wavelength and the compatibility to silicon-based photonics and electronics. GePDs monolithically integrated with silicon transistor technology is viewed as the essential part of infrared optical interconnects system.

However, many researchers have shown that the issue technology issue of GePD is high dark current, due to the 4.2% mismatch between Ge and Si, and efforts were done to suppress the dark current by means of improving fabrication process [5][6]

To improve GePD efficiency and speed, advanced GePD are developed to increase the photocurrent in regular P-i-N GePD by utilizing multiplication of carriers, for example, Avalanche photodetector (APD) and separate-absorption-charge-multiplication (SACM) photodiode [7]. Literature [8] proposed that creation of non-uniform electric field in germanium APD via nanoelectric engineering increases the gain-bandwidth product.

The purpose of this thesis is to systematically find the photo-electrical behavior based on the simplest P-i-N germanium photodiodes but with various structural parameters, with the aid of TCAD simulator; so that a basic guideline can be provided for the future advanced researches. In next section, working principles of P-i-N germanium photodiode is introduced.

1.2 Working principle of P-i-N GePD

Fig. 1-2 shows the illustration and the band diagram of a lateral P-i-N GePD in reverse bias. Green lines represent the conduction and valence band edge at equilibrium, and distance between $-X_{p0}$ and X_{n0} represent the depletion width at equilibrium. When a reverse bias is applied, depletion retrieves away from the center of diode (to $-X'_{p0}$ and X'_{n0}), and the exposed ionized dopants provide extra electric fields, which can be seen from the increasing slope of band edges.

When photodiode is under photon illumination, photons with sufficient energy and correct momentum can excite valence electrons; hence extra free electrons and corresponding free holes are generated. At intrinsic region, these photon-generated excess carriers are drifted by the electric field aroused by reverse bias. Electrons are driven to n side, and holes driven to p side. Current generated from this process is called photocurrent. The prompt photocurrent generated in the space charge region is of the main interest; therefore depletion region width can be made large to have a photodiode with high sensitivity. That's the reason P-i-N photodiode is used[9].

The current appeared without illumination is called dark current, which is undesirable since it would raise the consumption of power. Mechanisms behind dark current are given in next chapter.

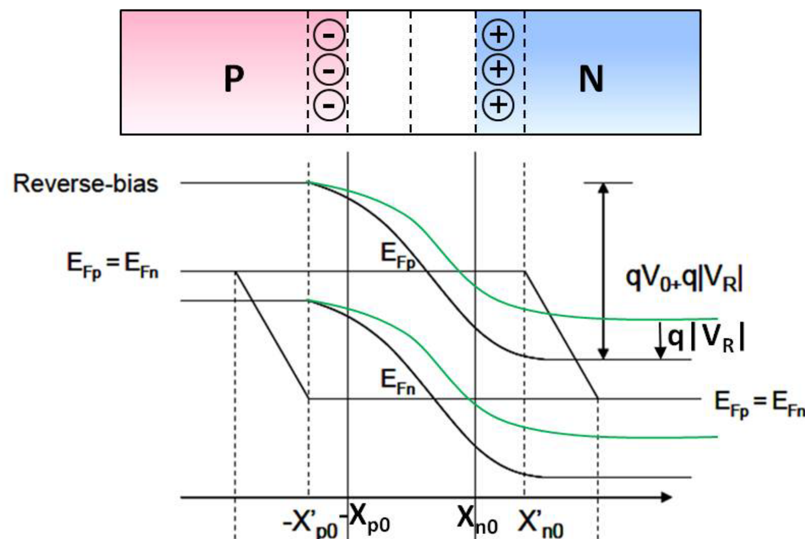

Fig. 1-2Illustration and band diagram of a lateral PiN GePD in reverse bias.

In the following chapters, operation conditions are all considered under a **reverse bias of absolute value 0.5** volt, and for short sometimes it is put as **-0.5V**.

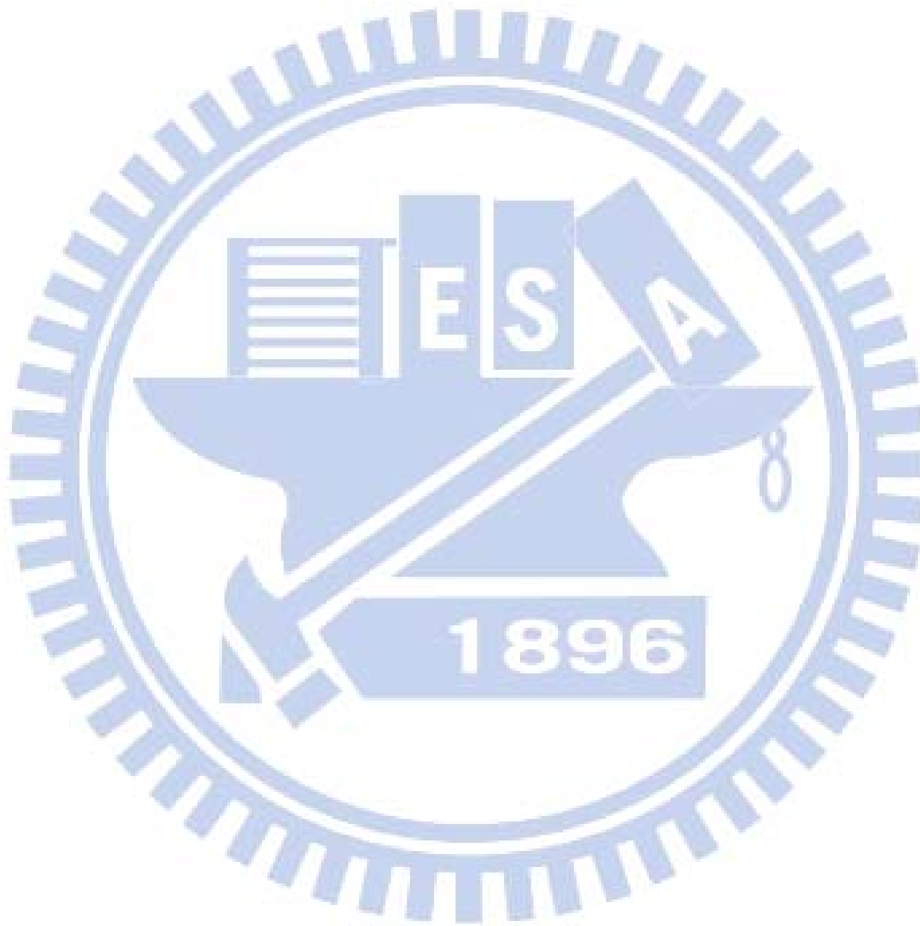

Chapter 2 Experimental Investigation of Dark Current in Germanium photodiodes

In this chapter, dark currents mechanisms are enumerated. Next, the results of temperature dependence measurement of GePD dark currents and the analysis are presented.

2.1 Dark Current Mechanisms in Ge Photodiode

To start with, several components of photodiode dark current which result from different mechanisms are considered before analysis. They are respectively diffusion current, thermal generation current, tunneling current and impact ionization current[10].

A well-performed photodiode needs to keep its dark current low enough, to avoid high power consumption at stand-by stage and even noise when light signals turned on. Compared to silicon devices, germanium diode is more likely to be suffered from higher junction leakage due to its small band gap (0.66 eV). What's more, high dark current leakage is the critical issue in Ge PDs technology as compared with III-V based photodiodes. Therefore, clarifying of the main recombination mechanisms is indispensable for of Ge photodiode electrical behavior simulation, and further for Ge photodiode optimization. In this chapter, the physical mechanisms behind dark current are viewed, and the experimental investigation of dark current is performed.

2.1.1 Diffusion Currents

Diffusion current is proportional to the gradient of the carrier concentration evaluated at the interface between the depletion and the neutral region[11]. Energy band diagram of a p-n junction in reverse bias is shown as Fig. 2-1. For example, in p-type quasi-neutral region areas, the equilibrium minority or electron concentration n_{p0} is:

$$n_{p0} = \frac{{n_i}^2}{N_A} \qquad \textbf{Eq. 2-1}$$

where N_A is acceptor concentration in p-type region. Those electrons would diffuse to n-type region if they are close to space-charge region, hence:

$$n_p = n_{p0}\left(1 - e^{-\frac{x}{L_n}}\right) \quad \textbf{Eq. 2-2}$$

$$I_{diffusion} = qD_n \frac{dn_p}{dx}\bigg|_{x=x0} = \frac{qD_n n_i^2}{N_A L_n} = q\sqrt{\frac{D_n}{\tau_n}}\frac{n_i^2}{N_A} \quad \textbf{Eq. 2-3}$$

Since n_i is positively correlated to temperature, we can tell from Eq. 2-3 that diffusion current would increases when rising temperature with an activation energy equals to the band gap of germanium [12].

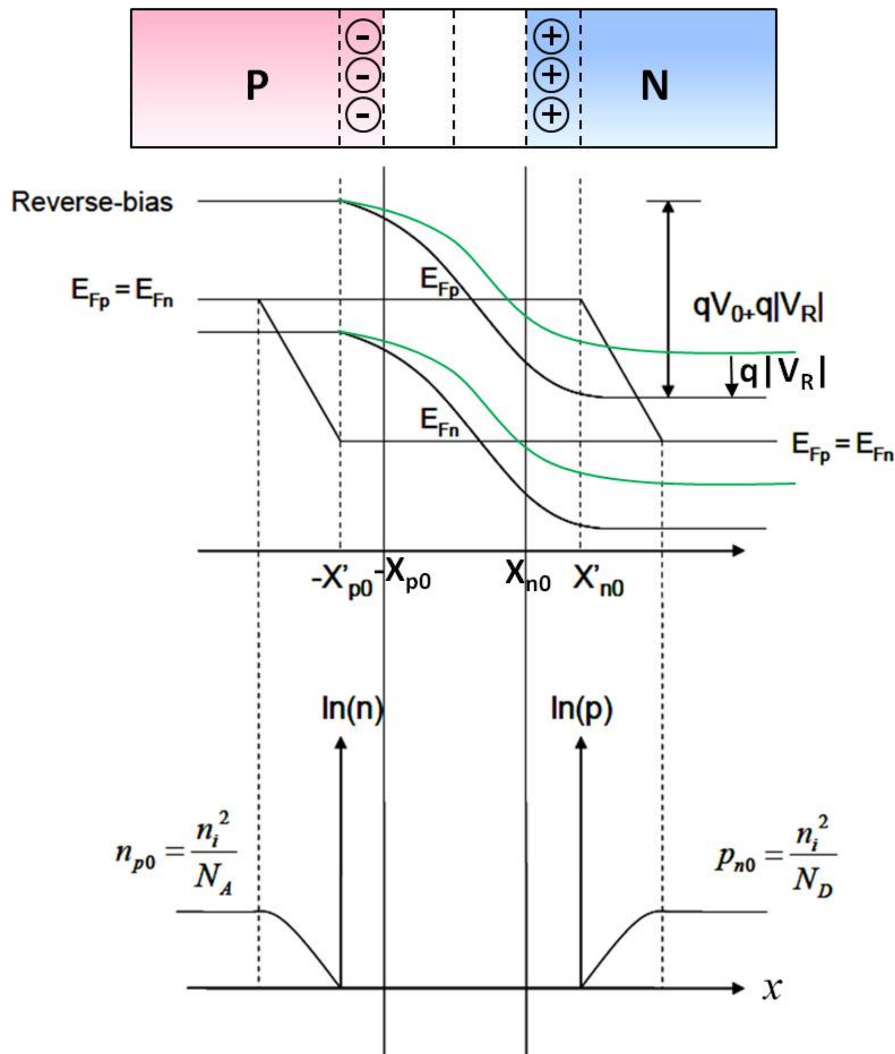

Fig. 2-1 Energy band diagram of p-n junction in reverse bias.

2.1.2 SRH current

Besides diffusion current, recombination-generation current should also be concerned. Since basically photodiode operates in -0.5 volts, under this reverse condition, the electric field in depletion region sweeps holes to the p-type region and electrons to n-type region. Because of the reduction in carrier concentration ($np \ll n_i^2$), system is prone to generate more carriers to meet equilibrium.

Many researchers have found dark current is greatly depends on the quality of junction layers. This indicates that the generation process involves impurities or imperfections. Those imperfections disrupt the lattice of semiconductor and introduce energy levels into the band-gap. In our case, most of the imperfections come from dislocations at the interface of silicon waveguide and germanium layer due to lattice mismatch. Fig. 2-2illustrates this generation process, or so-called Shockley-Read-Hall recombination.

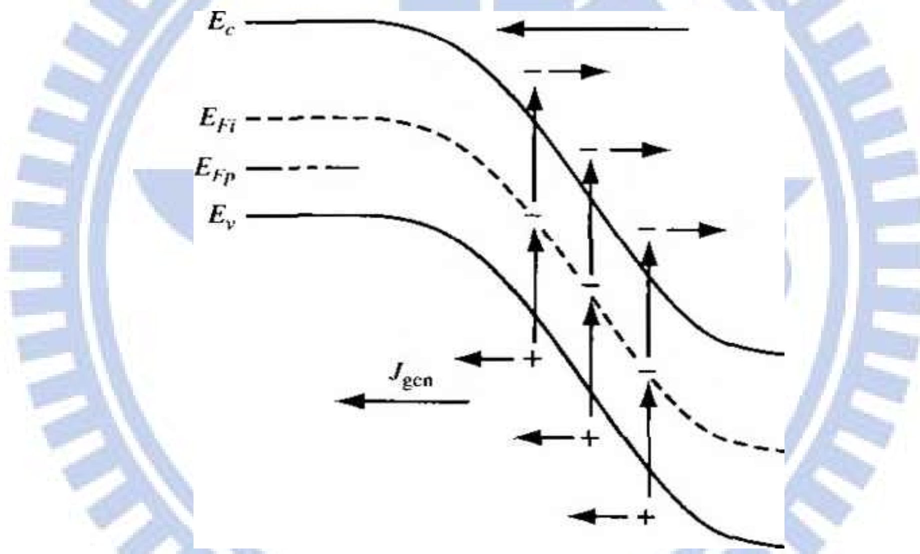

Fig. 2-2 Shockley-Read-Hall generation process[9].

The net generation-recombination rate, U, of carriers through these intermediate centers has been successfully described by Hall, Shockley and by Read[13][14]. It can be shown that:

$$U = \frac{\sigma_n \sigma_p v_{th} (pn - n_i{}^2) N_t}{\sigma_n \left[n + n_i \exp\left(\frac{E_t - E_i}{kT}\right)\right] + \sigma_p \left[p + n_i \exp\left(\frac{E_i - E_t}{kT}\right)\right]} \qquad \textbf{Eq. 2-4}$$

where σ_p and σ_n are the capture cross-sections for holes and electrons respectively, v_{th} is the thermal velocity, n is the electron concentration, p is the hole concentration, N_t is the concentration of bulk generation-recombination centers at the energy level E_t, E_i is the intrinsic Fermi level and n_i the intrinsic carrier concentration.

To summarize, components of diffusion and thermal generation currents in a p-n junction could be described as following equation [Sze, sensor]

$$J_{Reverse} = q\sqrt{\frac{D_n}{\tau_n}} \cdot \frac{{n_i}^2}{N_A} + q\frac{n_i}{\tau_{gen}}W \qquad \textbf{Eq. 2-5}$$

where q is elementary charge, D_n is the electron diffusivity, τ_n is the electron life time, N_A is the doping level of the p-type region, n_i is the intrinsic concentration of semiconductor, in this case, germanium, τ_{gen} is the generation lifetime, and W is the depletion width. A similar expression holds for holes.

The second term of Eq. 2-5 states SRH recombination/generation current is dependent on carrier life time τ_{gen}; namely, this source of dark current is influenced by the number of defects that served as recombination/generation sites[12]

More details will be discussed in section 2.3, while analysis of germanium dark current under different temperature and reverse bias based on experimental measurement is presented.

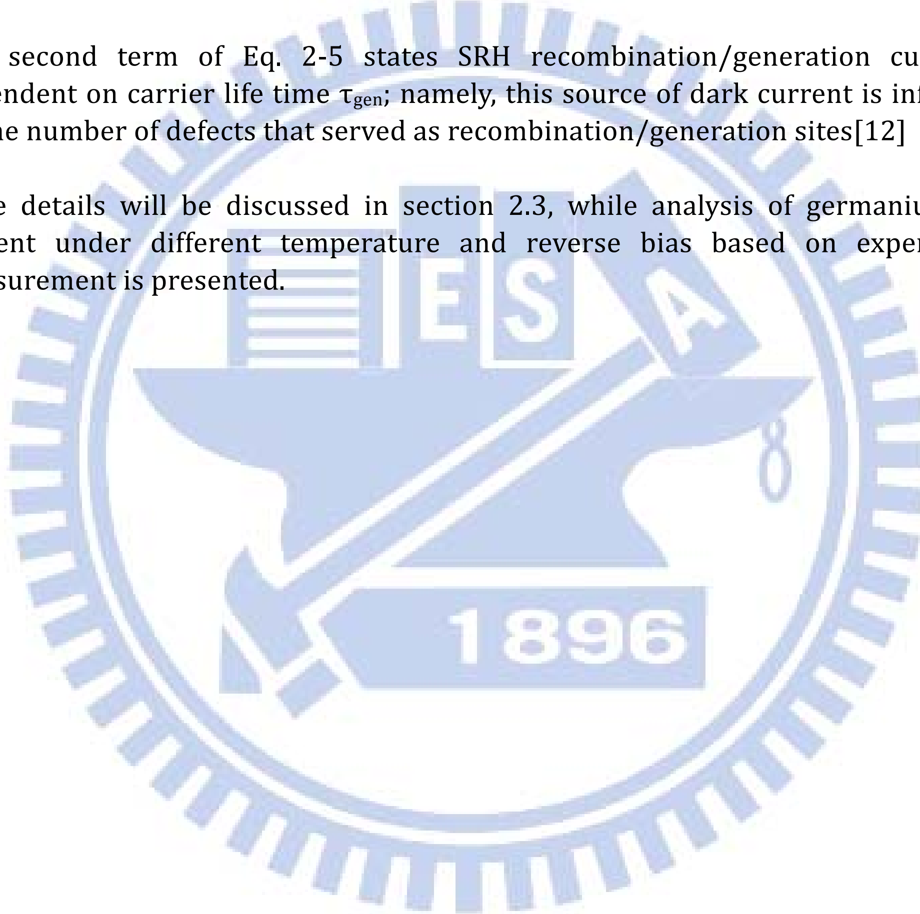

2.1.3 Tunneling and Impact Ionization

In a diode with degenerately doped p-n junctions, tunneling can be determining when reverse bias is above a certain value, since depletion region is relatively narrow in highly doped diodes and hence smaller tunneling barrier. The process is shown in Fig. 2-3. Tunneling current could be band-to-band tunneling (BTBT) and trap-assisted tunneling (TAT).

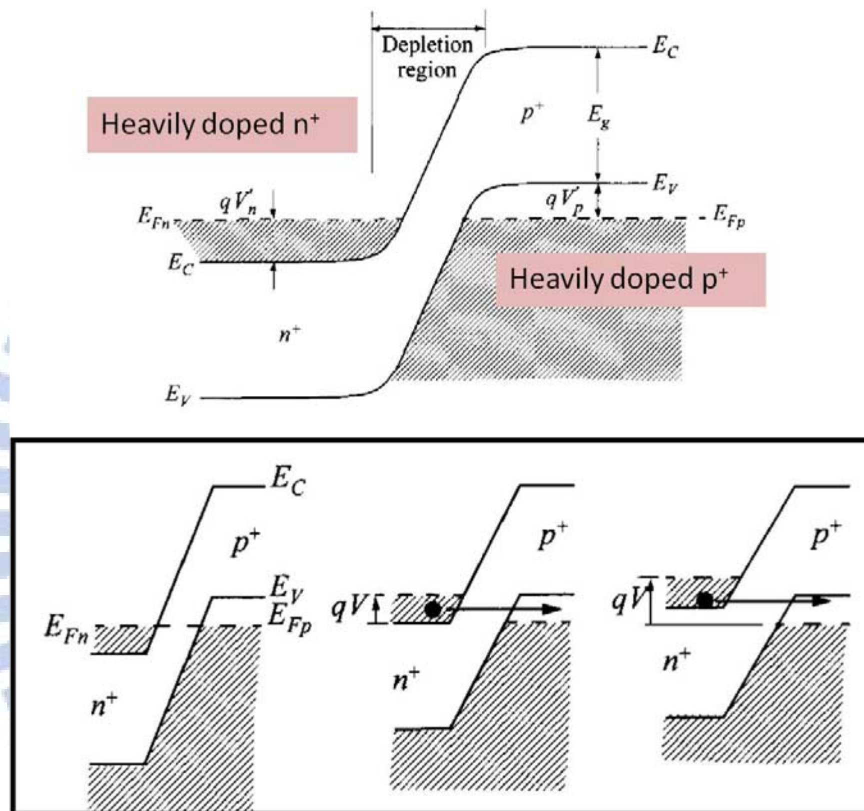

Fig. 2-3 Band diagram and tunneling process of heavily doped diodes[9][15].

At higher applied voltages, impact ionization plays a role followed by avalanche breakdown. The avalanche breakdown process occurs when carriers moving across the space charge region, acquire sufficient energy from the electric field to create electron-hole pairs by colliding with atomic electrons within the depletion region[9]. Analytical model describing reverse characteristics of a p-n diode including tunneling current and avalanche breakdown was presented in [16].

However, in this thesis, the structure we discussed is a P-i-N junction, whose intrinsic width is at least 0.5 μm. With this sufficient large tunneling barrier, and the operation condition that only under low electric field, it's reasonable to conclude that tunneling current and impact ionization currents are negligible.

2.2 Measurements of Germanium photodiodes

2.2.1 Structure of GePD

The structure GePD device used in this thesis looks like Fig. 2-4,in Fig. 2-4(bottom), silicon layer serves as an optical signal waveguide; it is recessed into trapezoidal shape by etch-back process, and from Fig. 2-4(right) we can see this trapezoidal shape is formed the (111), (113) and (100) facets of silicon. The taper angle (see (bottom)) is approximately 30°, which is used to increase the coupling efficiency for light to transmit through Si/Ge interface[17].

Lying on top of the silicon is the main body of photodetector, formed by germanium selective epitaxial growth. After annealing and CMP process, boron and phosphorus implantation is applied to form P+ and N+ side respectively, and after the process of oxide layer deposition and contact-hole formation, tungsten electrodes are filled in. The cross-section of GePD resembles a mushroom, and the "cap" of mushroom is called overlap region. Overlap region is designed to separate tungsten electrodes far away from light intensity, so that light intensity loss from metal absorption can be decreased. All the meanings of structural parameters are listed in Table 2-1.

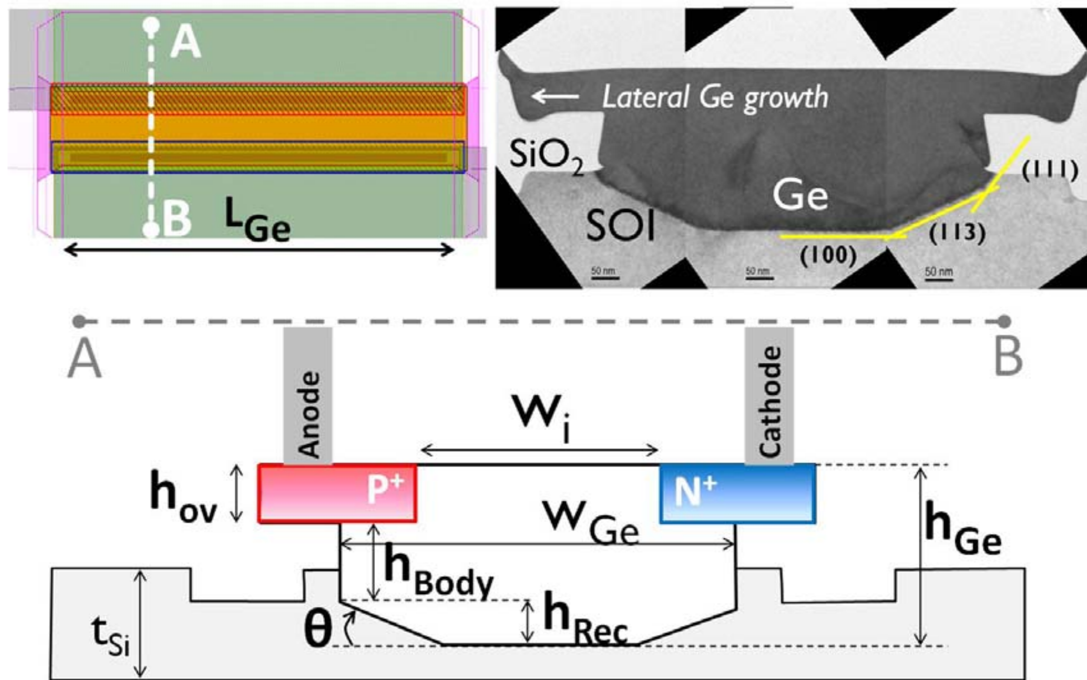

Fig. 2-4 Structure of germanium photodiode.
(left)Top view of GePD; (right)TEM structure of GePD; (bottom) GePD Structure illustration with parameters

Terms	Meanings
hGe	Total thickness of Germanium diode (=hov+hBody+hRec)
hBody	Thickness of Germanium body
hov	Thickness of overlap
hRec	Recession depth (= Si etched-back thickness)
wGe	Width of Germanium diode
Wi	Doping separation; Width of intrinsic region
θ	Tapered angle formed when silicon etch-back process
tSi	Thickness of silicon

Table 2-1 Structural parameters of GePD.

2.2.2 Temperature dependence measurement

To analyze dark current behavior, a series measurement of the current-voltage characteristic with varying temperature has been done. The temperature dependence measurement is performed by HP4156 Semiconductor Parameter Analyzer. Fig. 2-6shows the I-V characteristics of photodiode measured under different temperature from -10°C to 125°C, sweeping anode (connect to P^+ terminal of GePD) voltage from -2V to 1V.

However in Fig. 2-6, sets of curves is merging together as arrowed, which means that dark currents are interfered by exterior leakage path, for example, leakages that come along the edge of germanium. Furthermore, this parasitic current is difficult to be normalized with length because as we measured the leakage currents of diodes with 10, 20 and 50μmlongand there is no correlation between current and length. A large distribution is shown in Fig. 2-5.This phenomenon is also diverse from sample to sample throughout the whole wafer.

It is more meaningful to analyze the intrinsic behavior of leakage currents in germanium photodiode; after a series of "searching for the best die," measurement data that worthy discussing is put in the 2.3 section.

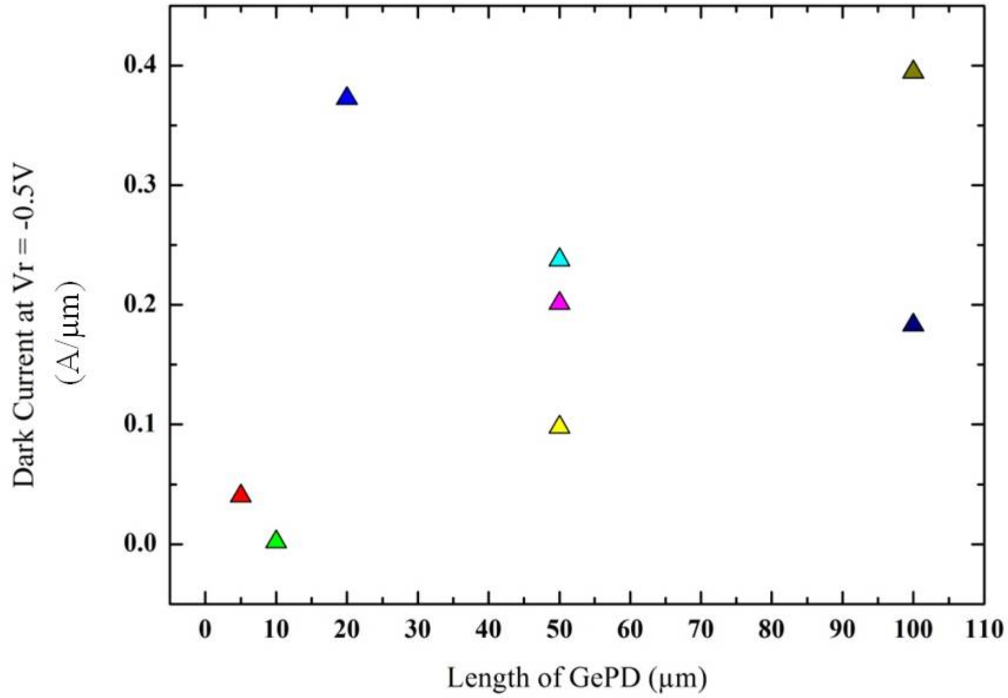

Fig. 2-5 Large distribution of dark current vs. Length of GePD. Large distribution prevents accurate extract of dark current.

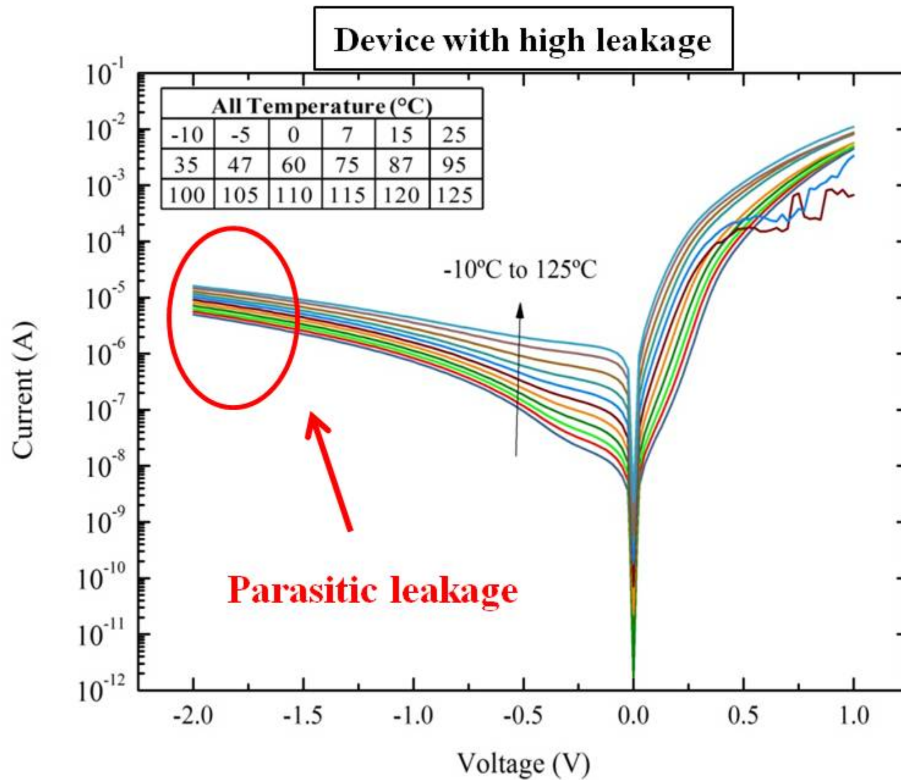

Fig. 2-6 Temperature dependence of I-V characteristics (with parasitic leakage).

2.3 Temperature Dependence of dark current

The result of measuring "the best die" is shown in Fig. 2-7, in which curves are more smooth compared to those interfered by parasitic leakages. And then, activation energy is estimated based on Arrhenius equation (Eq. 2-6) by fitting data with exponential function in the plotting of measured dark current at a given reverse bias versus 1/T (not shown), and extracting the exponent to calculate activation energy Ea at each reverse bias point.

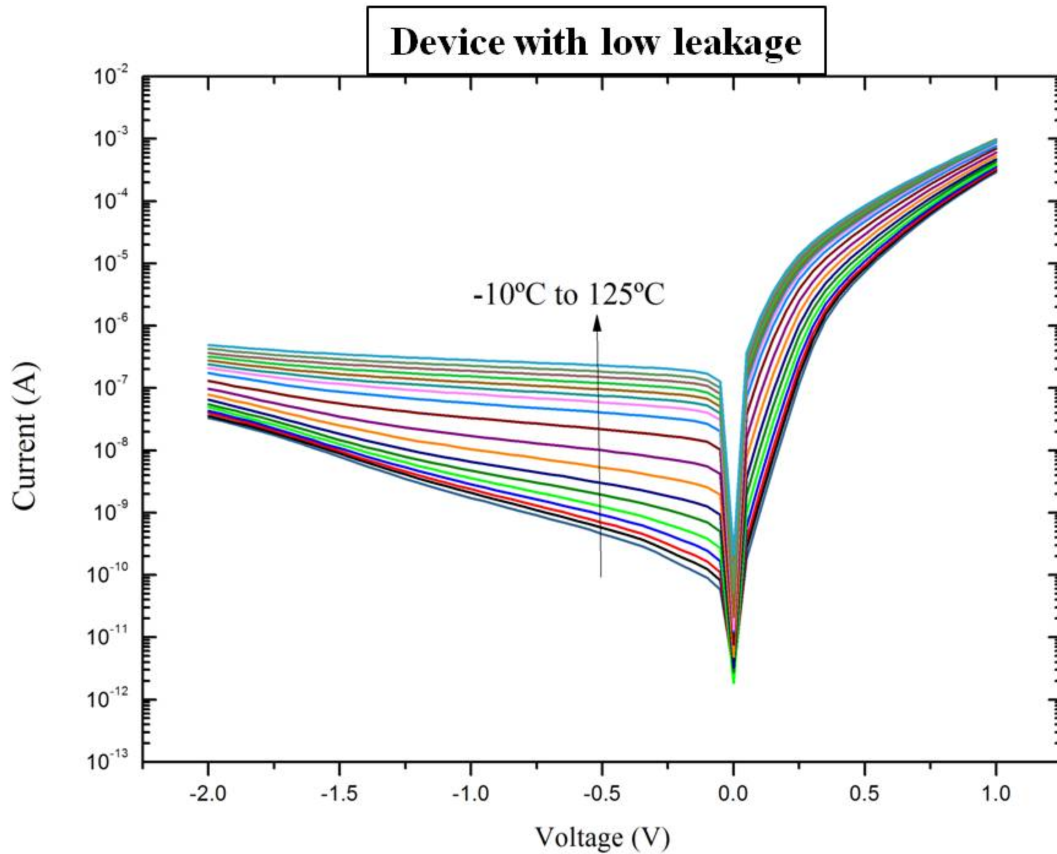

Fig. 2-7 Temperature dependence of I-V characteristics.

$$k = Ae^{-E_a/k_B T} \qquad \textbf{Eq. 2-6}$$

Activation energy is the energy needed for electrons to overcome process barrier. The activation energy for diffusion process is germanium bandgap 0.66 eV, and for SRH process with deep traps Ea should be close to half bandgap, 0.33 eV. Activation energy versus reverse bias is shown in Fig. 2-8.

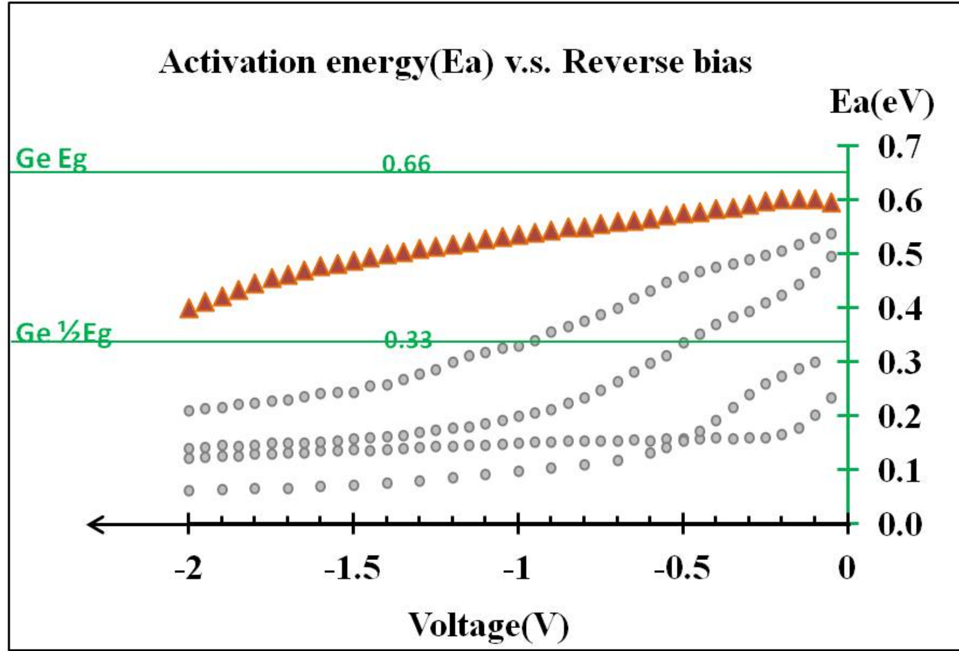

Fig. 2-8 Activation energy versus reverse bias from experimental data.
Dark current is initially dominated by diffusion mechanism near zero volts, and continually Shockley-Read-Hall generation takes place in higher reverse bias.

Ea of five samples as a function of reverse bias are shown in Fig. 2-8.Only the top curve (red solid triangles) maintains above Ge half bandgap (0.33 eV) until -2V, which is regarded behaving as intrinsic semiconductor leakage. Other four curves (small dots) reveal that these samples are more affected by leakages from parasitic conducting path.

Activation energy is dropping as reverse bias increases (goes to negative/left direction as arrowed). For the top curve, it starts with Ea ≈ 0.6 eV, which means that the average dark current over -10°C to 125°C is dominated by diffusion of minority carriers in small bias. As reverse bias gets higher, Ea gradually drops close to 0.3 eV, which means that at higher reverse bias, average dark current is subjected to SRH recombination process.

Another analysis shows this trend similarly. In Fig. 2-9, the logarithm of the measured leakage current (curves with blue solid symbols) at different applied voltages are plotted versus 1000/T together with **ni** and **ni²** dependencies (straight lines with open symbols). The inset of Fig. 2-9 is again Eq. 2-5, with first term related to diffusion current and second term related to SRH generation current as indicated. **ni** dependency on temperature is shown more clearly in Eq. 2-7. Bandgap correction with respect to temperature is taken into account when plotting of ni and ni^2 dependencies.

$$n_i = \sqrt{N_C N_V} exp\left[-\frac{E_g}{2kT}\right] = \sqrt{2\left(\frac{2\pi m_e^* kT}{h^2}\right)^{\frac{3}{2}} \cdot 2\left(\frac{2\pi m_h^* kT}{h^2}\right)^{\frac{3}{2}} exp\left[-\frac{E_g}{2kT}\right]} \quad \textbf{Eq. 2-7}$$

In Fig. 2-9, it shows that SRH generation leakage has a stronger dependence on reverse bias compared to diffusion current. It is because with higher reverse bias, the diode is more depleted (depletion region gets wider), which means more traps are exposed out as generation sites, resulting in higher generation current. Sets of curves show a trend that dark current of measured GePD is in a combination behavior of diffusion and SRH generation. Judged from the slope and tangent line, SRH generation is the main component in dark current at room temperature 25°C, while the GePD is at its operation point -0.5V. Above 87°C, diffusion current plays a role.

Fig. 2-10demonstrates this more clearly, which is the zoom in version of Fig. 2-9, while Y-axis is replaced as the amount of measured current subtracted by calculated diffusion current (first term of Eq. 2-5), which should give SRH generation behavior. A neat fitting with SRH equation lines (five parallel yellow lines) could be seen in temperature below 25°C. Deviations in higher temperature and higher reverse voltage regime are supposed to attribute to extra current from diode edge, which is randomly distributed as shown before.

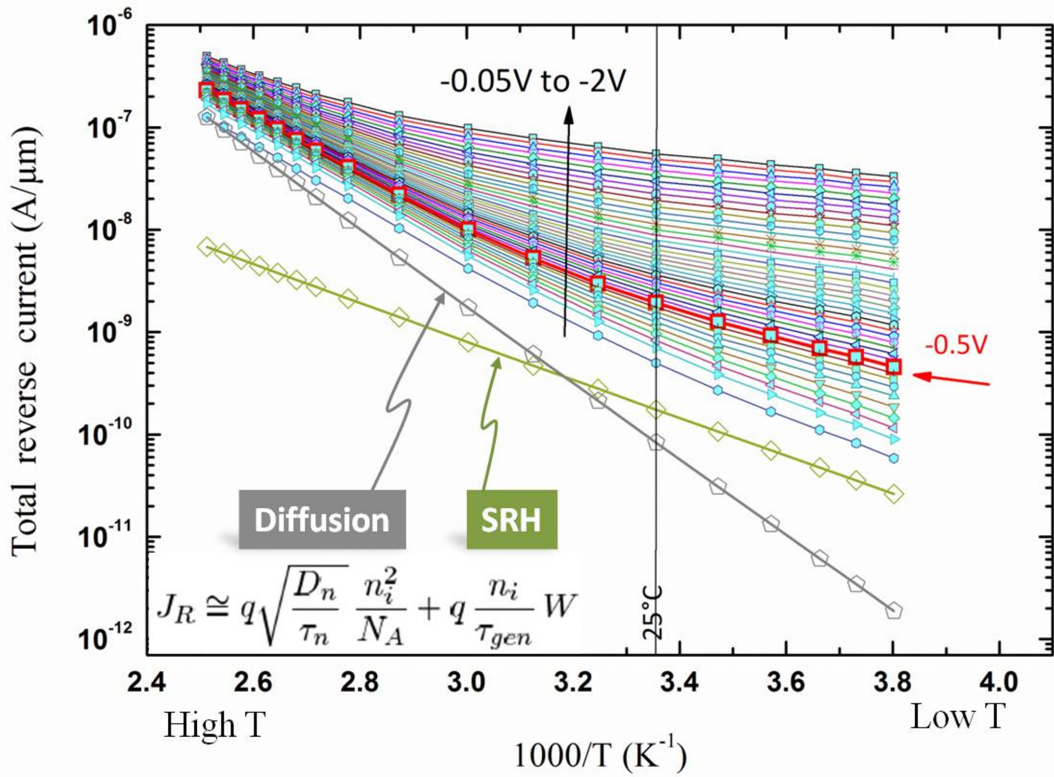

Fig. 2-9 Reverse Currents (A/μm) versus 1000/T(K^{-1}).

Measured current (solid symbols) at different temperature as a function of 1000/T. Two straight lines with open symbols are plotted from Eq. 2-5 **as in the inset, with first term related to diffusion current and second term related to SRH generation current as indicated.**

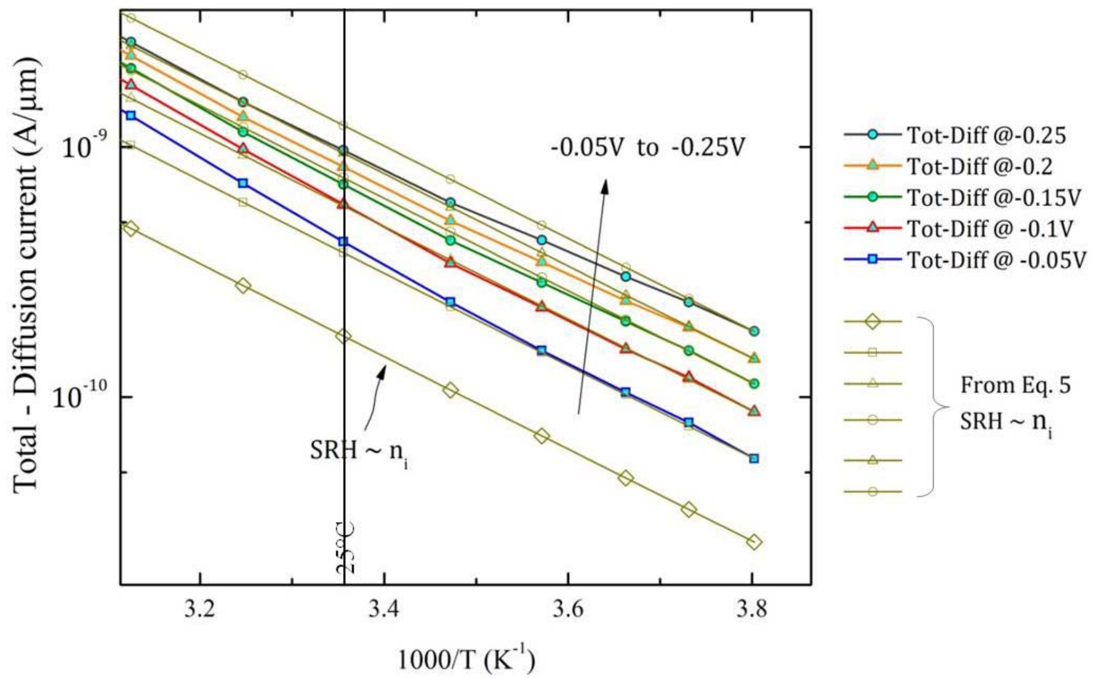

Fig. 2-10 Total reverse current subtracted by diffusion current.
Solid symbols are measured total current subtracted by pure calibrated diffusion current from Eq. 2-5, and empty symbols are pure calibrated Shockley-Read-Hall current from equation.

Lifetimes of electrons are also roughly calculated to be 0.06 μs. Based on literature[18], the defect density of the best die is estimated around 1e19/cm^3 from Fig. 2-11. In Chapter 3, defect density would be estimated by TCAD simulator.

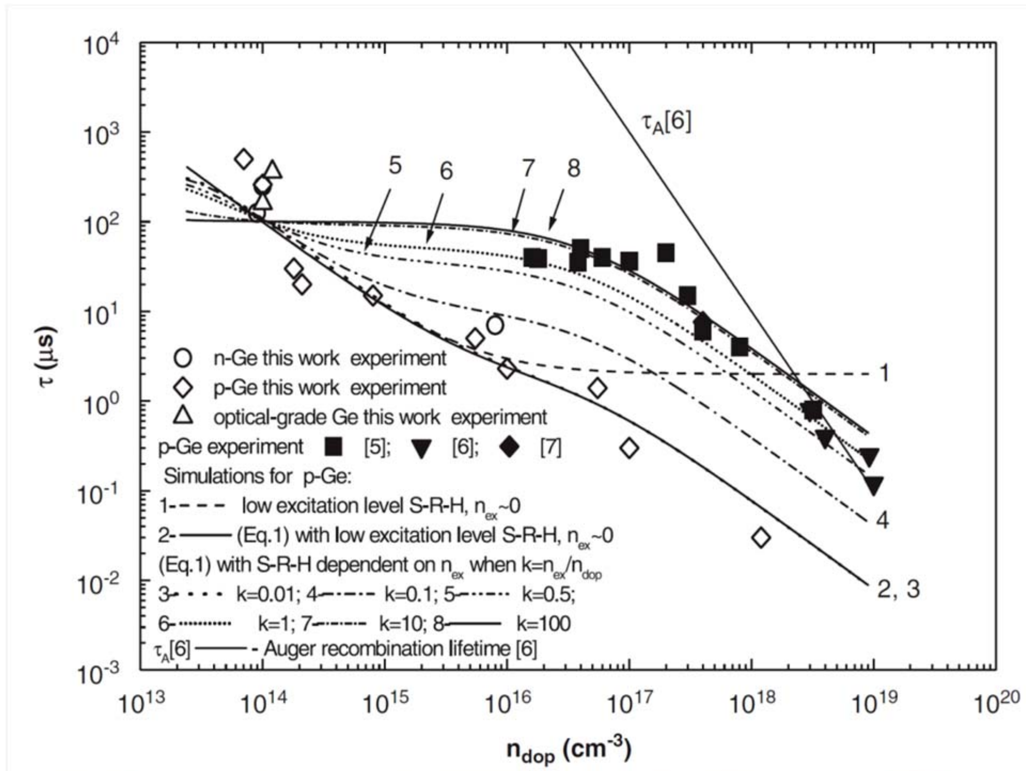

Fig. 2-11 Variation of recombination lifetime versus effective dopant concentration[18]**.**

2.4 Conclusion

At the beginning of this chapter, we overviewed physical mechanisms behind dark current in a germanium photodiode. Section 2.2 describes the structure of germanium photodiode used in this thesis, and the temperature dependence measurement method. Severe parasitic leakage was observed on many devices. Due to this yield issue, a meaningful analysis could only be performed on well-chosen devices.

Subsequently, in section 2.3, we show the investigation of dark current in germanium photodiode via experimental data.

Firstly, from the analysis of activation energy, when the bias is small, the average dark current over -10°C to 125°C is diffusion current; as bias gets more reversed, it would subject to SRH process. Secondly, it can be verified that dark current is in the combination behavior of diffusion current and SRH generation current. At room temperature, and at the bias -0.5V, SRH generation is the main component in dark current. There is a good qualitative agreement between formula trend and measured data. Thirdly, from a rough estimate of carrier lifetime, equivalent trap densities of our best samples are estimated to be around 1E19/cm^3.This will be more precisely estimated in Chap 3.

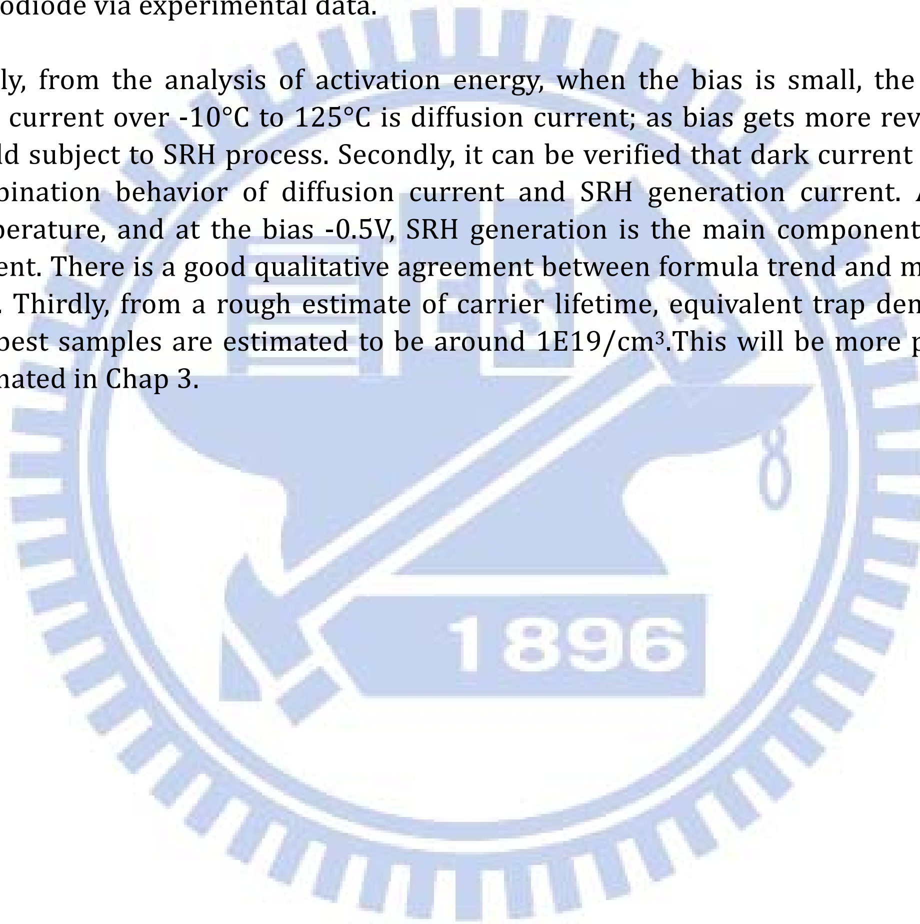

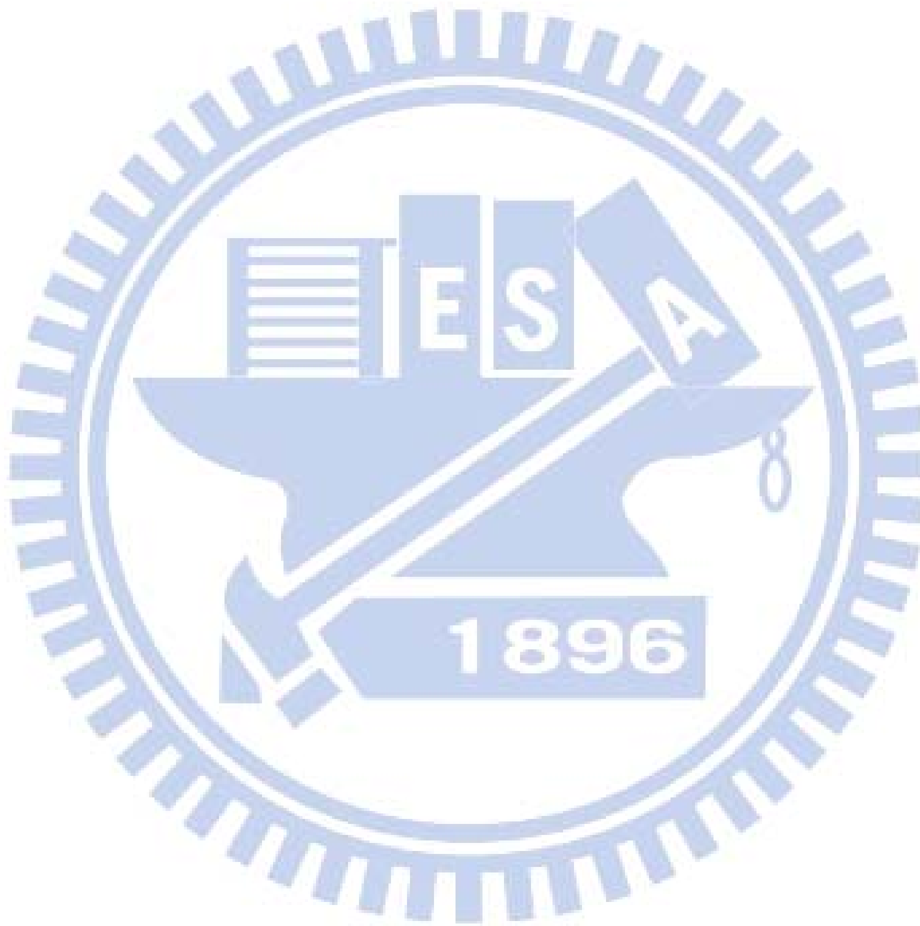
ESA
1896

Chapter 3 Dark Current in Germanium photodiodes: TCAD simulation

In the previous chapter we concluded that diffusion and SRH generation current are mainly the leakage sources of germanium photodiode. In this chapter, TCAD simulation is involved. This chapter starts with an overview of models that are used in our simulation, and the base structure we build in TCAD, finally we make alteration in the base structure and show an optimum structure that has minimum dark current.

3.1 TCAD Models

3.1.1Default Models in TCAD (including Diffusion)

Physical models used to simulate germanium photodiode are presented. Diffusion current can be treated as the intrinsic behavior of semiconductor. It is standardly activated in the TCAD simulator.

3.1.2 SRH: The Shockley-Read-Hall Model

As mentioned in Chapter 2, SRH model describes recombination/generation through deep-level defects in the semiconductor bandgap. The position of the dominating trap level in the bandgap is assumed at midgap energy level (0.33 eV) for Ge[19]. Basically, an expression of SRH is used in terms of minority carrier lifetimes (τ_n and τ_p), dependent on the local defect concentration.

3.2 Base structure formed in TCAD

The ultimate purpose of this thesis is to find an optimized structure of germanium photodiode through simulation, so it is important to get a base structure which is close to the measured diode, including similar geometry and effective defect density, and then we can utilize this base structure to simulate the currents of photodiodes with alteration. The inclusion of TCAD enables us to get the approximate form of defect density in the measured samples.

To form a base structure, the fabrication flow which is identical to experimental samples is simulated via TCAD sprocess tool, and the final simulated structure is shown in Fig. 3-1. Contacts are simulated as ideal ohmic contact, and in Fig. 3-1 they are shown in boundary only. Note that simulations are done in a two-dimensional GePD, so the current from electrical characteristic simulation is given by Ampere per μm (A/μm). That is, in simulation, the length of germanium (LGe) is always considered as 1 μm, only in Section 5.2 we would alter LGe to see the effects happen in length direction.

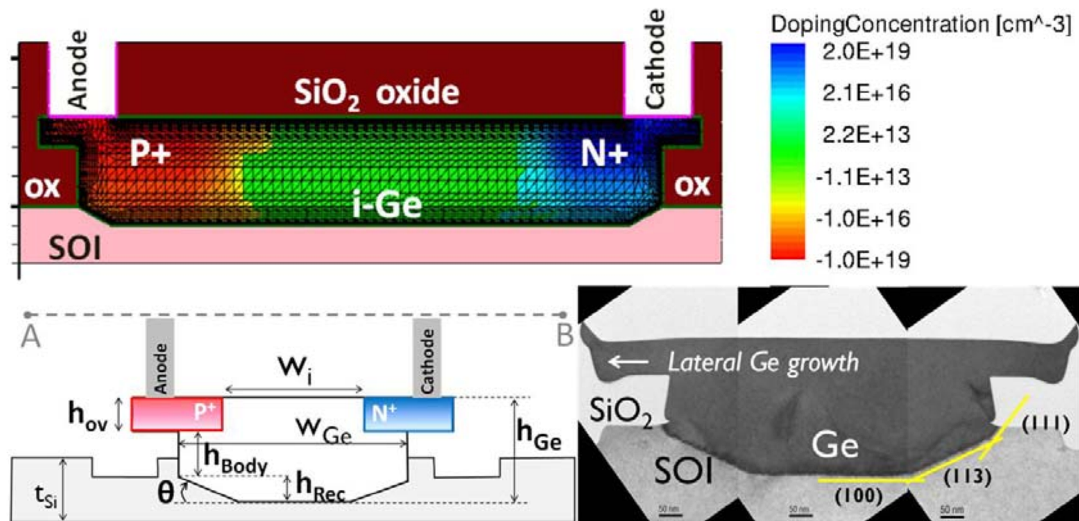

Fig. 3-1 Simulated structure of germanium photodiode in TCAD, showing dopant profiles, meshing.

In order to estimate the defect density inside germanium photodiodes, a constant defect distribution is introduced into simulator. That is, we build up a simulated germanium photodiode in which defects are uniformly distributed. Subsequently, a defect concentration is chosen to achieve a good agreement with measurements of the dark reverse current.

On the other hand, since dislocations are mostly generated at Si/Ge interface, and tend to annihilate as the epitaxial film thickens[5], we also introduce an exponential defect profile into another branch of simulation, by assuming that defect concentration is spatially peaked at the hetero-interface, and exponentially decayed as retreat away from the interface.

Fig. 3-2 shows the simulation structure of GePD with defects distributed in exponential profile and constant profile. Experimental data is also normalized to the length of GePD to make it comparable with electrical stimulation.

Fig. 3-3shows that simulation (black line) result fits nicely with experimental data (red open symbols) for the most part of reverse bias range. The density which fits best with measurement data is equal to 5e18/cm^3 for constant defect profile, and 1e20/cm^3 for exponential defect peak value.

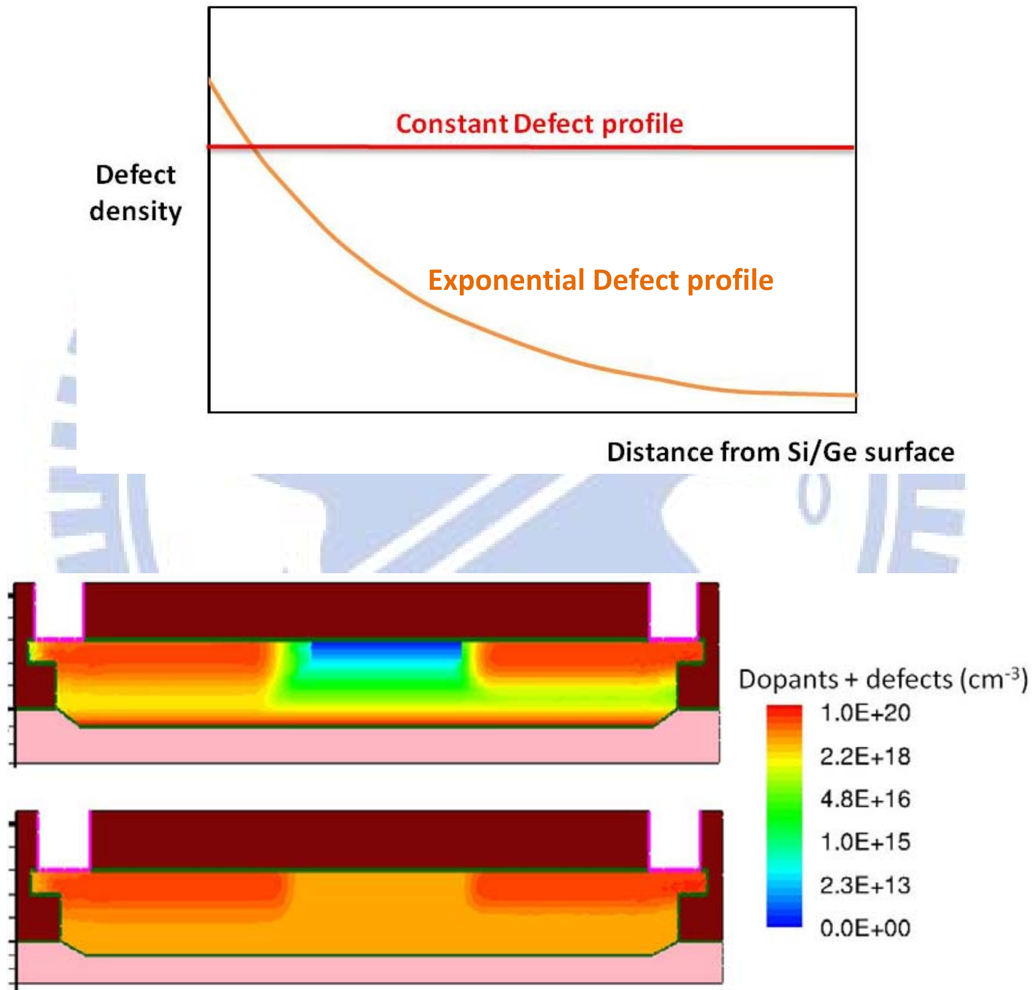

Fig. 3-2 Simulated structure with exponential (top) and constant (bottom) defect distribution profile.

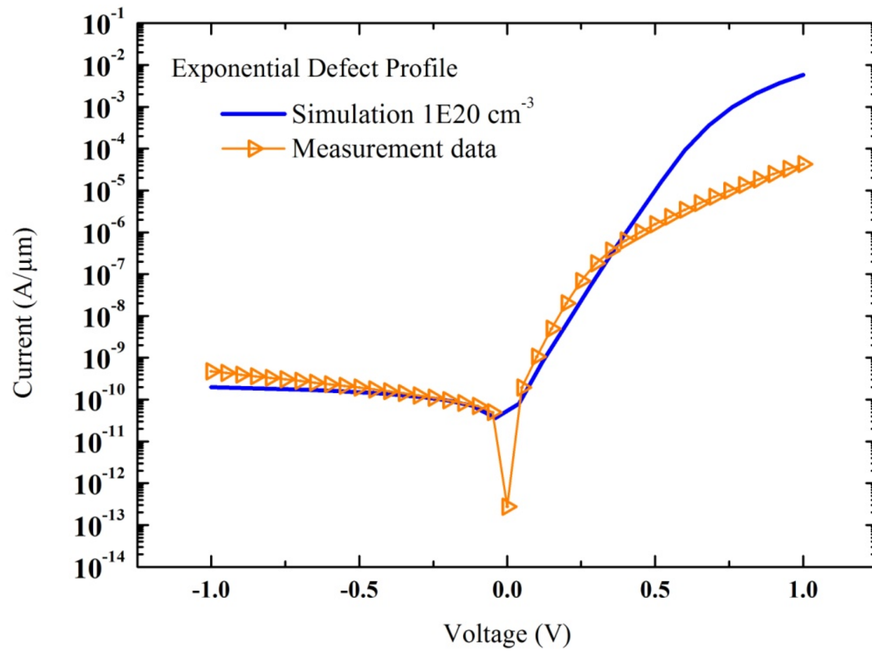

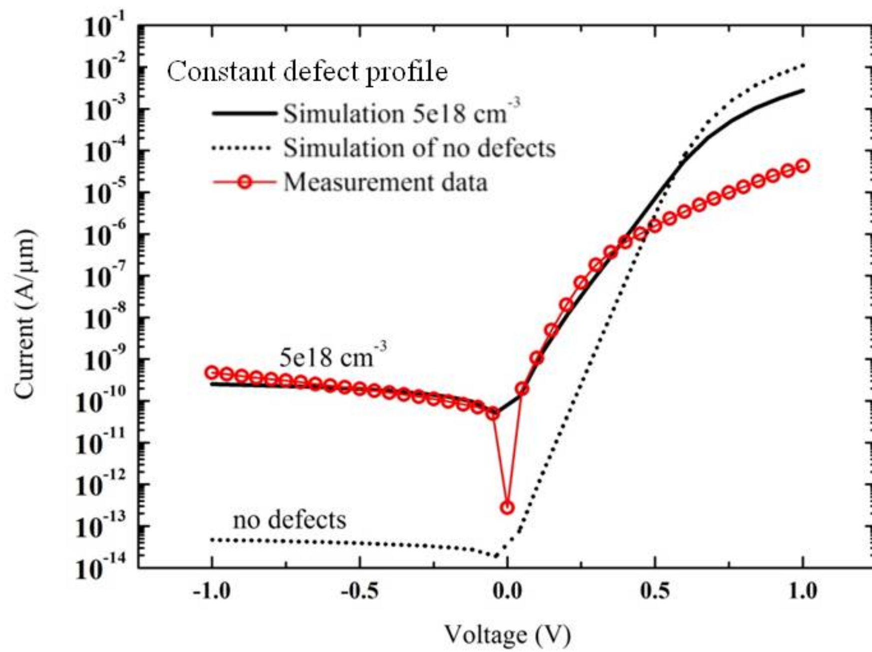

Fig. 3-3 Dark current experiment data and results of Exponential defect profile (Top) simulation and constant defect profile (bottom) simulation.

Furthermore, consistency not only shows up in the reverse region, it also shows in the forward bias region by examining forward swing. A split of diodes with different defect density has been simulated, and their forward swing behavior is shown in Fig. 3-4. Swing of experimental data is also calculated from measured I-V curves (solid symbols), and it could be seen that experimental data and simulation results are on the same level at the defect density corresponding to the one we obtained from reverse dark current simulation, 5e18 cm^{-3}. Consistency shows up in two sets of samples. This means defect density acquired from simulation is quite reliable.

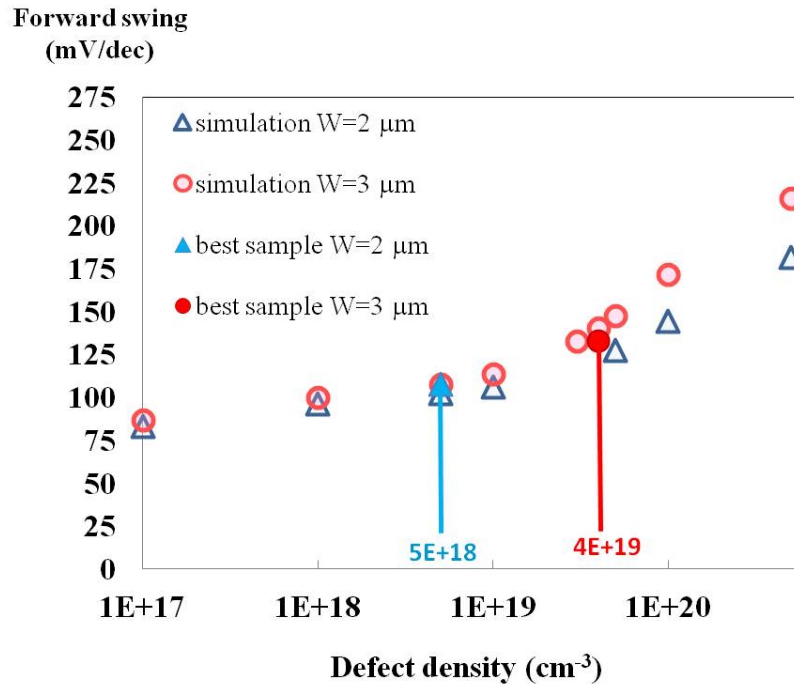

Fig. 3-4 Defect determined forward swing behavior indicated accuracy of the defect density level acquired from simulation of dark current.

To summarized, we have estimated the defect density of germanium photodiode via TCAD simulation tool. For constant defect profile assumption, defects are uniformly distributed with 5e18/cm^3 concentration. For exponential defect profile assumption, defects have a peak value 1e20/cm^3at the interface of Si/Ge, and exponentially decay towards top surface.

The result is found reliable because the fitting of simulated value and experimental data are well in dark current and forward swing. The following section, we will see the simulations based on these two structures.

3.3TCAD Optimization of Dark Current

3.3.1 Alterations in thickness

This section describe show we alter the base structure of germanium photodiode obtained in last section, and the results of how is the dark current affected by the modification. Note that in following sections including this one, simulations will be only performed on the base structure with **exponential defect profile**, which is more physically sensible.

The terms that are frequently used are in table 2-1 and Fig. 2-4. (Show again for convenience).

Terms	**Meanings**
hGe	Total thickness of Germanium diode (=hov+hBody+hRec)
hBody	Thickness of Germanium body
hov	Thickness of overlap
hRec	Recession depth (= Si etched-back thickness)
wGe	Width of Germanium diode
Wi	Doping separation; Width of intrinsic region
θ	Tapered angle formed when silicon etch-back process
tSi	Thickness of silicon

Table 2-1 Structural parameter of GePD.

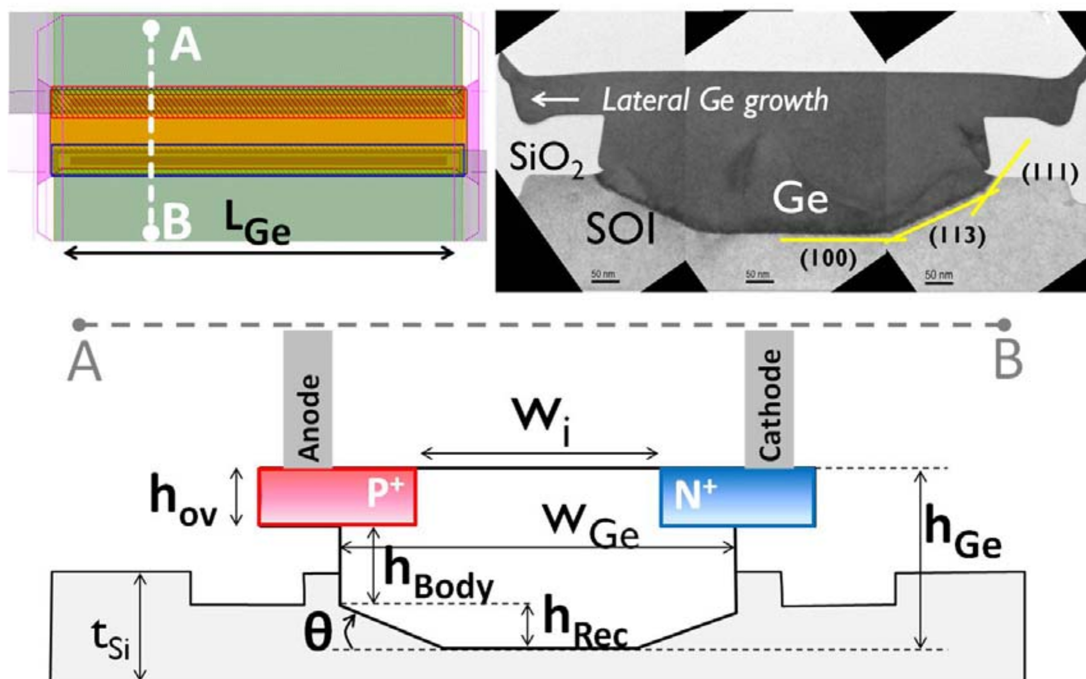

Fig . 2-4 Structure of germanium photodiode.

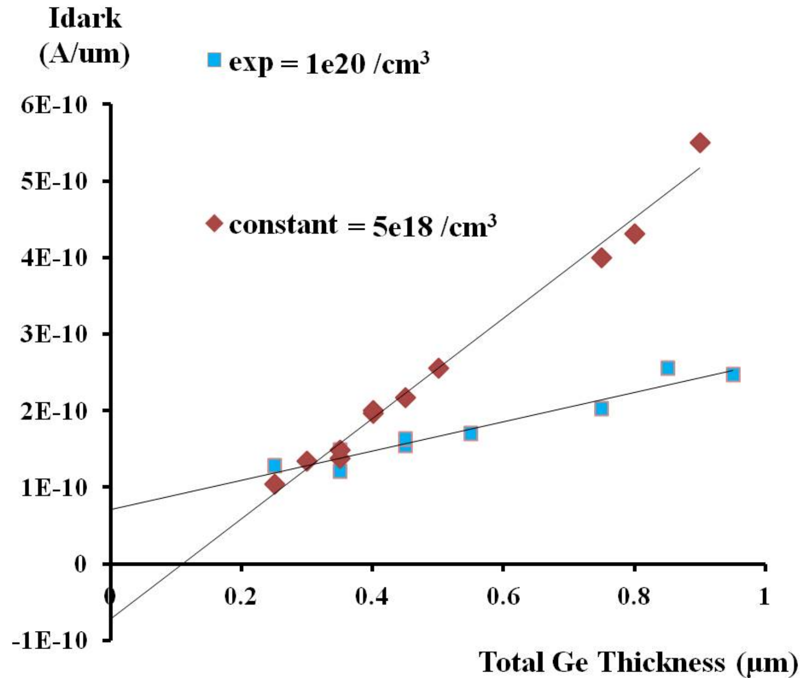

Fig. 3-5 Simulated dark current as a function of Total Ge thickness.

In the simulation of defects uniformly distributed in Ge layer with constant density, a linear dependence between dark current at -0.52 volt and total Ge thickness is seen. This is because with thicker Ge layer, the number of uniformly distributed defects also increases, which results in more carriers generated through defects.

First, h_{Body}, h_{ov} and h_{Rec} are altered, while holding doping energy, doping concentration and doping separation (Wi) fixed. Results show in Fig. 3-5. In Fig. 3-5, we can see that for both constant and exponential case, dark current merely changed by a little amount as hBody, hov and hRec are altered; there are no huge difference as long as the total thickness of germanium is the same, i.e. $h_{Ge}=h_{Rec}+h_{Body}+h_{ov}$ is the same. In other words, what really affects dark current is the total thickness of germanium, not the three individual parameters.

Besides, the slope of exponential defect profile data-set is apparently smaller than the slope constant defect profile; however, two of them increase as germanium gets thicker. This is can be explained by that with larger thickness, the number of traps increases since the volume of germanium increases, so there are more SRH generation happen in that diode.

As for the reason that current grows slower in the diode with exponential defect profile, it can be seen in Fig. 3-6, which shows that trap number is less in exponential density profile as hGe is over 0.6 μm.

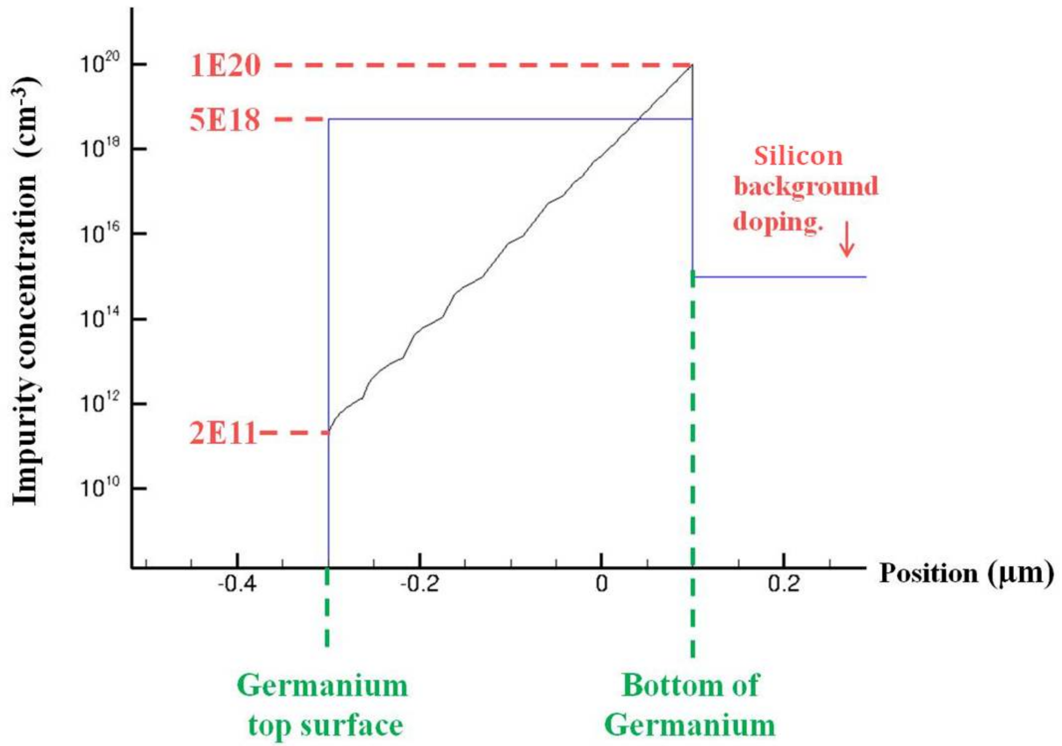

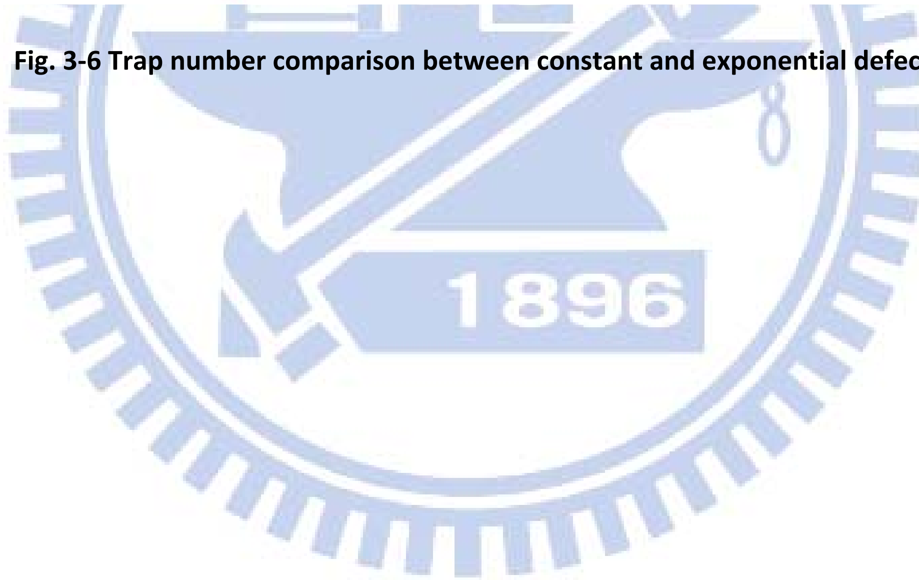

Fig. 3-6 Trap number comparison between constant and exponential defects.

3.3.2 Alterations in width

As to alterations in width parameters, the effects of width of germanium body (wGe) and doping separation (Wi) on dark current are discussed in this section.

In Fig. 3-7, it shows effects of width of germanium on dark currents in devices with three different thicknesses, while holding Wi and other parameters fixed. A trend can be seen that dark current is lower as wGe is at around 3 μm to 4 μm for each thickness.

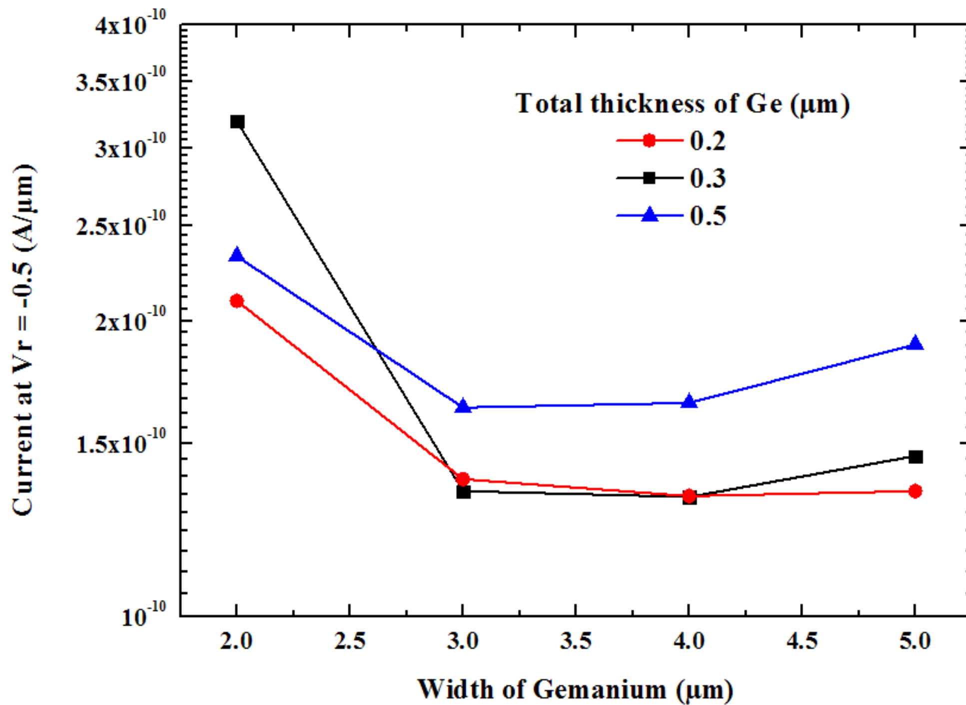

Fig. 3-7 Effects of the width of germanium on dark current.

Fig. 3-8 shows the behavior of dark current corresponding to differing doping separations (Wi). Dark current increases as doping separation gets wider, and the change is much larger than the effect of thickness or width of germanium (wGe).Similar trends show in samples with different thickness. Note that x-axis of Fig. 3-8 is the ratio of Wi over wGe, so that effects of wGe is excluded.

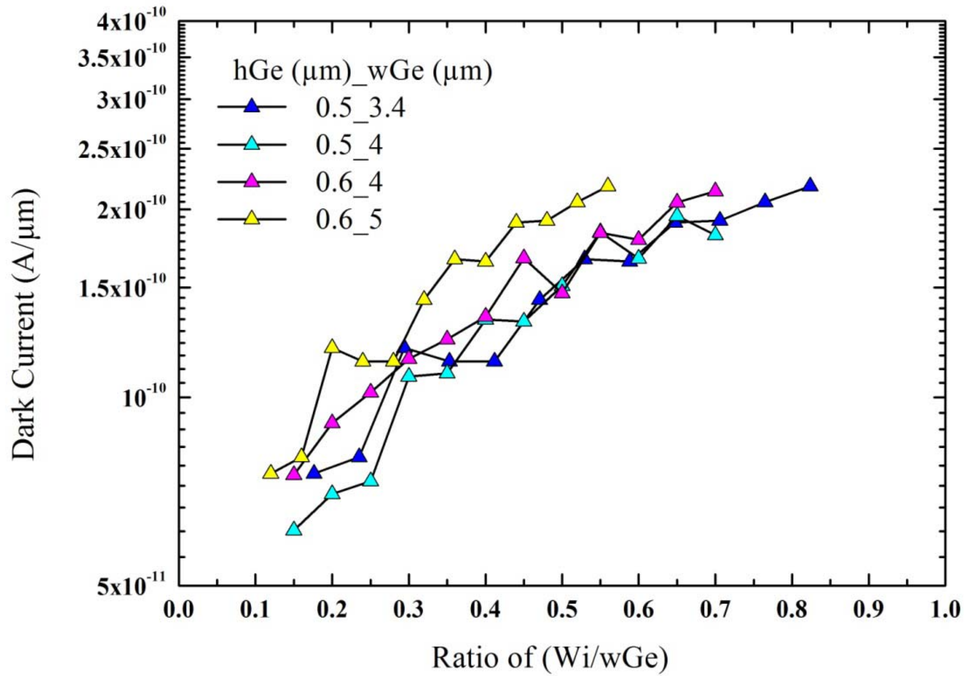

Fig. 3-8Dark current of different diodes versus doping separation ratio.

For a photodiode with fixed wGe, when Wi gets wider, traps in intrinsic region are uncovered by doping regions where carrier concentrations are very high. Although the peak value of electric field decreases as intrinsic region gets wider under same bias (see Fig. 3-9), dark current still ramps up as long as more and more traps are exposed out and located at a rather high field region.

To conclude, the location of traps is critical. When the number of traps that located at large electric field region is increased, not only the generation sites are increased, the generation process becomes more severely as well.

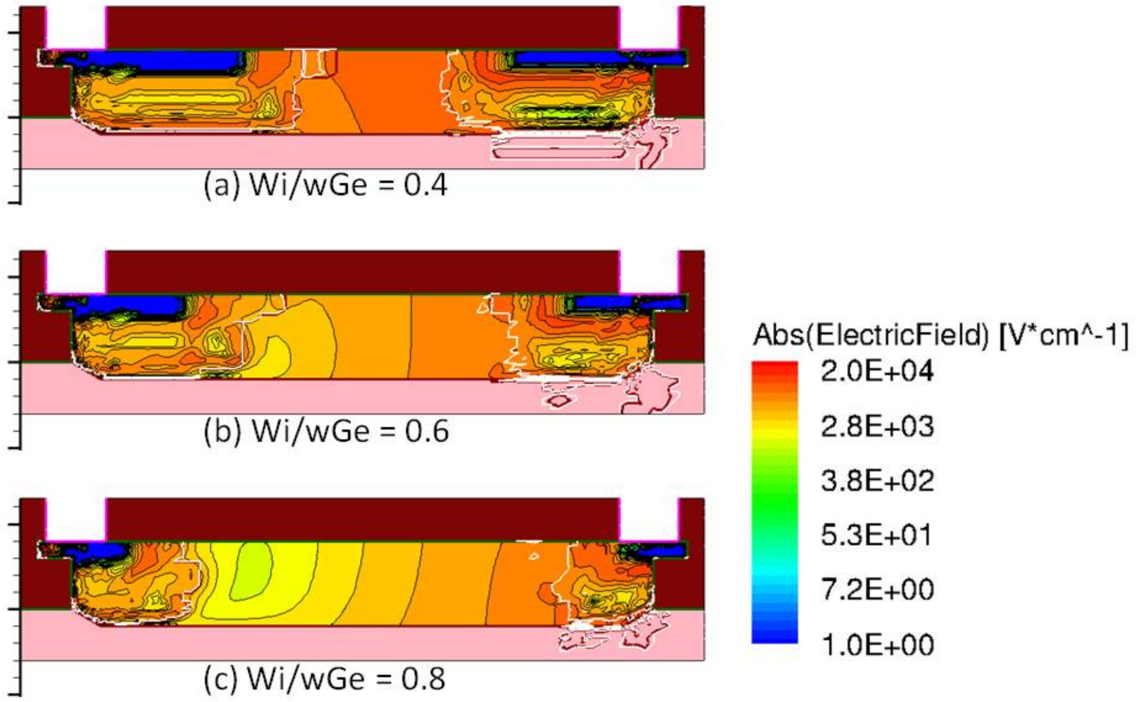

Fig. 3-9 Electric field distribution in diodes with different doping separation.

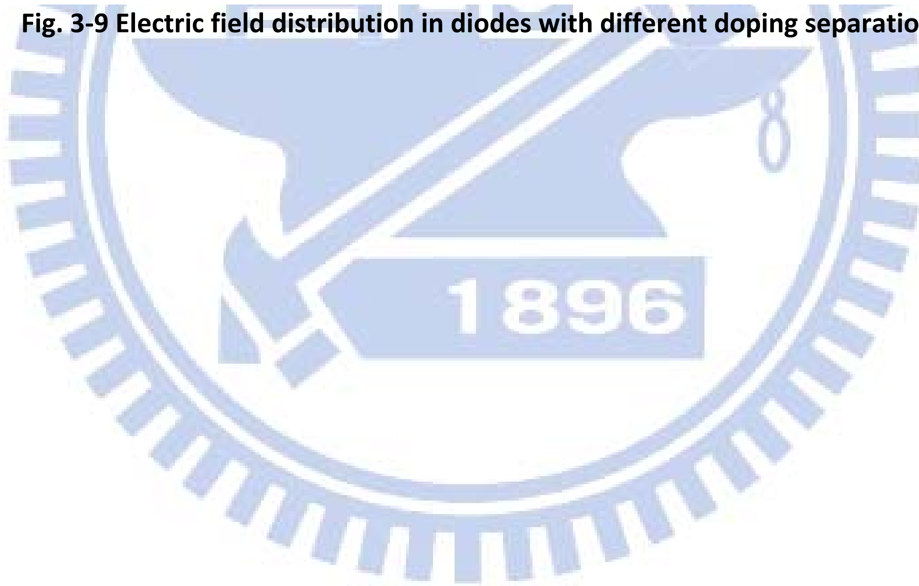

3.3.3 Alterations in implant energy

Implant energy determines junction depth. Fig. 3-10shows dark current of germanium photodiode as a function of implant energy (presented in E/E_0 ratio, where E_0 is the original implant energy). Dark current becomes higher when junctions become shallower. In Fig. 3-11 it can be seen that as junction depth decreases, electric field spreads out more such that it promotes SRH generation process.

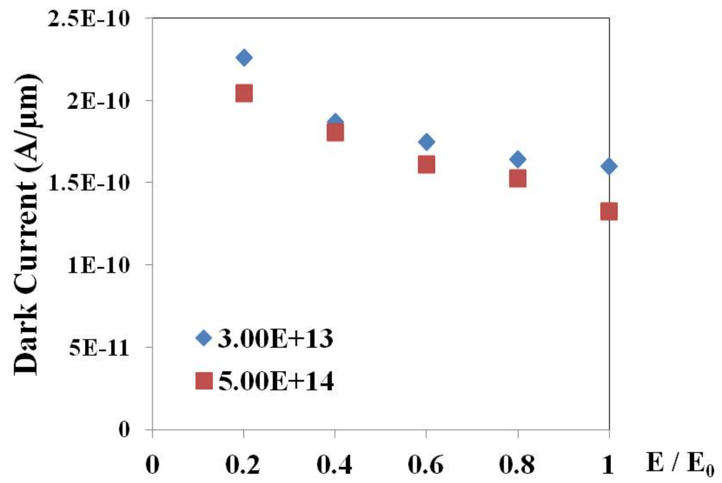

Fig. 3-10 Dark current versus implant energy ratio.

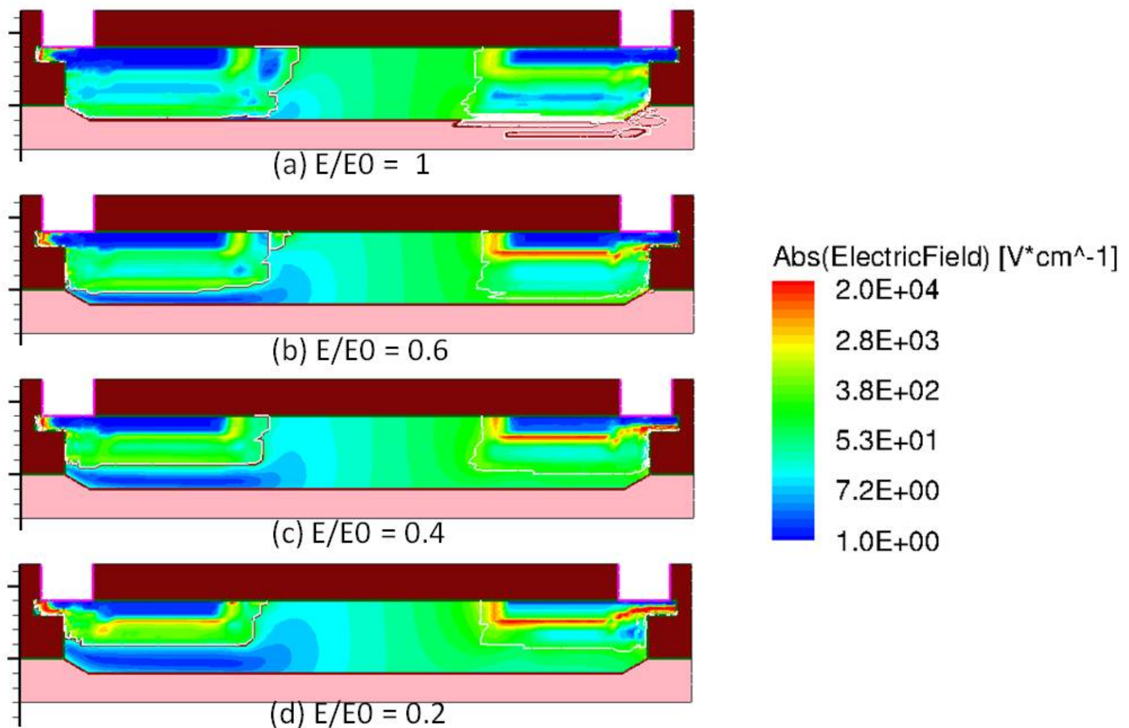

Fig. 3-11 Electric field distribution of diodes with different junction depth

.

3.4 Conclusion

In this chapter, TCAD simulation is involved. In the beginning, models used in our simulation are introduced, including SRH model. Then base structures with estimated defect density are built via TCAD sprocess tool; the estimated defect densities are $5e18/cm^3$ and $1e20/cm^3$ for simulations of constant defect profile and exponential defect profile respectively. Finally we make alteration in the base structure and show an optimum structure that has minimum dark current.

Generally speaking, to make a germanium photodiode with low leakage, a thin germanium layer is required to reduce the SRH volume (number of traps) as much as possible, a narrow doping separation is crucial to keep a small SRH volume within this large electric field region, and finally deep junctions are needed to circumvent the spreading electric field.

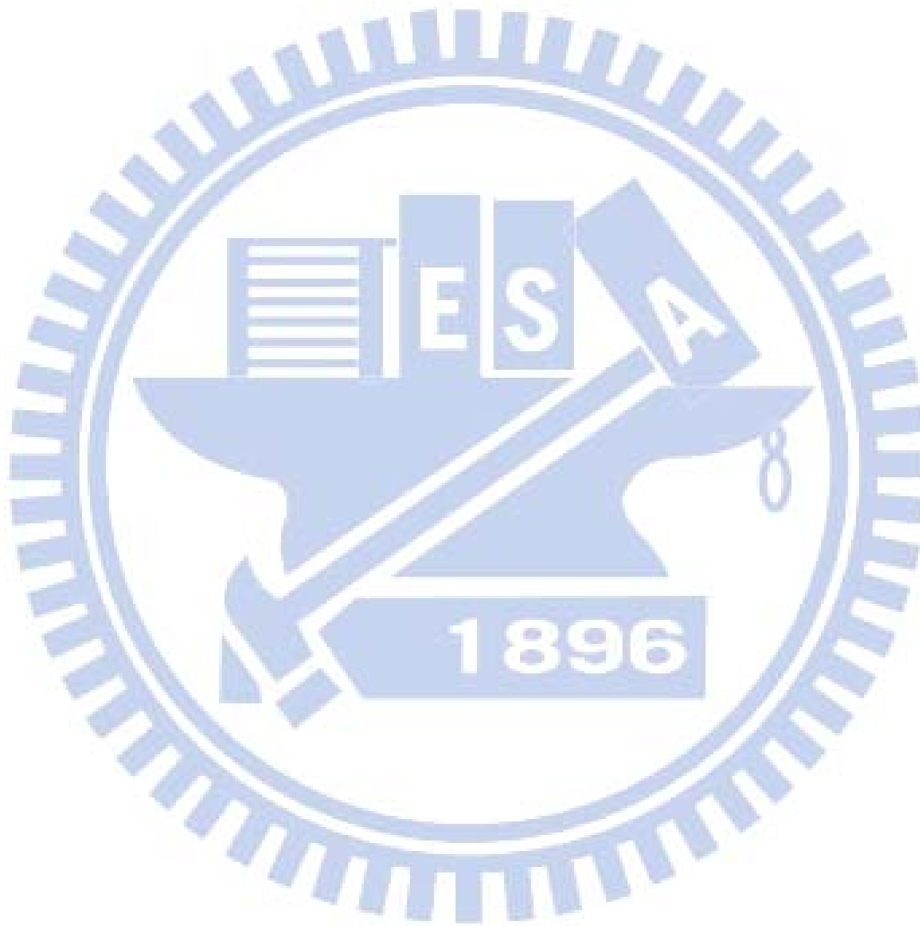

Chapter 4 Quantum Efficiency Optimization

In this chapter, an optical signal in implanted into the base structure obtained in chapter 2 as an input to simulate the illuminated photodiode. Optical generation method and definition of quantum efficiency (QE) are given. And again, we make alteration in the base structure and show an optimum structure that has maximum quantum efficiency.

4.1 Optical Generation and definition of Quantum Efficiency

4.1.1 Optical Generation Method

As shown in Fig. 4-1, a two-dimensional single-mode light intensity distribution of infrared optical signal at 1550 μm inside a two-dimension Germanium structure of 2-μm-wide and 0.2-μm-thick was obtained beforehand by using the commercial propagation tool FIMMWAVE by Photon Design (Photon Design, Inc., Oxford, U.K.). FIMMWAVE is a fully vectorial mode finder which provides rigorous solutions to the full Maxwell equations. It can quantitatively simulate the modal behavior and optical properties inside waveguides of arbitrary material and of almost any shape.

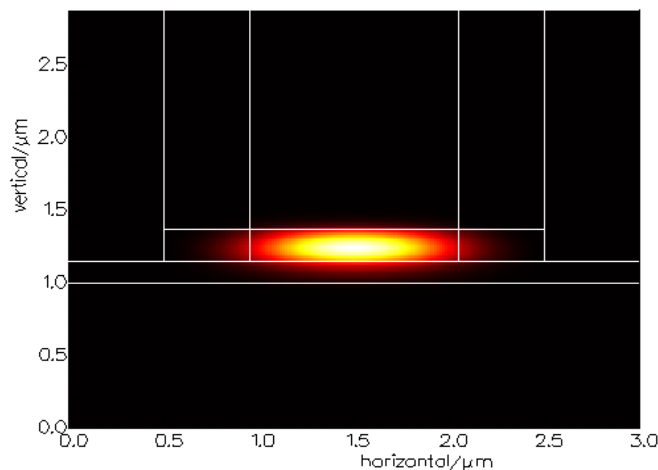

Fig. 4-1 The 2Dsingle-modeinfrared light intensity distribution inside a 2D Germanium structure of 2-μm-wide and 0.2-μm-thick.

From the result obtained by FIMMWAVE, the intensity distribution is found to be a two-dimensional Gaussian form with specific variance (σ_x^2,σ_y^2). Then, optical command codes expressed by two-dimensional Gaussian are added in TCAD simulator (codes in appendix) to mimic one photon in GePD. and the number we use in the following optimization simulations is 1e15 ($cm^{-3}s^{-1}$).Fig. 4-2 shows the illustration of light intensity in 2D Gaussian form and the GePD cross-section after optical signal is plugged in.

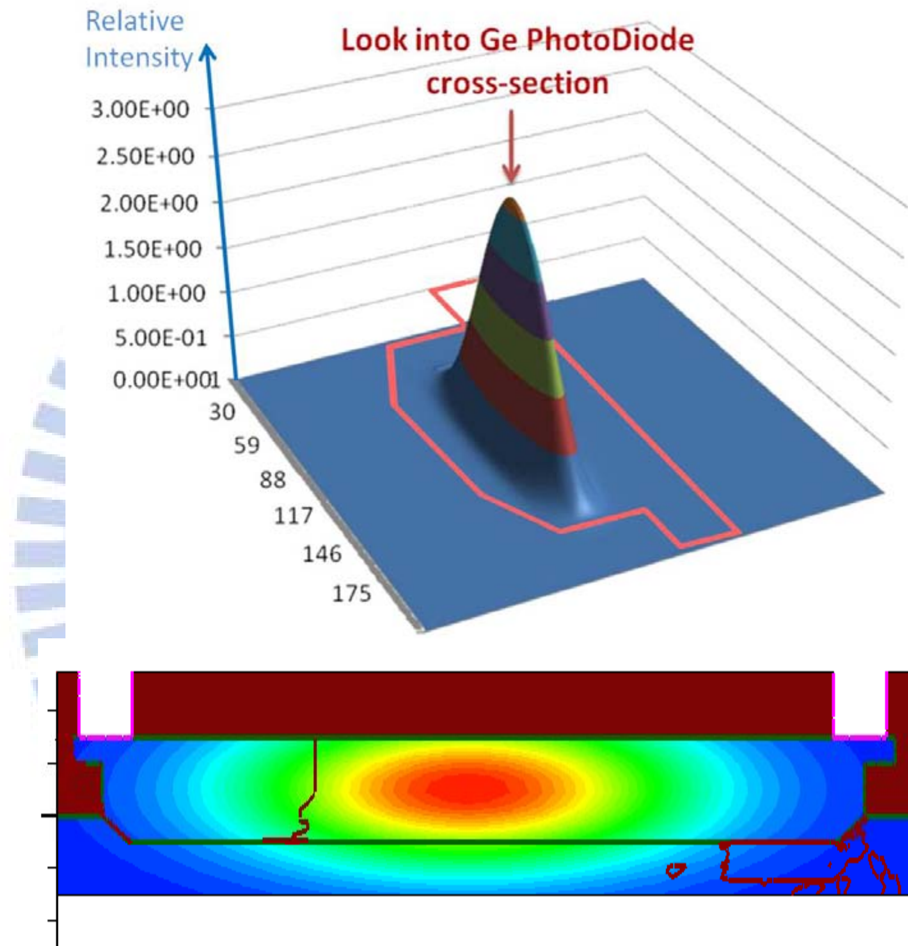

Fig. 4-2 Two-dim Gaussian optical signal in the TCAD simulator.
(Top) Illustration of light intensity in 2D Gaussian form; (bottom) GePD cross-section after optical signal is plugged in.

4.1.2 Definition of Quantum Efficiency (QE)

Quantum Efficiency(QE), or external quantum efficiency (EQE), is defined by the ratio to the number of incident photons of a given energy over the number of electrons that collected by photodiode, which is shown at Eq. 4-1.The value of quantum efficiency indicates the ability of a photodiode to transfer optical signal into electrical signal and collect them.

$$\mathrm{EQE} = \frac{\text{number of electrons/sec}}{\text{number of photons/sec}} \qquad \textbf{Eq. 4-1}$$

Another type of quantum efficiency is internal quantum efficiency (IQE), which is not used in the evaluation of our simulated photodiodes. The value IQE indicates the photon transmission ability of photodiodes, which is not the issue concerned in this thesis.

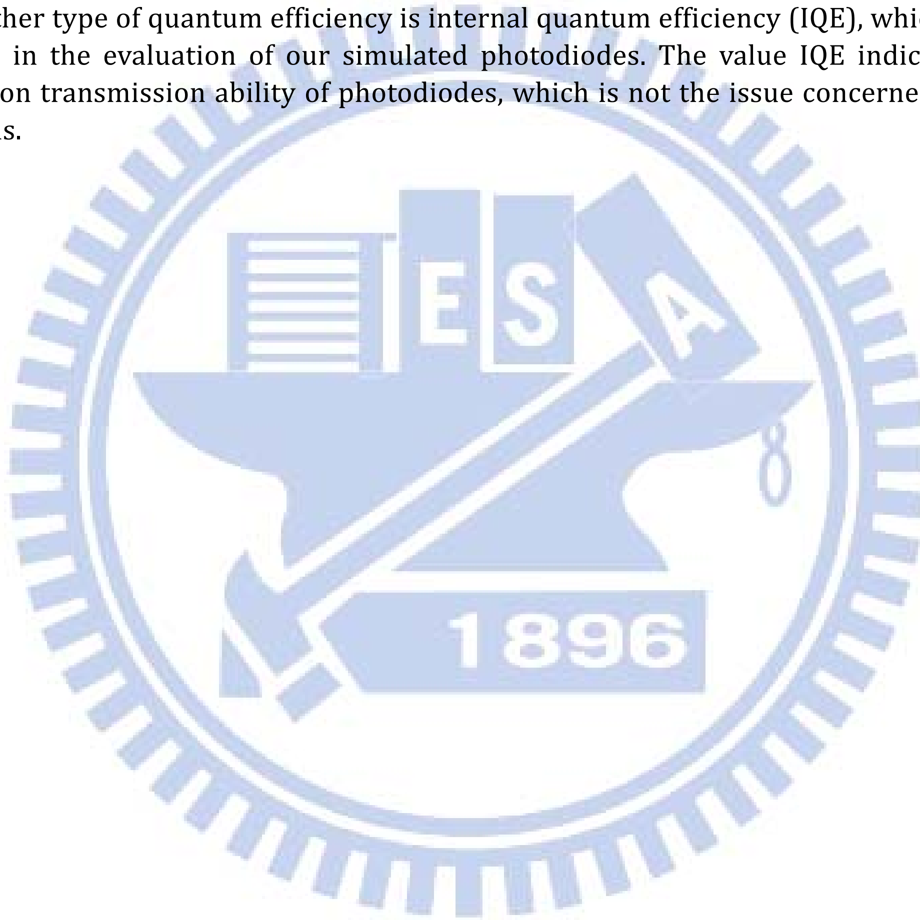

4.2 QE in respect of Structural parameters

Alterations are done mainly in total thickness of germanium, width of germanium, and the doping separation.

4.2.1 QE dependence on thickness and width of GePD

In Fig. 4-3, light distribution in photodiodes with various geometries is shown. One can see in small GePD, light intensity concentrates in the middle of the photodiode, where electric field is the largest. This is beneficial because the generated carriers can be quickly swept to electrodes by the strong electric field before they recombine. However, there are also lost of lights since some of lights distribute into oxide and silicon. And in the case of wide devices, light distribution broadens out, so averagely the number of carriers generated by photons that experience large force is reduced.

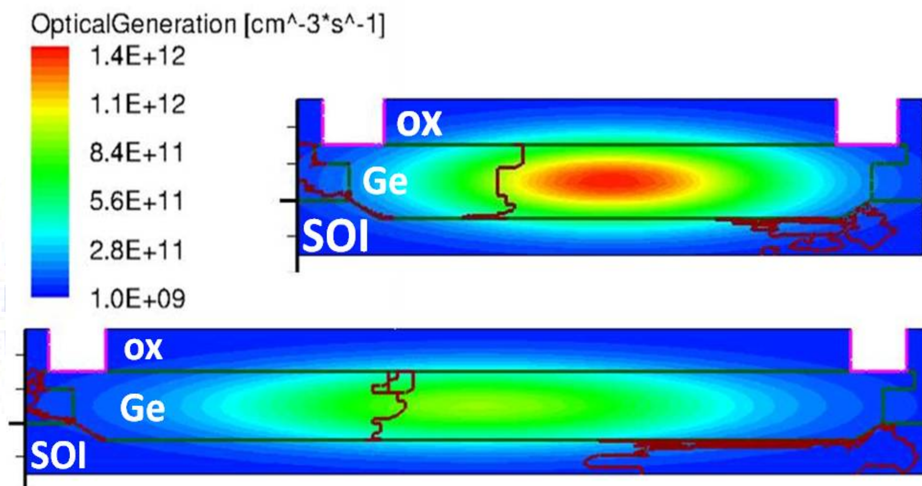

Fig. 4-3 Light distribution in photodiodes with different width and thickness.

As a result, we can expect an optimum happen at a specific germanium thickness and width. As shown in Fig. 4-4, maximum value happens at thickness of 0.5 μm and total Ge width of 3.4 to 4.5μm.

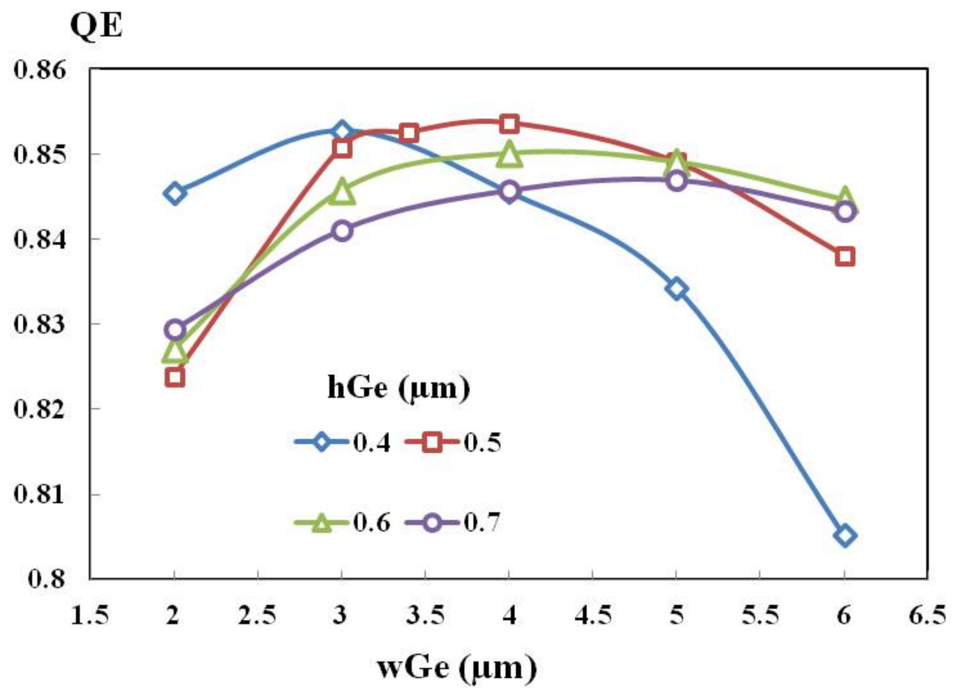

Fig. 4-4 Effects of Ge thickness and width on QE.

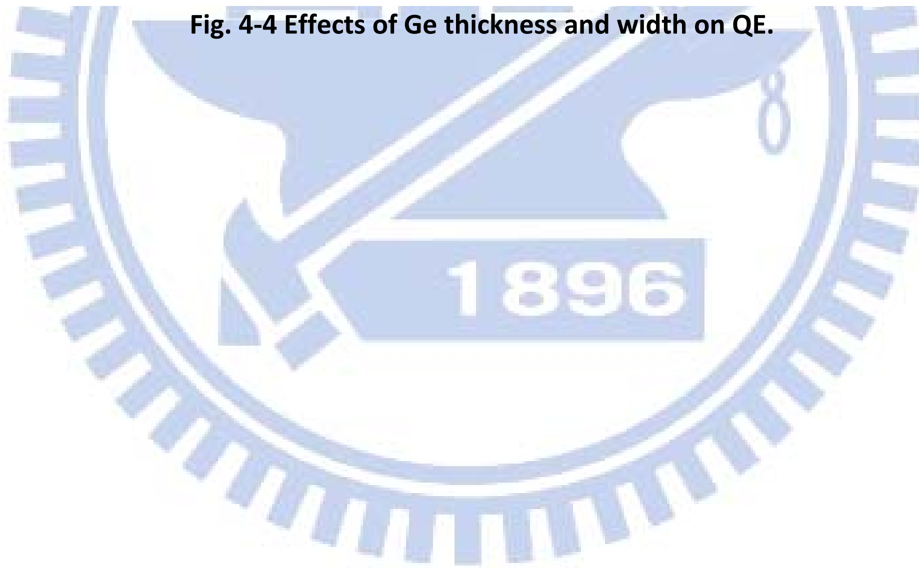

4.2.2 QE dependence on doping separation

In this section, photodiodes including different doping separation (Wi) are simulated with the GePD obtained in previous section that have lights mostly concentrate in the middle, and also be enclosed inside germanium layer. The width of doping separation determines firstly the window that enables electric field to act on generated electrons and holes, and secondly the strength of the electric field.

A large Wi indicates a large window to capture light, nevertheless we have shown in Fig. 3-9(show again below)that electric field decreases as Wi increases. That is, we should make Wi large enough to capture sufficient light, but not so large that electric field becomes too weak to drive electrons and holes to electrodes before they recombine.

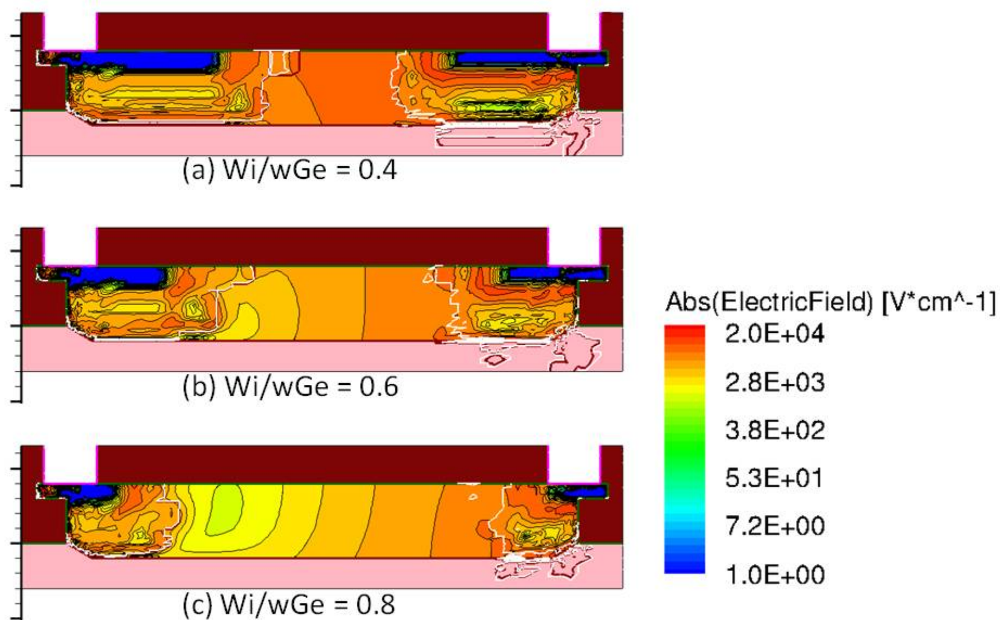

Fig. 3-9 Electric field distribution in diodes with different doping separation.

Fig. 4-5 shows how QE depends on doping separation. It can be seen that quantum efficiency reaches a maximum when Wi is 50% to 60% of the total width of germanium.

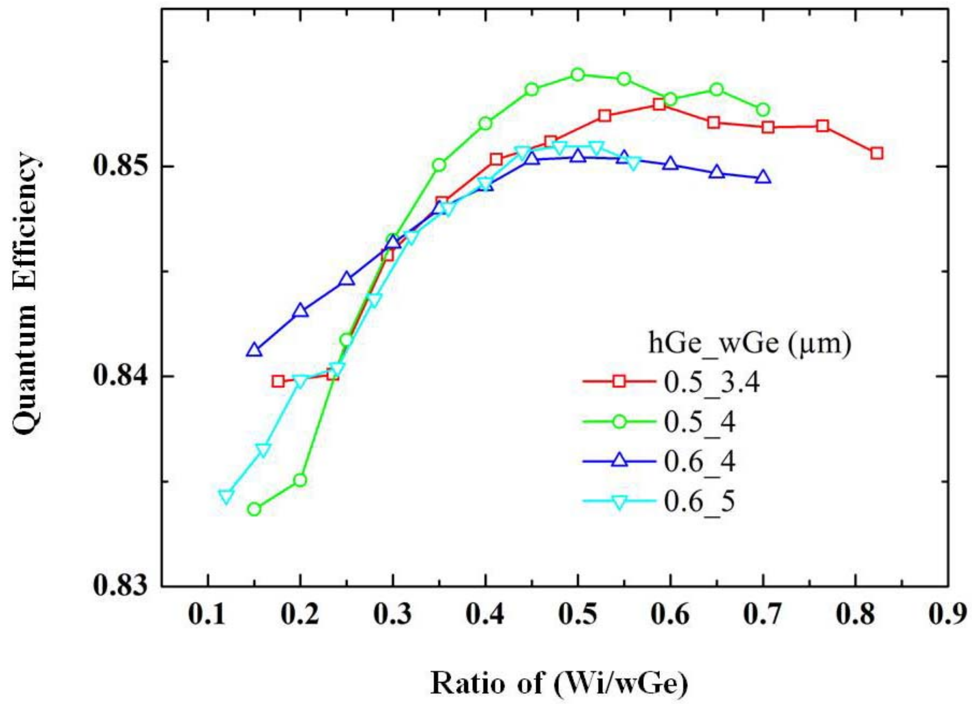

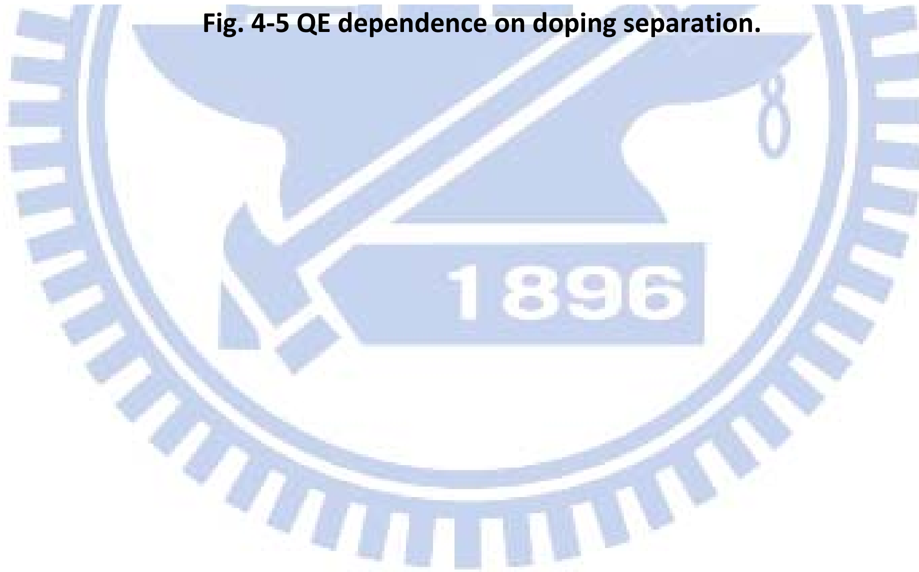

Fig. 4-5 QE dependence on doping separation.

4.3 QE improvement by Junction engineering

From the results of chapter 3 and previous sections in this chapter, one sees there is inevitable trade-off between low dark current and high QE. In this chapter, junctions engineering is performed and attempted to maintain or increase quantum efficiency at the same time keeping dark current at a low level.

To minimizing dark current with a given density of traps, it is important to separate trap locations from where electric field is high. Since traps mostly distribute at the bottom of germanium layer, making junctions shallower seems able to achieve this goal. However previously in Fig. 3-10(would be shown again later) we found that dark current rises as junction depth decreases due to electric field spreads out more in a shallow junction. Fig. 4-6 shows the simulation results of decreasing junction depth using original implantation method, and trade-off is seen between low leakage and high QE.

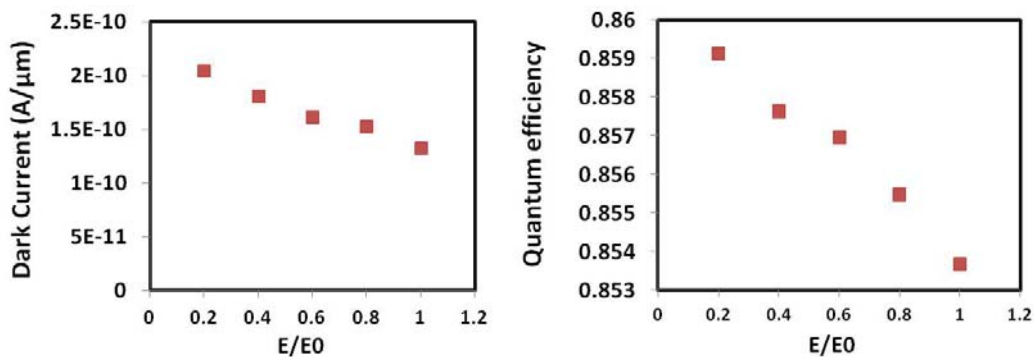

Fig. 4-6Dark current and QE as a function of implant energy.
(E_0 is the original implant energy, E is the variable.)

Consequently, a two-step implantation without extra masks is introduced into simulator, as the first implantation to form a deep junction with small doping concentration, and the second one to form a shallow junction with high doping concentration. The function of deep junction is to screen out the spreading electric field from the shallow junction, while it itself provides very small electric field so that SRH process through traps at the bottom of GePD wouldn't be very strong. Illustration of deep-and-shallow doping and the simulated structure with E/E_0 =0.2 are in Fig. 4-7.

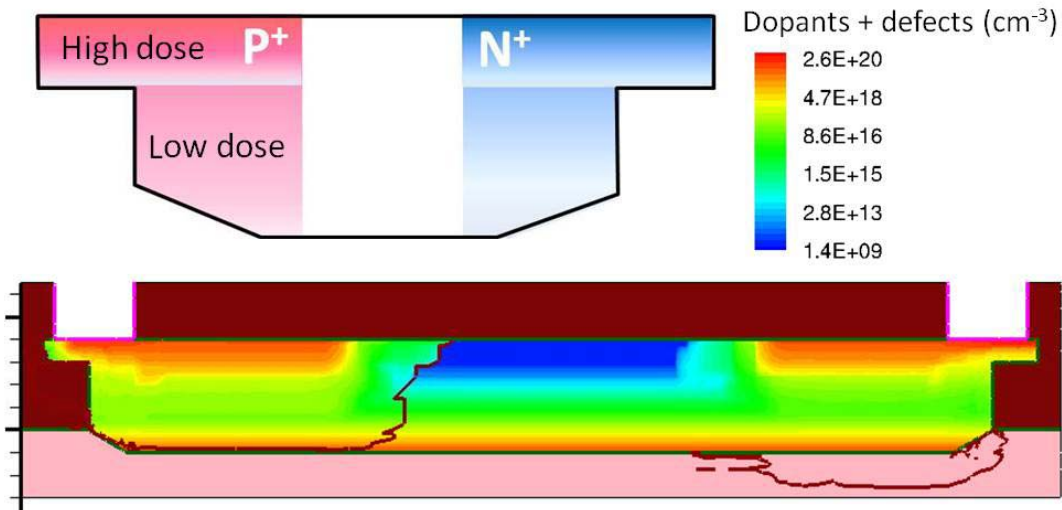

Fig. 4-7 Deep junctions and shallow junctions.

Results of simulation of deep-and-shallow junctions are in the following. Fig. 4-8 shows dark current and QE as a function of shallow doping dosages, and a set of curves differing by deep doping dosage is presented. Shallow doping concentration can be as heavy as activation maximum (for germanium is approximately $1e19/cm^3$), since high QE is achieved without promoting dark current. Dark current is suppressed compared to that of structure without the second step deep doping, and implantation dose of $3e13/cm^2$is chosen to be the optimum doping concentration for deep junction. Doses as low as $5e12/cm^2$ for deep doping cannot sufficiently screen out the electric fields form shallow junctions, and deep junctions with doses larger than$3e13/cm^2$might provide its own electric field and resulted in dark current rising, such as the behavior of devices with $5e13/cm^2$(red line with square).

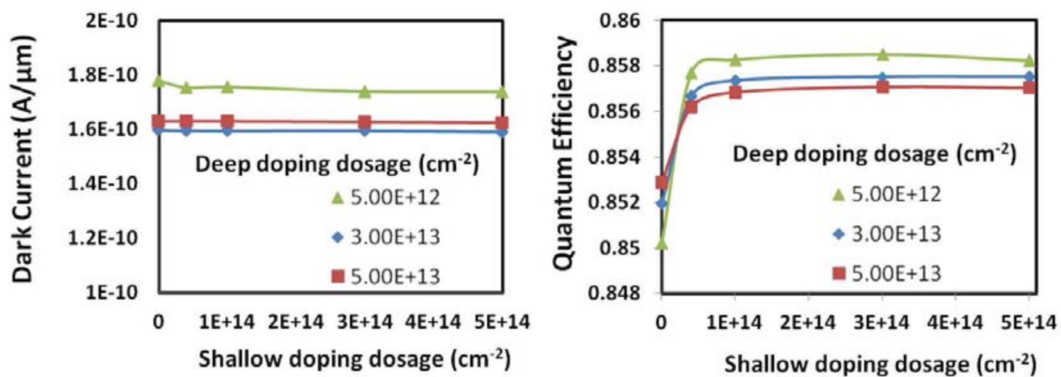

Fig. 4-8 Effects of deep-and-shallow junctions on dark current and QE.

4.4 Conclusion

Here in chapter 4, we start to simulate the photocurrent of GePD with optical signals. Optical signal is generated by putting the Gaussian form calculated by waveguide modal solver.

To have high quantum efficiency, we have an optimum with the width of germanium equals to 3.4 μm, the thickness of germanium equals to 0.5 μm, and the doping separation equals to half of the width, that is 1.7 μm.

To maintain high quantum efficiency while keeping low level of dark current, deep-and-shallow junction is proposed. Deep junction is doped slightly $3e13/cm^2$ to suppress dark current, and shallow junction is degenerately doped to prompt photo currents.

The optimum structure is shown in Fig. 4-9, where the color legend is for dopants and defect concentration, and round contours is illustrating the optical signal inside GePD.

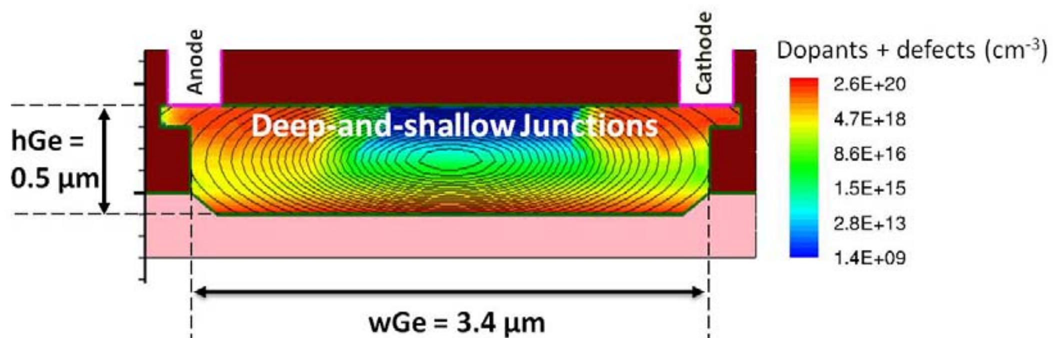

Fig. 4-9 The optimum structure for low dark current and high QE.

Chapter 5 Transient Response Optimization

In this chapter, the transient respond of photodiode to an optical pulse signal is presented, and the parasitic capacitance of our simulated photodiode without optical signal is obtained by C-V simulation. In the following sections, an equivalent circuit of GePD is given, the issue of the length of the photodiode is discussed, and finally frequency response of simulated photodiode is shown respectively.

5.1 The Role of Transient Response

The significant growth in computer processing power due to microelectronics scaling requires a corresponding increase in communication bandwidth. For on-chip applications, detectors with very small capacitance and high speed are crucial for low power, large bandwidth systems[17].

To estimate the transient behavior intrinsically from GePD device, an optical pulse signal is introduced into the TCAD simulator, while the simulated photodiodes are in the operation point -0.5V. Next we characterize the speed of simulated germanium photodetector in a unit of GHz by calculating the inverse of **Rise Time**, which is defined by: The time required for the response to rise from 10% to 90% of its final value. As shown in Fig. 5-1.

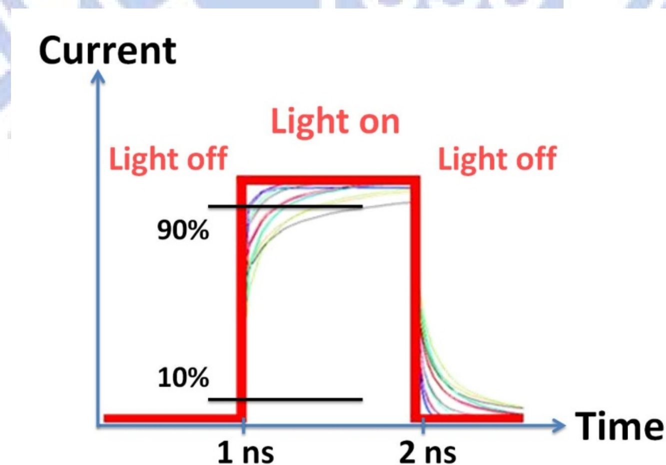

Fig. 5-1 Illustration of rise time definition.

To estimate the input-output transient respond from the system point of view, Fig. 5-2 shows the equivalent circuit of a P-i-N photodiode.

A photodiode is regarded as a current source with parasitic leakage resistance and junction capacitance, and parasitic capacitance, resistance and inductance of interconnect would also contribute to RC time delay. As I_{ph} is changing with the AC optical signal, the voltage–drop across is R_S also changing, and this leads to the charging/discharging behavior of C_{PD} and C_P.The ultimate goal is to acquire an equivalent circuit model of GePD, and after seeing the intrinsic speed of GePDs with different geometry in section 5.2, the value of component C_{PD} is obtained from C-V simulation in section 5.3.

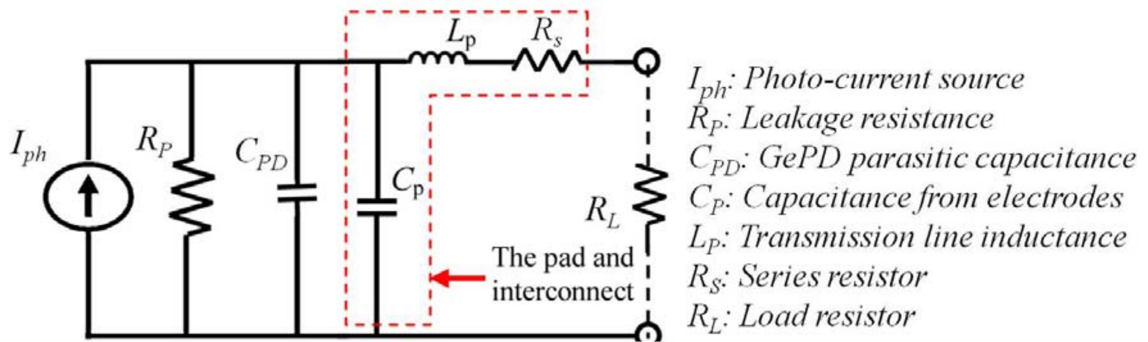

Fig. 5-2 Effective circuit of a PIN photodiode[20][21].

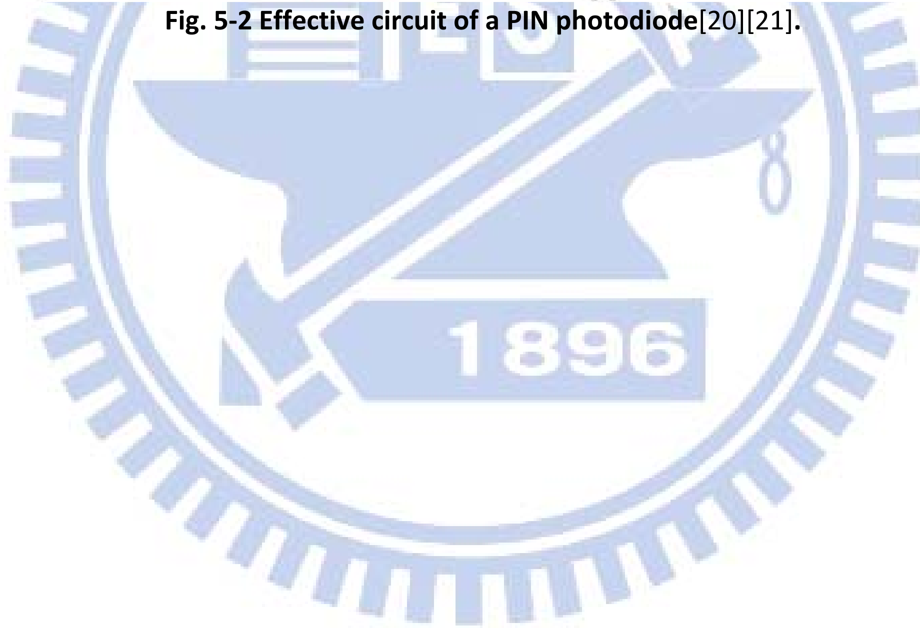

5.2Speed in respect of structural parameters

In this section, the effects of doping separation (Wi) and width of germanium (wGe) on the photodiode capacitance and speed are discussed.

C-V characteristic simulation is first performed on photodiodes with different Wi and wGe without injecting optical signal. Subsequently, an optical input with pulse width equals to 1 nanosecond is introduced into the electrical characterization section in simulator, and then speed (GHz) is calculated via rise time of the responds corresponding to every device.

Fig. 5-3 shows the C-V characteristics of simulated photodiode with various structures, and one sees from Fig. 5-3 (a) that capacitance increases dramatically as Wi decreases, and from Fig. 5-3 (b) capacitance increases as hGe increases, while wGe plays little role in capacitance. It is quite reasonable when seeing a well-known capacitance formulae Eq. 5-1. (Note that capacitance is in the unit of Farads per μm, because of the two-dimensional simulation)

$$C'(F/\mu m) = \varepsilon_{Ge}\frac{\text{Capacitor Area}}{\text{Capacitor thickness}} = \varepsilon_{Ge}\frac{\text{hGe} \times (\text{LGe} = 1\mu\text{m})}{\text{Wi}} \qquad \textbf{Eq. 5-1}$$

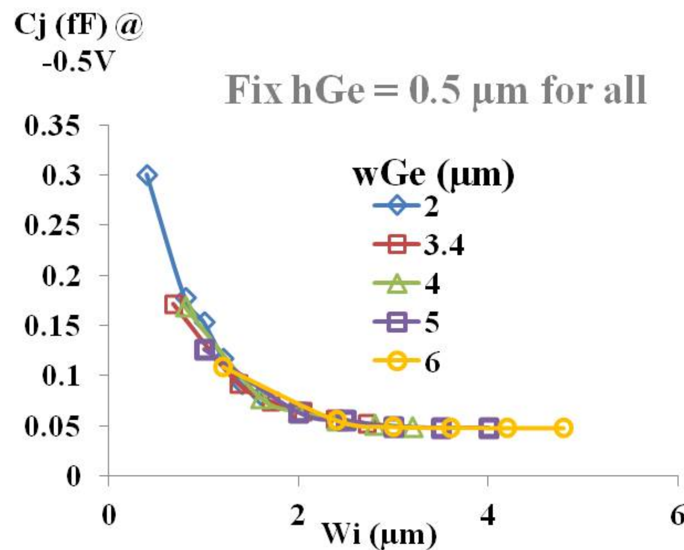

Fig. 5-3(a)

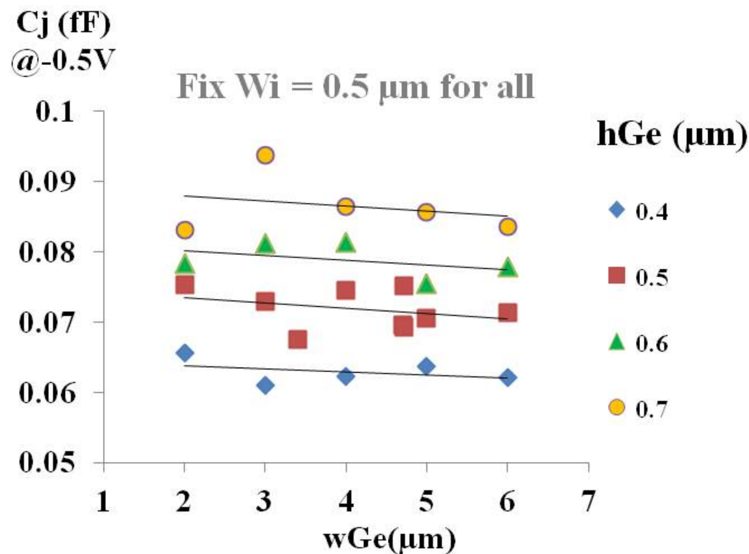

Fig. 5-3(b)

Fig. 5-3 C-V characteristics of simulated photodiode with various structures.

However, in Fig. 5-4speed dependencies on wGe appear to have an inverse linear relation despite the fact that wGe has little contribution to parasitic capacitance. (Note that Wi is fixed). It can be explained by the transition time for carriers to travel to electrodes, since there is a longer distance for electrons that generated in the middle of GePD to be driven to cathode in a rather wide photodiode, vice versa for holes.

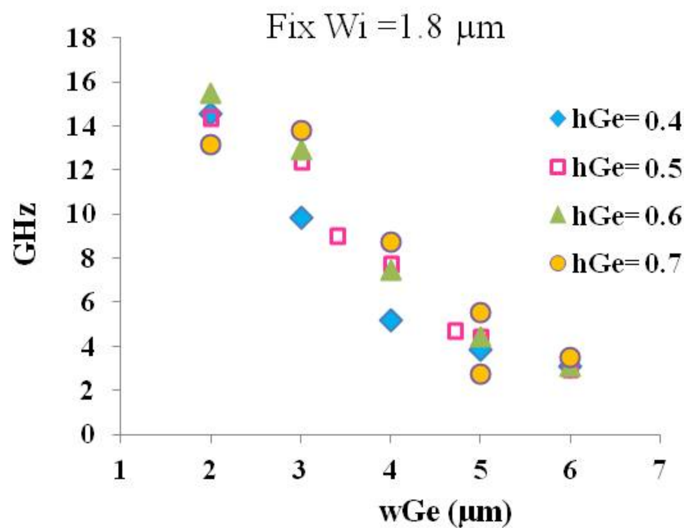

Fig. 5-4 Speed of GePD is inversely proportional to wGe.

In Fig. 5-5, speed above 30GHz is achieved in the device wGe equals to 2 μm, with doping separation equals to 1.2 μm. The photodiode with the structure which provides best quantum efficiency is indicated as well. Speed distribution over doping

separation is pretty sharp, and two machismos competing with each other. At region I, speed is affected by the large junction capacitance when Wi is small, In region II, speed is limited by the transition velocity of carriers since electric field decreases Wi increases.

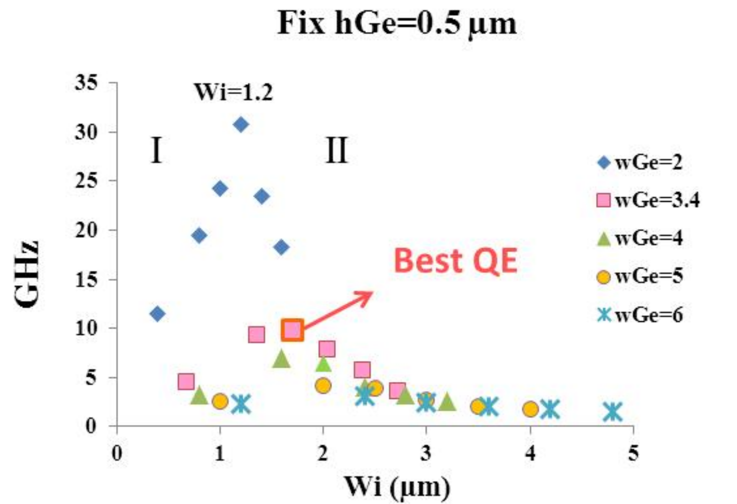

Fig. 5-5.Speed evaluation of GePDs with different Wi and wGe.

5.3 Length effect

In previous chapters, simulations are all done in a two-dimensional germanium photodiode; therefore in this section, we consider the effects of the length (LGe) on photodiode (L is shown inFig. 2-4), including the capacitance and the absorption efficiency of lights in long and short devices.

5.3.1 Capacitance in length direction

First estimation of transient respond of germanium photodiode is required from a system level point of view. To reduce RC delay, the capacitance of germanium photodetector for interconnect system should always be minimized. Fig. 5-6 shows the parasitic capacitance C_{PD} at -0.5V. In the structure of GePD in this thesis, the length of electrodes is approximately same with the length of implant junctions. Since capacitance is increasing with the GePD length, a short germanium photodiode is desirable for both lowering C_{PD} and pad capacitance C_P.

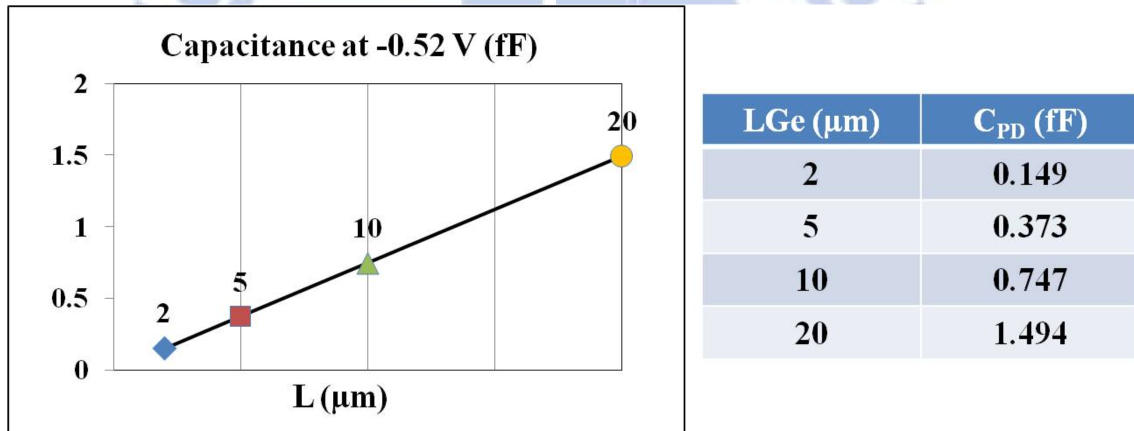

LGe (μm)	C_{PD} (fF)
2	0.149
5	0.373
10	0.747
20	1.494

Fig. 5-6Parasitic Capacitance C_{PD}obtained with length of GePD.

5.3.2 Absorption in length direction

From the transmission point of view, absorption coefficient measures how quickly the light signal would lose intensity due to the absorption of a material. But, as for photodiode, the more lights absorbed means the more photons can be utilize and contribute to carriers. In Fig. 5-7, the optical absorption of crystalline $Si_{1-x}Ge_x$ and the corresponding index of refraction of each material are shown from the literature[22].

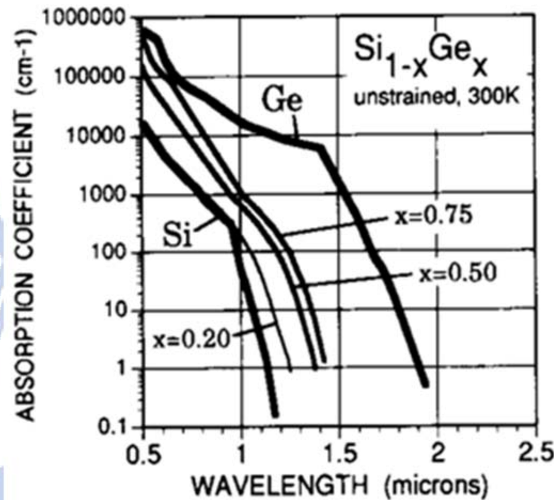

Fig. 5-7 Optical absorption coefficient of Si, Ge, and SiGe alloys[22].

Based on Beer-Lambert law (Eq. 5-2), where I, I_0, and α are intensity at L, input intensity and absorption coefficient respectively, the absorption ration as a function of the length of germanium photodiode can be calculated, as shown in Fig. 5-8. High absorption ration means that there are more number of photons that can be transferred into carriers, so photo-current would increase. (Note that QE doesn't change.)

$$I = I_0 \cdot e^{-\alpha L} \qquad \textbf{Eq. 5-2}$$

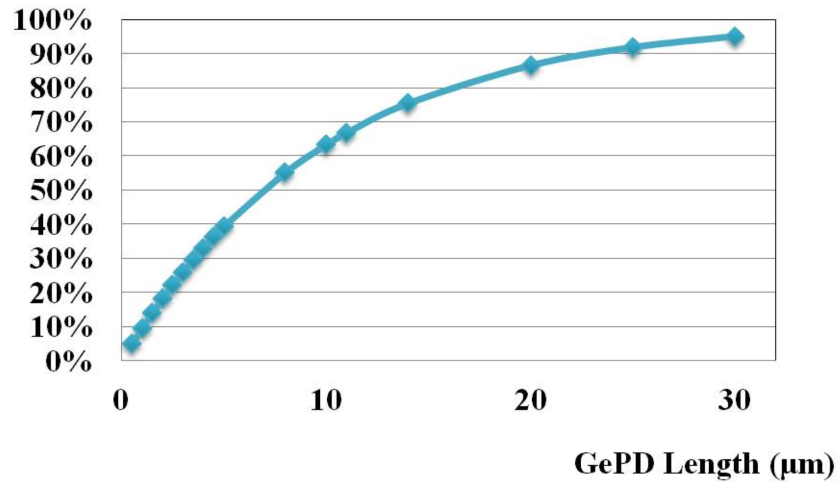

Fig. 5-8 Absorption ratio versus length of germanium photodiode.

As a result, this section reminds that in realist case, although we prefer a short photodiode to avoid large capacitance, the length of germanium photodiode still needs to be compromised with the absorption efficiency of light signals.

5.4 Frequency response

5.4.1 Bit stream input

As an input, the bit stream below in Fig. 5-9is pseudo random and has the most important transitions because it includes all the combinations of three bits.

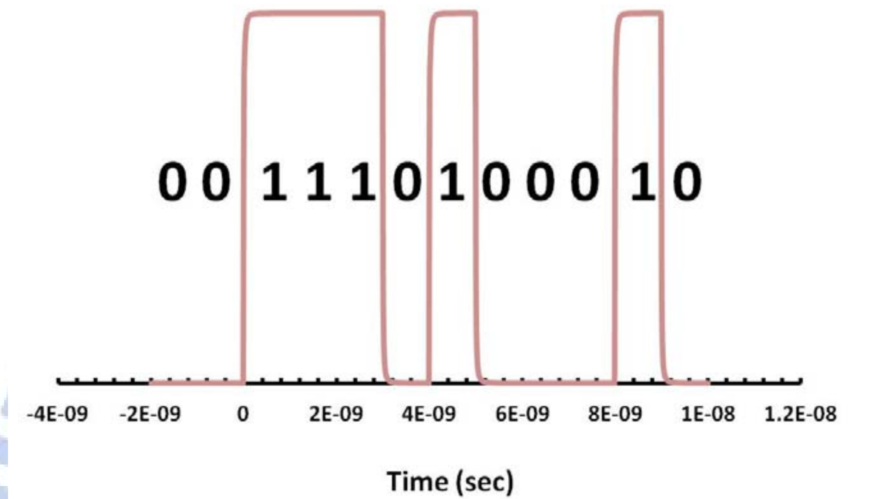

Fig. 5-9 The bit stream input contains combinations three bits.

5.4.2 Eye diagram

To evaluate system speed, eye diagrams are often used. An open eye interprets the nice transient respond of an electronic device. In Fig. 5-10, simulations of transients responds to the bit stream inputs with frequencies 1GHz, 10GHz, 20GHz, 40GHz, and 100GHz are performed. A regular trend can be seen that as the signal frequency is higher than the speed that GePD can handle with, signals distortion can be read as the "eye" getting closed. In realistic cases, eye diagrams needs to be extended with parasitic components, noises, and loads of amplifiers, depending on various interconnect systems.

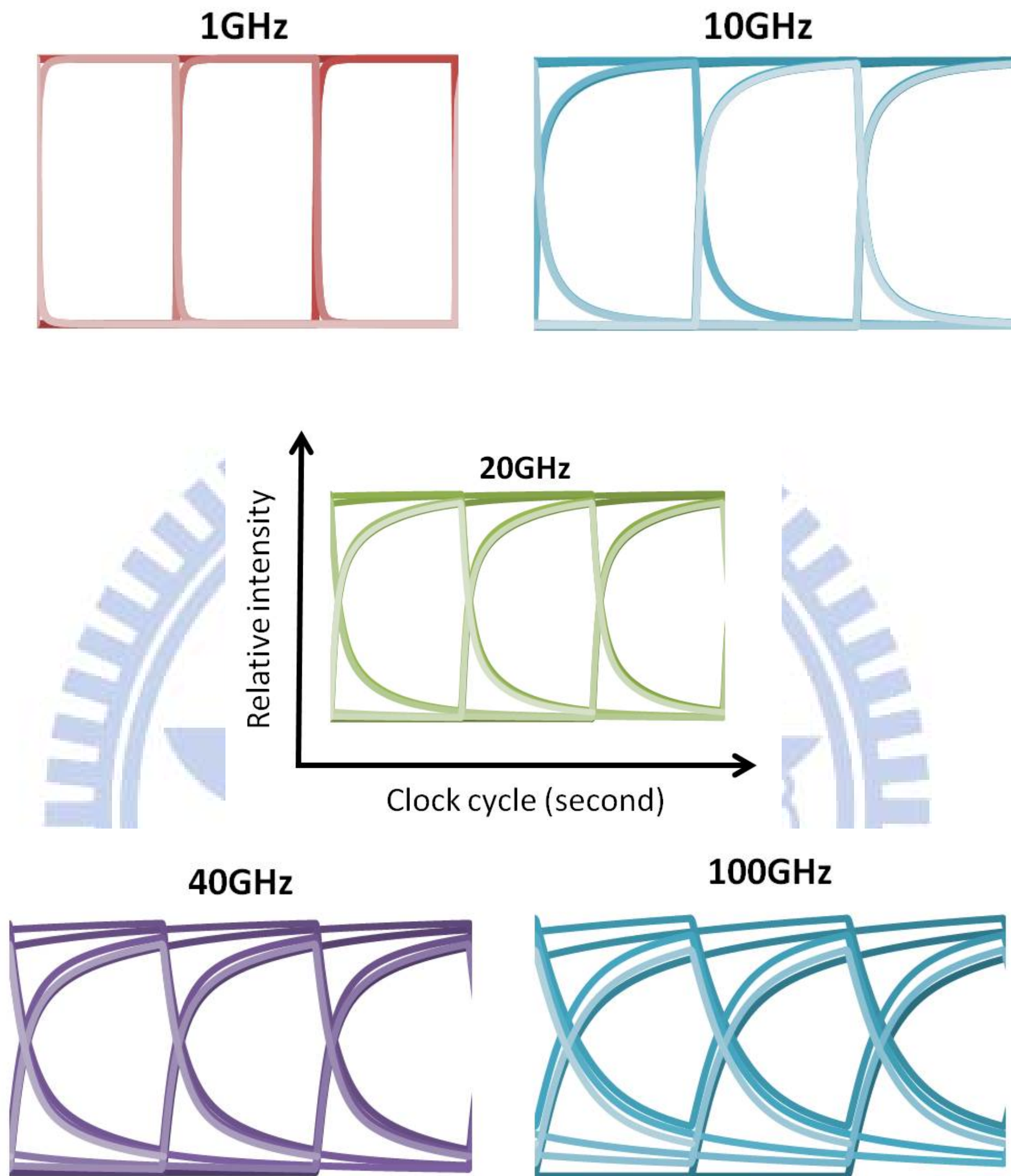

Fig. 5-10 Eye diagram of the GePD with speed 30GHz.

5.5 Conclusion

In this chapter, it is seen that the speed of GePD increases with the total width (wGe), while for each wGe there is an optimum doping separation (Wi) value. A maximum 32GHz is found at wGe equals to 2 μm, and Wi equals to 0.2 μm. For optimization in length direction, we should note that length of GePD needs to be compromised with the absorption efficiency of light signals and the junction capacitance.

Value of junction capacitance of GePD with different length is obtained by C-V simulation. The simulation of C-V might seem redundant, since capacitance is of course increasing linearly with effective capacitor area (hGe × LGe), but it helps us to demonstrate the model of equivalent circuit of GePD, which would be shown in chapter 6.

Finally, frequency respond is shown in eye diagrams while a bit stream of optical signal with various frequencies.

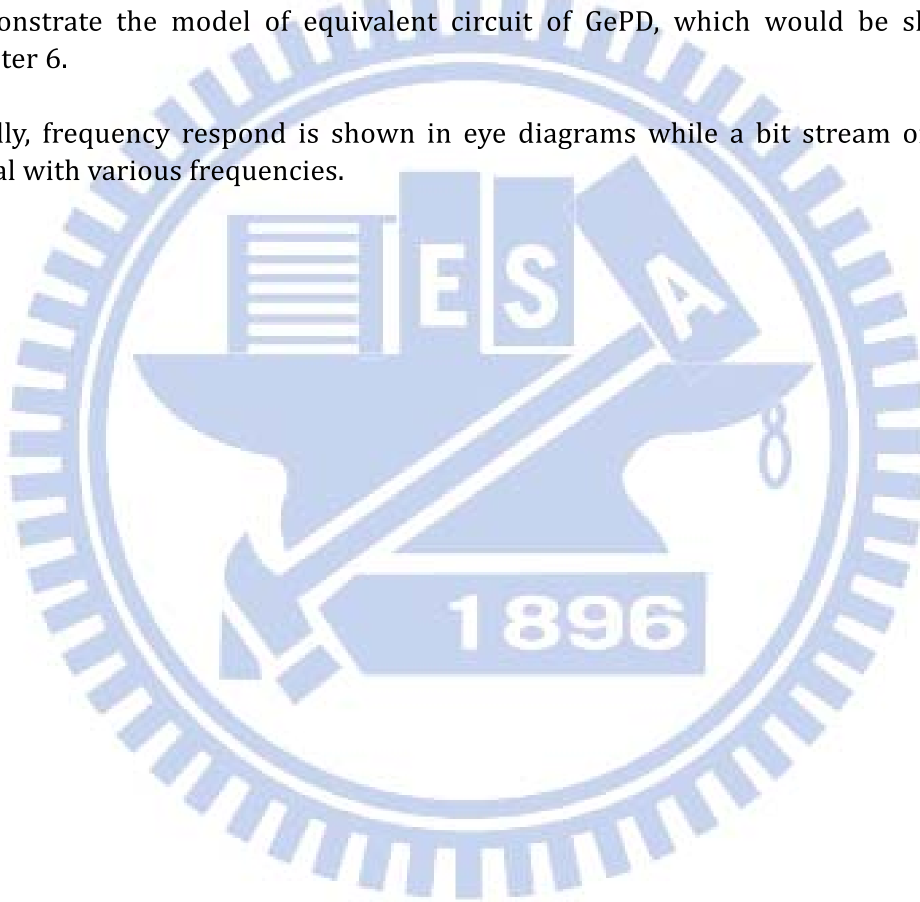

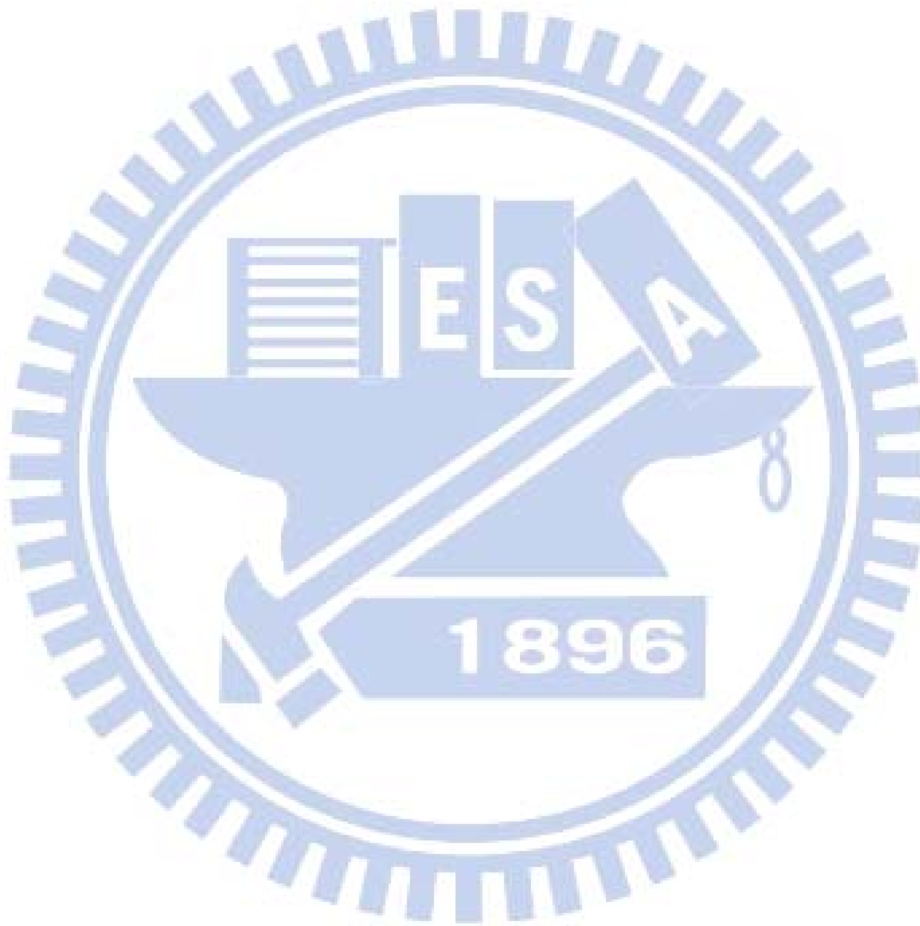
E S A
1896

Chapter 6 Conclusion

As one of the crucial components in optical interconnect system, germanium photodiodes are promising due to its corresponding bandgap to absorb infra-red light and the compatibility to silicon-based photonics and electronics. However, many researchers have shown that GePD is suffering from high dark current, and efforts were done to suppress the dark current and to increase gain-bandwidth product by improving GePD efficiency and speed.

Several guidelines toward the GePD structure are provided in this thesis with the aid of investigation of measured dark current and TCAD simulation, to help fabricating high-efficiency and low-power consumption germanium photodetector with the structure resembles following figure. A table of guidelines is put at the end of this chapter after statements of conclusions chapter by chapter.

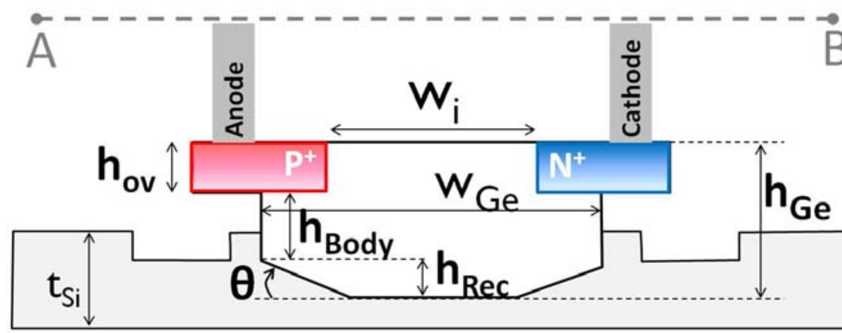

In chapter 2, we show the investigation of physical mechanisms behind the dark current in germanium photodiode via experimental data. It can be verified that dark current is in the combination behavior of diffusion current and Shockley-Read-Hall generation current. At room temperature, and at the bias -0.5V, SRH generation is the main component in dark current. There is a good qualitative agreement between formula trend and measured data.

In chapter 3, TCAD simulation is involved with inclusion of SRH model. We constructed base structures similar to measured photodiodes in TCAD sprocess tool with defect densities are estimated as 5e18/cm³ and 1e20/cm³ for simulations of constant defect profile and exponential defect profile. Alterations were made in the base structures to find the structure that has minimum dark current. Generally speaking, to make a germanium photodiode with low leakage, a thin germanium layer is required to reduce the SRH volume, i.e. number of traps, as much as possible. A narrow doping separation is crucial to keep a small SRH volume within the large electric field region. Finally, deep junctions (junction depth ≈ hGe) are needed to circumvent the dark current arouse by the spreading electric field of shallow junctions.

In chapter 4, we start to simulate the photocurrent of GePD with optical signals. To have high quantum efficiency, we have an optimum when the width of germanium equals to 3.4 μm, the thickness of germanium equals to 0.5 μm, and the doping separation equals to half of the width, which is 1.7 μm. To maintain high quantum efficiency while keeping low level of dark current, **deep-and-shallow junction** is proposed. Deep junction is with slightly doping 3e13/cm^3 to suppress dark current, and shallow junction is degenerately doped to prompt photo currents. The final GePD structure with optimized geometries and junction engineering is shown below, where the color legend is for dopants and defect concentration, and round contours is illustrating the optical signal inside GePD.

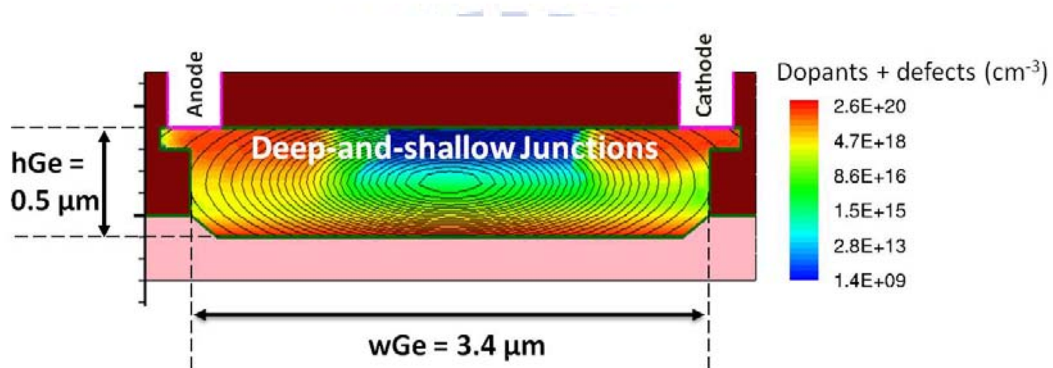

In chapter 5, transient respond of GePD to AC optical signal is presented. The speed increases as total width (wGe) decreases, while for each wGe there is an optimum doping separation (Wi) value. A maximum 32GHz is found at wGe equals to 2 μm, and Wi equals to 0.2 μm. For optimization in length direction, we should note that length of GePD needs to be compromised with the absorption efficiency of light signals and the junction capacitance. The value of junction capacitance of GePD with different length is obtained by C-V simulation to demonstrate the model of equivalent circuit of GePD.

To summarize the whole thesis, contributions from above chapters are generalized in two aspects, as described in the following two paragraphs:

In device aspect, we provide guidelines toward the GePD structure, which are summarized above, and arranged in Table 6-1on next page. Each parameter is discussed while others are fixed.

In system aspect, we provide a simulation framework such that values of electronic components in the equivalent circuit of GePD become available or computable. In this way, evaluation of speed at the system level could be achieved by applying equivalent circuit of germanium photodiode connects to arbitrary known interconnection systems. For a germanium photodiode with length L, components can be obtained as shown in Table 6-2.

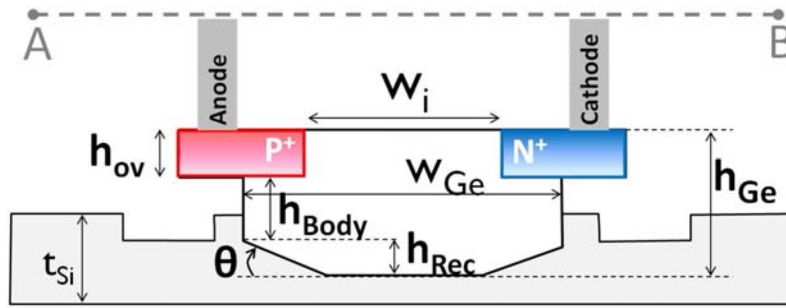

Parameters	Guidelines	Reasons
To lower Dark current		
hGe	Smaller, better	I_{dark} increases linearly with hGe, due to number of traps increases as germanium has a larger volume.
wGe	≥ 3 µm (Wi=1.8µm)	For same Wi, many traps at the tapered facets are more close to the middle in a narrow GePD, where electric field is stronger.
Wi	Smaller, better	Number of traps increases at the intrinsic region where electric field is large.
Junction	Deeper, better	Electric field spreading out from shallow junction would increase I_{dark}.
To increase Quantum efficiency		
hGe	0.5 µm	The optimum reached in the structure which lights mostly contribute in the center of GePD while not being squeezed out of germanium.
wGe	3.4 µm	
Wi	½ of wGe	
Junction	Shallower, better	Strong electric fields from shallow junction improve QE
Low Dark Current and High QE at same time		
Optimized geometry and Deep-and-shallow two-steps implant		Strong electric field of shallow junctions is away from defects at bottom of GePD, and it provides a strong driven force to carriers. Deep junction with slight doping can screen the electric fields spreading from top to defects at the bottom.
To boost speed		
LGe	Depends on application	L influences absorption of light and parasitic capacitance
wGe	Smaller, better	Narrow GePD means shorter distance for carriers to travel to electrodes.
Wi	The optimum exists, depending on wGe	Maximum happened at different Wi values in GePD with different wGe, because there are two mechanisms competing each other: Junction capacitance and drift velocity

Table 6-1 Several Guidelines for designing GePD.

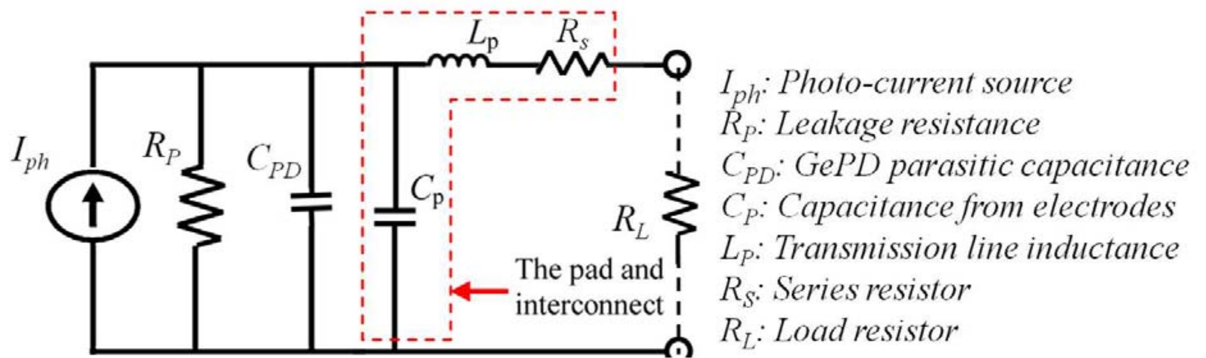

Components	Resource	Expression
I_{ph} (A)	Ch 4 of this thesis	$Photons_{absorbed}(L) \times QE(ratio)$
R_P (ohm)	Ch 2, Ch3 of this thesis	$V_{bias}(V)$ / I_{dark} (A/μm) × L(μm)
C_{PD} (Farads)	Ch 5 of this thesis	As simulated in Sec. 5.3.1
C_P, L_P, R_S	Estimated from circuit layout	
R_L	Depends on next circuit stage (amplifier...etc.)	

Table 6-2GePD equivalent circuit [20][21]**and acquired value of components.**

1896

Appendices

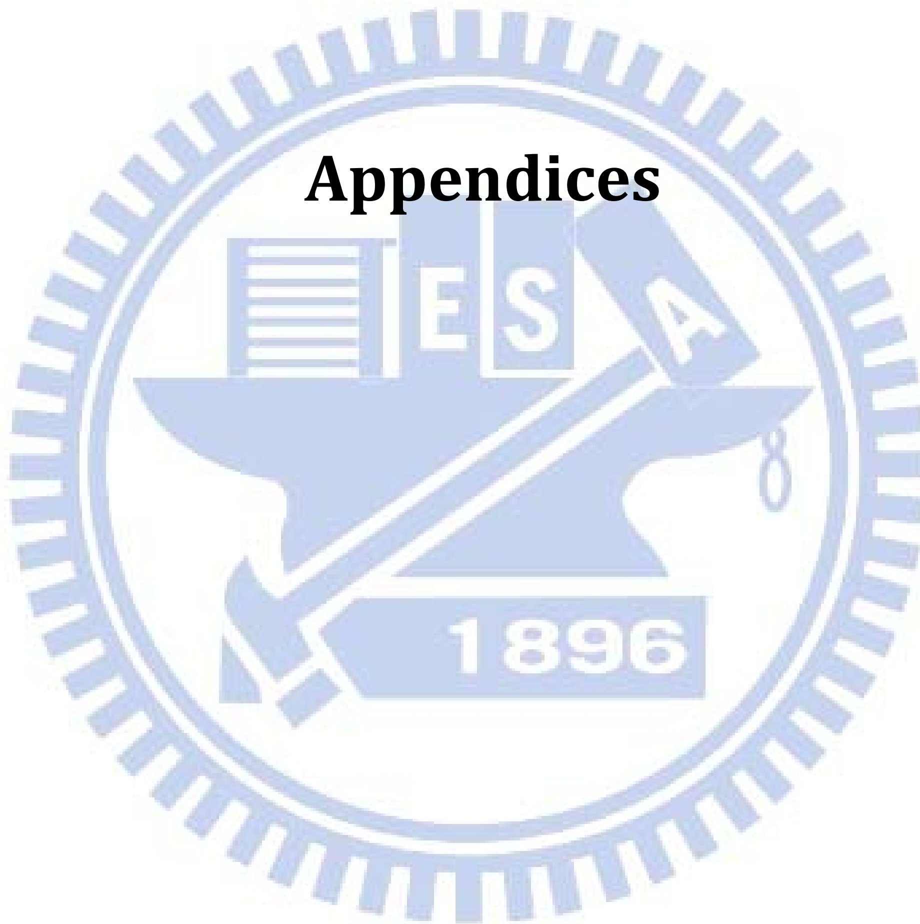

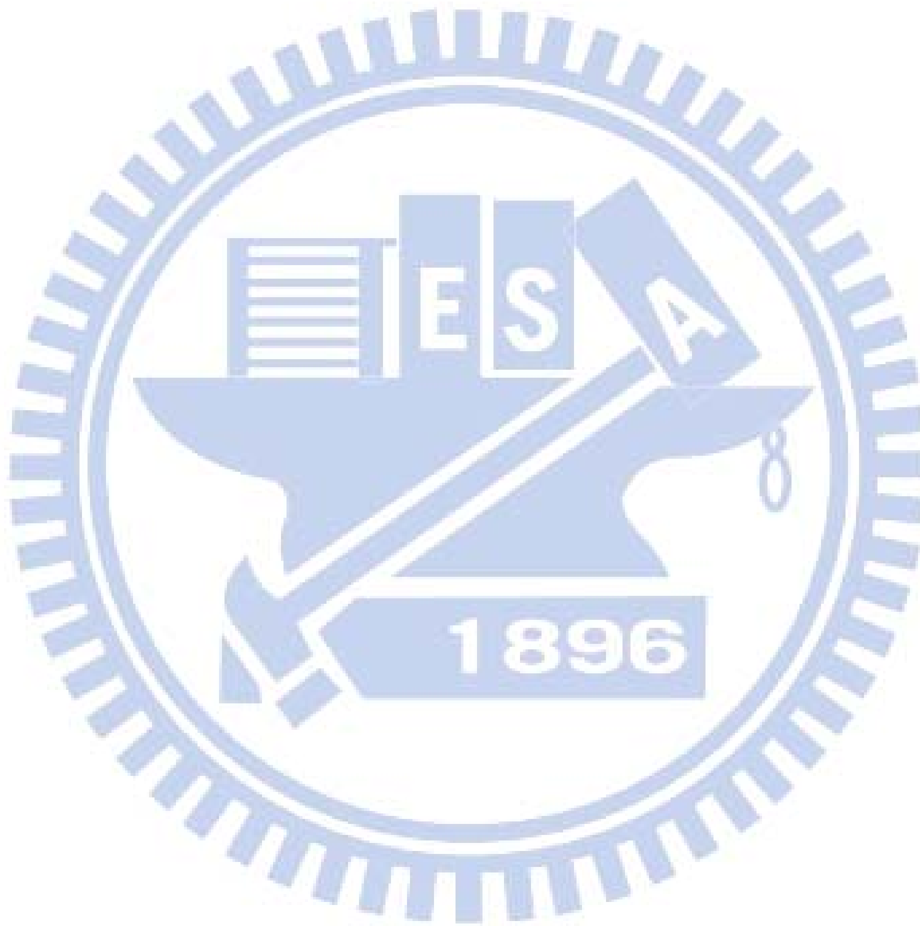
ESA
1896

Appendix A: Command codes in TCAD simulator

In this appendix, command codes used in TCAD Sprocess, TCAD Sdevice simulators are given. Note that here "hGe" stands for h_{body} only, not the total germanium thickness.

Sprocess

```
define garden 0.1
define hOX [expr (@hov@+@hGe@)]
define Wtot [expr (2*(@wov@+$garden)+@wGe@)]
define theta [expr (3.14159265*@angle@/180)]
define wPN [expr (@wGe@*@wPN_ratio@)]
define imp_long [expr (($wPN+$Wtot)/2)]

line x loc= 0   tag=SiTop     spacing=50<nm>
line x loc= 300<nm> tag=SiBottom  spacing=50<nm>

line y loc= 0   tag=SiLeft    spacing=50<nm>
line y loc= $Wtot tag=SiRight   spacing=50<nm>

region silicon xlo=SiTop xhi=SiBottom ylo=SiLeft yhi=SiRight
init concentration=1e15 field=Boron !DelayFullD

mgoals on  min.normal.size=2<nm> max.lateral.size=2<um> normal.growth.ratio=1.3


# PHYSICAL MODELS FOR GERMANIUM
        pdbSetDouble ImplantData Germanium AtomicMass 72.61
        pdbSetDouble ImplantData Germanium AtomicNumber 32
        pdbSetDouble Germanium LatticeConstant 5.64613
        pdbSetDouble Germanium LatticeDensity 4.41e22
        pdbSetDouble Germanium AmorpGamma 1.0
        pdbSetDouble Germanium AmorpDensity 1.1e22
        pdbSetDouble Germanium AmorpThreshold 1.1e22
        pdbSetDouble Germanium LatticeSpacing [expr pow(1/4.41e22,1.0/3.0)]
        pdbSetString Germanium LatticeType Zincblende
        pdbSetDouble Germanium MassDensity 5.35
        pdbSetBoolean Germanium Amorphous 0
        pdbSetString Germanium LatticeAtom COMPOSITION
        pdbSetString Germanium Composition Component0 Name Germanium
        pdbSetDouble Germanium Composition Component0 StWeight 1
        pdbSetDouble Germanium CompoundNumber 1
        pdbSetDouble Germanium DebyeTemperature 519
```

```
        pdbSetBoolean Germanium ElectronicStoppingLocal 1
        pdbSetDouble Germanium SurfaceDisorder 5e-4



# NUMERICAL PARAMETERS FOR TaurusMC (please consult manual)
        pdbSet MCImplant TrajectoryReplication 1
        pdbSet MCImplant TrajectorySplitting 1
        pdbSetDouble Germanium Phosphorus MaxSplits 8.0
        pdbSetDouble Germanium Phosphorus MaxSplitsPerElement 1.0
        pdbSetDouble Germanium Boron MaxSplits 8.0
        pdbSetDouble Germanium Boron MaxSplitsPerElement 1.0
        pdbSetDouble Germanium Arsenic MaxSplits 8.0
        pdbSetDouble Germanium Arsenic MaxSplitsPerElement 1.0

# Monte Carlo Implant paramerters implanted species (TaurusMC)
        pdbSetDouble Germanium Phosphorus amor.par 1.0
        pdbSetDouble Germanium Phosphorus casc.amo 1.0
        pdbSetDouble Germanium Phosphorus disp.thr 15
        pdbSetDouble Germanium Phosphorus casc.dis 15
        pdbSetDouble Germanium Phosphorus surv.rat 0.75
        pdbSetDouble Germanium Phosphorus casc.sur 0.75
        pdbSetDouble Germanium Phosphorus MCVFactor 1.0
        pdbSetDouble Germanium Phosphorus MCDFactor 1.0
        pdbSetDouble Germanium Phosphorus MCIFactor 1.0

        pdbSetDouble Germanium Boron amor.par 1.0
        pdbSetDouble Germanium Boron casc.amo 1.0
        pdbSetDouble Germanium Boron disp.thr 15
        pdbSetDouble Germanium Boron casc.dis 15
        pdbSetDouble Germanium Boron surv.rat 0.225
        pdbSetDouble Germanium Boron casc.sur 0.225
        pdbSetDouble Germanium Boron MCVFactor 1.0
        pdbSetDouble Germanium Boron MCDFactor 1.0
        pdbSetDouble Germanium Boron MCIFactor 1.0

        pdbSetDouble Germanium Boron LSS.pre 1.25
        pdbSetDouble Germanium Boron nloc.exp 0.075
        pdbSetDouble Germanium Boron nloc.pre 0.44
        pdbSetDouble Germanium Boron casc.sat 0.02
        pdbSetDouble Germanium Boron sat.par 0.02
                                        # THESE PARAMETERS makes B only partially amorphizing in
Germanium,
                                        # damage saturates when 2% of lattice atoms have been
                                        # displaced. This number is based on LIMITED SIMS data
                                        # and should be considered an estimate.

        pdbSetDouble Germanium Arsenic amor.par 1.0
        pdbSetDouble Germanium Arsenic casc.amo 1.0
        pdbSetDouble Germanium Arsenic disp.thr 15
        pdbSetDouble Germanium Arsenic casc.dis 15
        pdbSetDouble Germanium Arsenic surv.rat 2
        pdbSetDouble Germanium Arsenic casc.sur 2
        pdbSetDouble Germanium Arsenic MCVFactor 1.0
        pdbSetDouble Germanium Arsenic MCDFactor 1.0
        pdbSetDouble Germanium Arsenic MCIFactor 1.0
        pdbSetDouble Germanium Arsenic LSS.pre 1
        pdbSetDouble Germanium Arsenic nloc.exp 0.075
        pdbSetDouble Germanium Arsenic nloc.pre 0.5
```

```
###1_oxide_pattertn

#mask
mask name=hov left=-0.001 right=0.1
mask name=hov left=$Wtot-$garden right=$Wtot+0.001

mask name=hGe left=-0.001 right=0.1+@wov@
mask name=hGe left=$Wtot-$garden-@wov@ right=$Wtot+0.001


deposit material= {Oxide} type=isotropic thickness=$hOX
etch material= {Oxide} type=anisotropic thickness=@hov@ mask=hov
etch material= {Oxide} type=anisotropic thickness=[expr (@hGe@+0.001)] mask=hGe


###2_silicon_etch_back
# X1 0
define Y1 [expr @wov@+$garden]
define Y2 [expr $Y1+@hRec@/tan($theta)]
define Y3 [expr $Wtot-$Y2]
define Y4 [expr $Wtot-$Y1]

etch material= {Silicon} type=polygon polygon= {0 $Y1 @hRec@ $Y2 @hRec@ $Y3 0 $Y4 0 $Y1 }

###3_Germanium Growth
deposit material= {Germanium} type=fill coord=-$hOX

###4_N++ implant (masked)
mask clear

mask name=N_imp left=-1<nm> right=$imp_long  negative
mask name=N_imp left=[expr ($Wtot-$garden)] right=[expr ($Wtot+0.001)] negative

deposit material= {Nitride} type=anisotropic thickness=1000<nm> mask=N_imp
implant Phosphorus dose=5e14<cm-2> energy=80<keV> sentaurus.mc info=1
strip Nitride


###5_P++ implant (masked)
mask clear
mask name=P_imp left=-1<nm> right=$garden negative
mask name=P_imp left=[expr ($Wtot-$imp_long)] right=[expr ($Wtot+0.001)] negative
deposit material= {Nitride} type=anisotropic thickness=1000<nm> mask=P_imp
implant Boron dose=5e14<cm-2> energy=30<keV> sentaurus.mc info=1
strip Nitride



select z=(min(Phosphorus,2e19)-min(Boron,1e19)) name=DopingConcentration store
select z=(DopingConcentration) name=Netactive store



!( if { "@Dtype@" == "con" } {

    puts "
    select Germanium z=(Phosphorus+Boron+@Dpeak@) name=TotalConcentration store
    select Silicon z=(Phosphorus+Boron) name=TotalConcentration store "

     } else {
```

```
    puts "
    select                Germanium                z=(Phosphorus+Boron+@Dpeak@*exp(-(@hRec@-x)/0.02))
name=TotalConcentration store
    select Silicon z=(Phosphorus+Boron) name=TotalConcentration store "

      }
}!

###6_Contact formation

#contact mask
mask clear
mask name=contact left=-1<nm> right=[expr ($garden+0.05)]
mask name=contact left=[expr ($garden+0.05+0.35)] right=[expr ($Wtot-($garden+0.05)-0.35)]
mask name=contact left=[expr ($Wtot-($garden+0.05))] right=[expr ($Wtot+0.001)]

deposit material= {Oxide} type=anisotropic thickness=250<nm>
etch material= {Oxide} type=anisotropic thickness=251<nm> mask=contact
deposit material= {Aluminum} type=fill coord=[expr (-1*($hOX+0.25))]

contact name=anode   Aluminum x=[expr (-1*($hOX+0.1))] y=[expr ($garden+0.05+0.1)] replace point

contact  name=cathode  Aluminum  x=[expr  (-1*($hOX+0.1))]  y=[expr  ($Wtot-($garden+0.05+0.1))]
replace point

###7_optical Gaussian profile

set C1 [expr (0.08653/0.22)]
set C2 [expr (0.40018/2)]

set sigmaX   [expr ((@hov@+@hGe@+@hRec@)*$C1)]
set sigmaY   [expr ((2*($garden+@wov@)+@wGe@)*$C2)]
set rX      [expr ((@hov@+@hGe@+@hRec@)/2)-@hRec@]
set rY      [expr ($garden+(@wGe@+@wov@+@wov@)/2)]

select                                                    z=(1e12/($sigmaX*sqrt(2*3.14159))*exp(-
(x+$rX)*(x+$rX)/(2*$sigmaX*$sigmaX))*1/($sigmaY*sqrt(2*3.14159))*exp(-(y-$rY)*(y-
$rY)/(2*$sigmaY*$sigmaY))) \
name=OpticalGeneration store

struct tdr=n@node@ !Gas

exit
```

Sdevice for IV

```
File {
  * input files:
  Grid=   "@tdr@"

Parameter="/imec/users/hellings/public/Doctoraat/TCAD/otherprojects/tables/Jan2010/Germaniu
m_hellings_v2.par"
  OpticalGenerationInput = "@tdr@"

  * output files:
  Plot=   "@tdrdat@"
  Current="@plot@"
  Output= "@log@"

}


Electrode {
  { Name="anode"   Voltage=0.0}
  { Name="cathode"  Voltage=0.0}
}



Physics{

Mobility(
        DopingDependence
)

Recombination (
         SRH (  DopingDependence
                ElectricField (
                Lifetime = Hurkx
                DensityCorrection = None
                )
        )
)


Optics (
        OpticalGeneration (
                ReadFromFile ( DatasetName = OpticalGeneration
                        Scaling = 1)
        )
)


}



Plot{
*--Density and Currents, etc
  eDensity hDensity
  TotalCurrent/Vector eCurrent/Vector hCurrent/Vector
  eMobility hMobility
  eVelocity hVelocity
  eQuasiFermi hQuasiFermi
```

```
*--Temperature
  * eTemperature
  * hTemperature Temperature

*--Fields and charges
  ElectricField/Vector Potential SpaceCharge

*--Doping Profiles
  Doping TotalConcentration * DonorConcentration AcceptorConcentration

*--Generation/Recombination
  SRHRecombination Auger
  Band2BandGeneration
  * AvalancheGeneration eAvalancheGeneration hAvalancheGeneration

*--Driving forces
eGradQuasiFermi/Vector hGradQuasiFermi/Vector
  eEparallel hEparalllel

*--Band structure/Composition
  BandGap
  * BandGapNarrowing
  * Affinity
  ConductionBand ValenceBand
  *xMoleFraction

*--Traps
  *eTrappedCharge  hTrappedCharge
  *eGapStatesRecombination hGapStatesRecombination

*--Heat generation
  * TotalHeat eJouleHeat hJouleHeat RecombinationHeat


*OpticalGeneration
  *OpticalIntensity

}



Math{

*          Error(Electron) = 1e-5
*          Error(Hole)       = 1e-5
*          RelErrControl
*          ErrRef(Electron) = 1e12
*          ErrRef(Hole)     = 1e12
Extrapolate
*          TrapDLN = 100
*          eDrForceRefDens = 1e12
*          hDrForceRefDens = 1e12
            NoSRHperPotential
*          hMobilityAveraging=ElementEdge
*          eMobilityAveraging=ElementEdge

}



Solve {
```

```
*- Creating initial solution
                        Coupled(Iterations=100) { Poisson }
                        Coupled(Iterations=100 LineSearchDamping=0.01) { Poisson Electron Hole}

*- Ramp to negative bias
                      Quasistationary(
                          InitialStep=0.25 Increment=1.2 Decrement=4
                          MinStep=1e-4 MaxStep=1
                          Goal { Name="anode" Voltage=-1 }
                        ){ Coupled(Iterations=15 ) { Poisson Electron Hole} Plot (FilePrefix = "n@node@_Dark_05" Time= (0.5))}


NewCurrentFile="sweepdark_"
Plot (FilePrefix = "n@node@_dark")
*- Ramp to positive bias
                      Quasistationary(
                          InitialStep=0.04 Increment=1.2 Decrement=4
                          MinStep=1e-4 MaxStep=0.04
                          Goal { Name="anode" Voltage=1 }
                        ){ Coupled(Iterations=15 ) { Poisson Electron Hole} }



NewCurrentFile="sweeplight_"
Plot (FilePrefix = "n@node@_light")

 *- switch on the light
                      Quasistationary(
                          InitialStep=1 Increment=1.2 Decrement=4
                          MinStep=1e-4 MaxStep=1
                          Goal { ModelParameter="Optics/OpticalGeneration/ReadFromFile/Scaling" value=@Iphg@ }
             ){ Coupled(Iterations=15 ) { Poisson Electron Hole} }


 *- Ramp to negative bias
                      Quasistationary(
                          InitialStep=0.04 Increment=1.2 Decrement=4
                          MinStep=1e-4 MaxStep=0.04
                          Goal { Name="anode" Voltage=-1 }
                        ){ Coupled(Iterations=15 ) { Poisson Electron Hole} Plot (FilePrefix = "n@node@_Light_05" Time= (0.75))}



}
```

Sdevice for C-V

```
Device DIODE {
Electrode {
            { Name="anode" Voltage=@StartVoltage@}
            { Name="cathode" Voltage=0.0 }
}

File {
            Grid = "@tdr@"
            Current = "@plot@"
            Plot = "@tdrdat@"

    Parameter="/imec/users/hellings/public/Doctoraat/TCAD/otherprojects/tables/Jan2010/Germanium_hellings_v2.par"
}

Physics {
            Mobility ( DopingDep)
            Recombination (
             SRH (  DopingDependence
                        ElectricField (
                        Lifetime = Hurkx
                        DensityCorrection = None
                        )
            )
    )
}

Plot {
            eDensity hDensity eCurrent hCurrent
            ElectricField eEparallel hEparallel
            eQuasiFermi hQuasiFermi
            Potential Doping SpaceCharge
            DonorConcentration AcceptorConcentration
ConductionBandEnergy ValenceBandEnergy
}

}

Math{

*           Error(Electron) = 1e-5
*           Error(Hole)       = 1e-5
*           RelErrControl
*           ErrRef(Electron) = 1e12
*           ErrRef(Hole)     = 1e12
Extrapolate
*           TrapDLN = 100
*           eDrForceRefDens = 1e12
*           hDrForceRefDens = 1e12
             NoSRHperPotential
*           hMobilityAveraging=ElementEdge
*           eMobilityAveraging=ElementEdge

}

File {
            Output = "@log@"
            ACExtract = "@acplot@"
}
```

```
System {
            DIODE GePD (anode=elect_p cathode=elect_n)
            Vsource_pset vp (elect_p 0) {dc=@StartVoltage@}
            Vsource_pset vn (elect_n 0) {dc=0}
}

Solve {
#-a) zero solution
Coupled { Poisson }
Coupled { Poisson Electron Hole }
Coupled { Poisson Electron Hole Circuit Contact}
#-d) ramp bottom contact
            Quasistationary (
            InitialStep=@MaxStep@ MaxStep=@MaxStep@ MinStep=1.e-7
            Goal { Parameter=vp.dc Voltage=@TargetVoltage@ }
            ){
                        ACCoupled (
                                    StartFrequency=1e6 EndFrequency=1e6
                                    NumberOfPoints=1 Decade
                                    Node(elect_p elect_n) Exclude(vp vn)

    )
{ Poisson Electron Hole Circuit Contact}
}

}
```

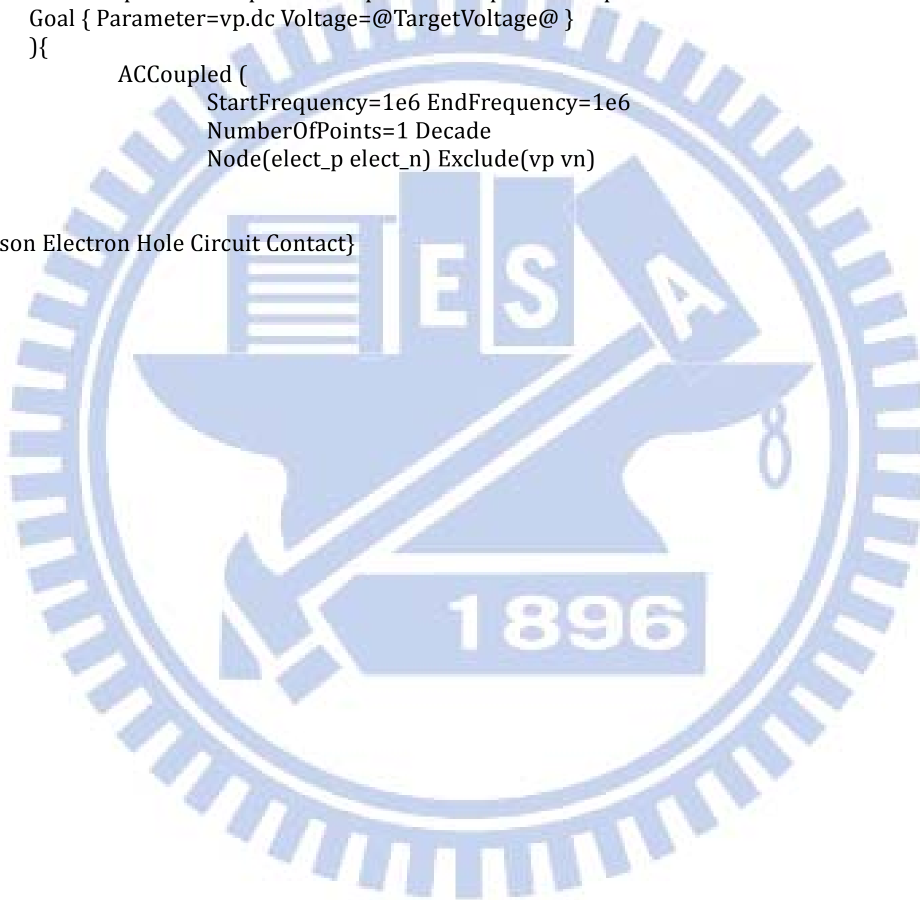

Sdevice for transient

```
File {
  * input files:
  Grid=   "@tdr@"

Parameter="/imec/users/hellings/public/Doctoraat/TCAD/otherprojects/tables/Jan2010/Germaniu
m_hellings_v2.par"
  OpticalGenerationInput = "@tdr@"

  * output files:
  Plot=   "@tdrdat@"
  Current="@plot@"
  Output= "@log@"

}


Electrode {
  { Name="anode"    Voltage=0.0}
  { Name="cathode"  Voltage=0.0}
}

Physics{

Mobility(
          DopingDependence
)

Recombination (
           SRH (  DopingDependence
                    ElectricField (
                    Lifetime = Hurkx
                    DensityCorrection = None
                    )
          )
)

Optics (
          OpticalGeneration (
                    ReadFromFile ( DatasetName = OpticalGeneration
                              Scaling = 1)
          )
)

}

Plot{
*--Density and Currents, etc
  eDensity hDensity
  TotalCurrent/Vector eCurrent/Vector hCurrent/Vector
  eMobility hMobility
  eVelocity hVelocity
  eQuasiFermi hQuasiFermi

*--Temperature
  * eTemperature
  * hTemperature Temperature

*--Fields and charges
  ElectricField/Vector Potential SpaceCharge
```

```
*--Doping Profiles
  Doping TotalConcentration * DonorConcentration AcceptorConcentration

*--Generation/Recombination
  SRHRecombination Auger
  Band2BandGeneration
  * AvalancheGeneration eAvalancheGeneration hAvalancheGeneration

*--Driving forces
eGradQuasiFermi/Vector hGradQuasiFermi/Vector
  eEparallel hEparalllel

*--Band structure/Composition
  BandGap
  * BandGapNarrowing
  * Affinity
  ConductionBand ValenceBand
  *xMoleFraction

*--Traps
  *eTrappedCharge  hTrappedCharge
  *eGapStatesRecombination hGapStatesRecombination

*--Heat generation
  * TotalHeat eJouleHeat hJouleHeat RecombinationHeat


*OpticalGeneration
  *OpticalIntensity

}


Math{

*         Error(Electron) = 1e-5
*         Error(Hole)       = 1e-5
*         RelErrControl
*          ErrRef(Electron) = 1e12
*          ErrRef(Hole)     = 1e12
Extrapolate
*         TrapDLN = 100
*         eDrForceRefDens = 1e12
*         hDrForceRefDens = 1e12
           NoSRHperPotential
*         hMobilityAveraging=ElementEdge
*         eMobilityAveraging=ElementEdge

}


Solve {
*- Creating initial solution
                        Coupled(Iterations=100) { Poisson }
                        Coupled(Iterations=100 LineSearchDamping=0.0001) { Poisson Hole Electron}

*- Ramp to negative bias
                      Quasistationary(
                          InitialStep=0.25 Increment=1.2 Decrement=4
                          MinStep=1e-4 MaxStep=1
```

```
                    Goal { Name="anode" Voltage=-0.5 }
                  ){   Coupled(Iterations=15      )  {   Poisson   Electron   Hole}   Plot   (FilePrefix  =
"n@node@_Dark_05" Time= (0.5))}

NewCurrentFile="transient_"

Transient (
        InitialTime = 0 FinalTime = 3e-9
        InitialStep=1 MaxStep=1e-11
        Bias{      ModelParameter="Optics/OpticalGeneration/ReadFromFile/Scaling" value=( 1 at 0, 1
at 0.99e-9, 1e15 at 1e-9, 1e15 at 1.99e-9, 1 at 2e-9, 1 at 2.99e-9) }
) { Coupled { Poisson Electron Hole } }

}
```

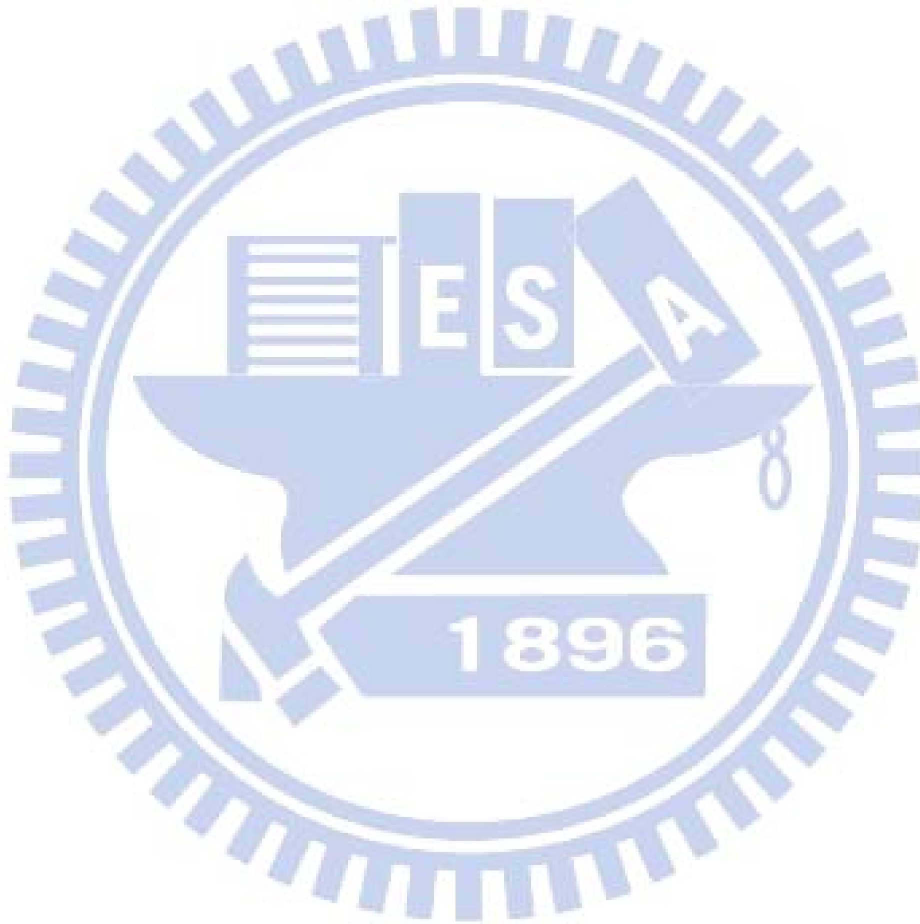

Bibliography

[1] D. A. B. Miller, "Rationale and Challenges for Optical Interconnects to Electronic Chips," *proceedings of the IEEE*, vol. 88, no. 6, p. 728, 2000.

[2] D. A. B. Miller, "Optical Interconnects to Silicon," *IEEE Journal of Selected Topics in Quantum Electronics*, vol. 6, no. 6, pp. 1312-1317, 2000.

[3] D. A. B. Miller, "Physical reasons for optical interconnection," *Int. J. Optoelectronics*, vol. 168, 1997.

[4] L. Chen, K. Preston, S. Manipatruni, and M. Lipson, "Integrated GHz silicon photonic interconnect with micrometer-scale modulators and detectors," *Optics Express*, vol. 17, no. 17, pp. 15248-15256, 2009.

[5] S. B. Samavedam, M. T. Currie, T. A. Langdo, and E. A. Fitzgerald, "High-quality germanium photodiodes integrated on silicon substrates using optimized relaxed graded buffers," *Applied Physics Letters*, vol. 73, no. 15, pp. 2125-2127, 1998.

[6] M. Takenaka, K. Morii, M. Sugiyama, Y. Nakano, and S. Takagi, "Ultralow-dark-current Ge photodetector with GeO 2 passivation and gas-phase doped junction," *IEEE International Conference on*, pp. 36-38, 2011.

[7] J. E. Bowers, D. Dai, Y. Kang, and M. Morse, "High-gain high-sensitivity resonant Ge / Si APD photodetectors," *Proc. SPIE*, vol. 7660, pp. 1-8, 2010.

[8] S. Assefa, F. Xia, and Y. A. Vlasov, "Reinventing germanium avalanche photodetector for nanophotonic on-chip optical interconnects," *Nature*, vol. 464, no. 7285, pp. 80-84, 2010.

[9] D. A. Neamen, *Semiconductor Physics and Devices.pdf*, 3rd ed. McGraw-Hill, 2003.

[10] N. V. Loukianova et al., "Leakage Current Modeling of Test Structures for Characterization of Dark Current in CMOS Image Sensors," *IEEE Transactions on Electron Devices*, vol. 50, no. 1, pp. 77-83, 2003.

[11] R. Widenhorn, M. M. Blouke, A. Weber, A. Rest, and E. Bodegom, “Temperature dependence of dark current in a CCD,” *Proc. SPIE*, vol. 4669, pp. 193-201, 2002.

[12] G. Eneman et al., “Impact of Donor Concentration , Electric Field , and Temperature Effects on the Leakage Current in Germanium p + / n Junctions,” *IEEE Transactions on Electron Devices*, vol. 55, no. 9, pp. 2287-2296, 2008.

[13] R. N. HALL, “Electron-Hole Recombination in Germanium,” *Physical Review*, vol. 87, no. 2, pp. 387-387, 1952.

[14] C.-T. Sah and W. Shockley, “Carrier Generation and recombination in P-N Junctions and P-N Junction Characteristics,” *proceedings of the IRE*, vol. 1, p. 1228, 1956.

[15] L. Esaki, “New Phenomenon in Narrow Germanium p-n Junctions,” *Physical Review*, vol. 109, no. 2, pp. 603-604, 1958.

[16] G. A. M. Hurkx and H. C. D. Graaff, “A New Analytical Diode Model Including Tunneling and Avalanche Breakdown,” *IEEE Transactions on Electron Devices*, vol. 39, no. 9, pp. 2090-2098, 1992.

[17] L. Chen and M. Lipson, “Ultra-low capacitance and high speed germanium photodetectors on silicon,” *Optics Express*, vol. 17, no. 10, pp. 7901-7906, 2009.

[18] E. Gaubas, M. Bauz, A. Uleckas, and J. Vanhellemont, “Carrier lifetime studies in Ge using microwave and infrared light techniques,” *Materials Science in Semiconductor Processing*, vol. 9, pp. 781-787, 2006.

[19] “Synopsys, Inc., Mountain View, CA, C-2009.06 ed. Sentaurus Device Reference Manual.” 2009.

[20] D. Dai, M. J. W. Rodwell, J. E. Bowers, Y. Kang, and M. Morse, “Derivation of the Small Signal Response and Equivalent Circuit Model for a Separate Absorption and Multiplication Layer Avalanche Photodetector,” *IEEE Journal of Selected Topics in Quantum Electronics*, 2009.

[21] S. Assefa et al., “CMOS-Integrated Optical Receivers for On-Chip Interconnects,” *IEEE Journal of Selected Topics in Quantum Electronics*, vol. 16, no. 5, pp. 1376-1385, 2010.

[22] R. A. Soref and S. Member, “Silicon-Based Optoelectronics,” *proceedings of the IEEE*, vol. 81, no. 12, p. 1687, 1993.